REPORT DOCUMENTATION PAGE	Form Approved OMB No. 0704-0188

1. AGENCY USE ONLY *(Leave blank)*	2. REPORT DATE	3. REPORT TYPE AND DATES COVERED
	7.Jan.99	THESIS

4. TITLE AND SUBTITLE
SYNOPTIC DISTURBANCES FOUND IN PRECIPITABLE WATER FIELDS NORTH OF EQUATORIAL AFRICA

5. FUNDING NUMBERS

6. AUTHOR(S)
1ST LT PATLA JASON E

7. PERFORMING ORGANIZATION NAME(S) AND ADDRESS(ES)
TEXAS A&M UNIVERSITY

8. PERFORMING ORGANIZATION REPORT NUMBER

9. SPONSORING/MONITORING AGENCY NAME(S) AND ADDRESS(ES)
THE DEPARTMENT OF THE AIR FORCE
AFIT/CIA, BLDG 125
2950 P STREET
WPAFB OH 45433

10. SPONSORING/MONITORING AGENCY REPORT NUMBER
FY99-27

11. SUPPLEMENTARY NOTES

12a. DISTRIBUTION AVAILABILITY STATEMENT
Unlimited distribution
In Accordance With AFI 35-205/AFIT Sup 1

12b. DISTRIBUTION CODE

13. ABSTRACT *(Maximum 200 words)*

14. SUBJECT TERMS	15. NUMBER OF PAGES
	97
	16. PRICE CODE

17. SECURITY CLASSIFICATION OF REPORT	18. SECURITY CLASSIFICATION OF THIS PAGE	19. SECURITY CLASSIFICATION OF ABSTRACT	20. LIMITATION OF ABSTRACT

SYNOPTIC DISTURBANCES FOUND IN PRECIPITABLE WATER FIELDS NORTH OF EQUATORIAL AFRICA

A Thesis

by

JASON EDDY PATLA

Submitted to the Office of Graduate Studies of
Texas A&M University
in partial fulfillment of the requirements for the degree of

MASTER OF SCIENCE

December 1998

Major Subject: Meteorology

SYNOPTIC DISTURBANCES FOUND IN PRECIPITABLE WATER FIELDS NORTH OF EQUATORIAL AFRICA

A Thesis

by

JASON EDDY PATLA

Submitted to Texas A&M University
in partial fulfillment of the requirements
for the degree of

MASTER OF SCIENCE

Approved as to style and content by:

James P. McGuirk
(Chair of Committee)

John F. Griffiths
(Member)

Benjamin S. Giese
(Member)

Gerald R. North
(Head of Department)

December 1998

Major Subject: Meteorology

ABSTRACT

Synoptic Disturbances Found in Precipitable Water Fields

North of Equatorial Africa. (December 1998)

Jason Eddy Patla, B.S., Purdue University

Chair of Advisory Committee: Dr. James P. McGuirk

The origin and structure of tropical synoptic scale precipitable water (PW) anomalies estimated from TOVS satellite observations are analyzed as they propagate eastward across northern Africa during MAM 1988. Previous studies, accomplished by Mackey (1996), determined the location and season for the strongest and most coherent 3 to 8 day filtered PW signal.

NCEP/NCAR reanalysis (2.5° resolution) provides data for a case study analysis of seven prominent anomalous PW events during the period. Six case wind field composite analysis is accomplished with both actual winds and reduced shear winds (zonal mean removed at each latitude band). Case study analysis revealed a doppler shifted propagating Rossby Wave (k = 6, c = -5 m/sec) at 500hPa and 250hPa that moved onto the west African coast imbedded within a mean zonal flow of approximately 17 m/sec. The wave then moved east across the continent at approximately 12 m/sec near 20°N. The wave's associated cusp-like feature advects deep tropical moisture northward, resulting in Mackey's PW anomaly.

Analysis of potential vorticity, specific humidity, temperature, and wind field composites at 850hPa, 500hPa and 250hPa fit well within the range of Rossby wave structure. Descriptive statistical analysis established confidence

intervals for the composites at two resolutions within the localized grid (20°W to 40°E, 0° to 30°N).

A sample structure of the anomalies is displayed for each variable found to be statistically significant. The strongest correlation between observed PW and analyzed specific humidity and temperature is observed at 500mb and 250mb. Composite analysis of specific humidity and the appropriate standard deviation field supports this finding. PW amounts much greater than the climate mean state over the Gulf of Guinea are found within the PW anomaly structure, indicating an additional moisture source, possibly convection enhanced by the wave passage. 850mb upward vertical motion is also found to be slightly enhanced due to the anomalous flow associated with the wave passage.

An empirical model is provided showing a four stage development of the PW anomalies during the five primary days of their life cycle and days prior.

DEDICATION

I dedicate this thesis to my parents, Norbert and Judy, and my brother and sister, Jonathan and Jennifer, for all the help and encouragement they have provided over the years. Their love and persistence has guided me towards a happy life, an advanced education and an enjoyable career in the United States Air Force.

I also dedicate this to many of my friends, including Fr. Michael Burrows, OSB of Marmion Academy, who have also pushed and supported me throughout my life in order to succeed.

ACKNOWLEDGEMENTS

I acknowledge the members of my committee for their time and assistance towards completing this research. Their knowledge and insight will always be appreciated. I thank Prof. James P. McGuirk for going to bat for me in order to give me a chance at Texas A&M, even with borderline undergraduate grades. His sense of humor and wit kept the most stressful days at bay, and I appreciate his willingness to give me a chance and advance my education as my advisor. I thank Prof. John F. Griffiths for serving on my committee and providing help when necessary. I thank Prof. Benjamin S. Giese for serving on my committee and occasionally looking away from mainstream ideas and towards considering every possibility. I thank Prof. John W. Nielsen-Gammon for his programming prowess enabling my utilization of the NCEP/NCAR reanalysis data.

I would also like to thank other graduate students that assisted me over the years: Steve Schroeder, for his open-minded and thorough approach to pretty much everything; Patricia Taft, for her constant drive and encouragement toward completion; and Gordon Carrie, for his patience and assistance during the programming portion of my research. Additionally, I would like to thank Robert White and Jerry Guynes for their professional and personal support of our computer facility. I still don't know how they did what they did so well.

Lastly, I thank the United States Air Force for allowing me the opportunity to earn my M.S. degree in order to follow my father's footsteps towards a successful military career.

TABLE OF CONTENTS

LIST OF FIGURES

FIGURE Page

FIGURE Page

FIGURE Page

LIST OF TABLES

CHAPTER I

INTRODUCTION

The tropics contain many source regions for the initiation of atmospheric disturbances. Some features of these disturbances are readily detectable through various sources of atmospheric analysis, while others are less obvious and often go overlooked. Sources for the study of tropical behavior involve a number of varying methods, including remotely sensed data (satellites), in situ observations (unfiltered time data), field experiments (GATE, TOGA COARE, TRMM), and operational model analysis (NMC, NCEP/NCAR reanalysis, ECMWF).

In many locations, in situ observations are so sparse in coverage density that satellite imagery is the only reliable source of data. The satellite data can then, in turn, be manipulated to observe signals and patterns that may not be obvious within the in situ data. Time filtering, as well as observing the raw data, may help locate these regions of persistent or organized cyclic behavior occurring in certain atmospheric fields. Some common fields observed by satellites include OLR (outgoing longwave radiation), visible, infrared, and water vapor imagery. Television Infra-Red Observational Satellite (TIROS) Operational Vertical Sounder (TOVS) precipitable water (PW) is another such observable field. This field can then be presented as a spatially continuous dataset, allowing for the study of synoptic scale events.

The style is that of the *Journal of Atmospheric Sciences.*

It is important to note that all data sources have their various shortcomings, particularly those involving moisture variables (McGuirk et al., 1989). Some satellite retrievals, unlike the PW data used in this study, depend on a first guess field to interpolate between data points in data sparse regions. This may invariably under-analyze synoptic scale events in particular regions. Recent numerical model analysis, however, has been used to assimilate most of the available data sources in an attempt to create the most detailed and error-free (analysis and forecasts) product possible. A state-of-the-art analysis/forecast system, (National Centers for Environmental Prediction) NCEP/(National Center for Atmospheric Research) NCAR provides the most recent advancement of such a numerical model. This fixed numerical model uses data from 1957 to present, incorporating the various sources of input as they became available (Kalnay et al., 1996).

This study utilizes TOVS-estimated PW at 2.5° grid point resolution, both filtered and unfiltered, to locate and track positive or negative anomalies. The PW algorithm and global analysis was developed by Chung (1993), Yin (1994) and Hatfield (1994). Mackey (1996) first used this PW analysis to identify the most pronounced source regions and seasonal signals of eastward and westward propagating synoptic systems. NCEP/NCAR analysis is used to determine their evolution and structure in specific fields at various atmospheric levels. The result of this analysis is a qualitative conceptual model of the development and evolution of these propagating disturbances north of equatorial Africa.

CHAPTER II

BACKGROUND

Western Africa is frequently studied as a source region for convective wave development. Whether developing over land south of the ITCZ in the southern Sahara (Carlson, 1969a, b), or maintaining an "inverted V" appearance over the Atlantic Ocean (Frank, 1969), *westward* propagating tropical disturbances are known to originate from across this region. Intense systems occasionally develop from these disturbances threatening the North Atlantic with nearly half the ocean's destructive tropical cyclones during particular months of the year (Frank, 1970). The far reaching effects of these systems necessitates a strong need to study their origin's structure and dynamics, possibly allowing better forecast of convective wave development. The area around western Africa, therefore, has been the site of numerous studies of westward propagating disturbances over the past few decades.

Landsea et al. (1997), for example, use a statistical parameterization of rainfall for three regions of West Africa to help develop seasonal forecasts of Atlantic hurricanes. Many studies, however, credit the Sahel for the development of synoptic scale disturbances. Lau and Chang (1987) include such worldwide tropical activity as easterly waves, tropical upper tropospheric troughs (TUTTs), westerly wind bursts, tropical plumes and mid-latitude intrusions within this synoptic scale of three to eight days.

To fully understand synoptic scale occurrences, one must first understand the larger scale patterns and means. Newell et al. (1972) were able to construct one of the first atlases across the globe, describing mean circulations and

atmospheric structure based solely on surface observations and balloon soundings. His data found the mean zonal wind across the lower levels of the tropics to be easterly, becoming westerly in the mid and upper levels, as well as with increasing latitude away from the equator. This is important because this predominant steering flow should carry low and up to mid level synoptic disturbances to the west in most cases across the tropics.

On a more regional scale, studies have been accomplished across the continent of Africa determining large-scale flow, circulation and convective patterns. Krishnamurti (1979), for example, discusses the monthly progression of weak southerly flow and convergence regions out of the Gulf of Guinea that may be an important moisture source for PW anomaly development and maintenance.

Though all scales of atmospheric events have an impact on the region's rainfall, Duvel (1988) determined that about 50% of the region's interdiurnal variation of outgoing longwave radiation (OLR), representing the region's significant summer convection, is induced by events within the synoptic scale (Druyan et al., 1997). These events include easterly waves that develop in the lower levels of the atmosphere near north-central Africa and propagate westward with the flow. Numerous factors, though, play an important role in the overall weather of the region when only considering rainfall. The Northern Hemisphere's summer monsoon, for example, usually with a July onset across the Guinea Coast, brings ample moisture for simple diurnal rainfall.

The structure of various African disturbances, especially easterly waves, has been analyzed using a number of methods. Burpee (1972), using power- and cross-spectrum analysis, tested a number of causative theories for the development of these disturbances. He determined that disturbances first

appear and are most intense near the 700mb level over east central Africa, with a periodicity of 3.2 days and a horizontal wavelength of 4000km. The disturbance formation is due to baroclinic instability in the zonal flow caused by a strong baroclinic zone found south of the mid-troposphere easterly jet core. Additionally, composite analysis reveals a reversal in the absolute vorticity gradient just south of the easterly jet's core (Reed et al., 1977), known to be a necessary condition for such a development of barotropic instability (Kuo, 1949). The study by Reed et al. (1977), though, found the disturbances most intense at 650hPa with a periodicity of 3.7 days and a horizontal wavelength of 2700km. Neither study, however, discussed significant upper level structure or moisture characteristics.

A common and relatively simple way to develop a representative structure of a disturbance is to create composites of wave profiles, partially overcoming problems resulting from data sparseness. The Global Atmospheric Research Program (GARP) Atlantic Tropical Experiment (GATE), a groundbreaking experiment that opened a world of study to the eastern Atlantic region, is one of the best sources for such composites. A grid of ships off the west African coast, centered at about 8.5°N, 23.5°W within the eastern Atlantic ITCZ, collected the data for the experiment from from mid-August to mid-September 1974. The data included surface observations, pibals, rawinsondes, aircraft, and satellite data.

Reed et al. (1977) composited numerous events to show a distinguishing wind, temperature, moisture, and vorticity structure within easterly waves as they moved westward off the coast. Composited winds exhibited a low-level easterly jet core, centered at about 650hPa and just north of the disturbance center, flowing over a shallower and weaker southwesterly monsoon current.

The mean temperature field revealed an upper-level (150hPa) cool region just south of the disturbance center and a strong low-level temperature gradient to the north separating the cool ocean air from warm Saharan air. The moisture pattern displayed a large low-level region of high relative humidity values to the south of the disturbance that decreases with height and tilts towards the center of the disturbance. The lowest moisture values were found near 850hPa over the Sahara Desert, increasing slightly below and moderately above this level. Absolute vorticity values again displayed a reversal in the gradient just south of the easterly jet core and north of the disturbance center.

The composite structure found in the GATE data has been compared to synoptic wave structure in other regions. Thompson et al. (1978) compared GATE composites of the east Atlantic's ITCZ to the structure of similar disturbances within the ITCZ of the western Pacific. The research determined that the primary differences between the two locations included: 1) the strongest vertical motion at both locations is found within and ahead of the disturbance, though with the western Pacific's maximum at 150hPa, and the east Atlantic's maximum at 700-800hPa; and, 2) a much shallower and more intense low-level convergence region ahead of the disturbances of the eastern Atlantic ITCZ, including two levels of divergence (500-600hPa and 200-300hPa) as opposed to one primary upper tropospheric divergence region found in the western Pacific ITCZ.

Reed et al. (1977) further noted differences in wave structure over land versus over the ocean. Wavelengths over the ocean were about 500km shorter than over land. Vorticity values were also greater at all levels over the oceans. Additionally, waves over the ocean showed a less positive NE/SW tilt of the horizontal wave axis, weakening the momentum flux.

Another method of comparison included gridded analysis such as ECMWF. Druyan et al. (1997) undertook more of a land-bound study on a day to day basis and compared the output to a particular surface station. This type of comparison is important in order to verify model output. If in situ observations from a station remain adequately close to model output, higher confidence may be placed in future model output. Niamey (13°N, 2°E) station data, in southwest Niger, was the focus of a study in which station data updated the numerical model every 6 hours at two separate resolutions, 2° X 2.5° and 4° X 5°. Utilizing July to August data revealed a structure of vertical motion and divergence fields, though the relationship between the two variables did not always correlate. For example, low-level convergence did not always yield mid-level upward vertical motion patterns above the region. Previous studies of African waves indicated the level of maximum vertical velocity exists near 700hPa. The Druyan et al. (1997) study revealed a maximum closer to 500hPa and indicated that not all rainfall activity coincides with the strongest values of uplift. This discrepancy may be due to either daily moisture variability across the region or the ability to distinguish mesoscale convective activity from the broad-scale patterns.

One of the more recent analysis datasets, such as the ECMWF, is the NCEP/NCAR Reanalysis Project. This particular program has two unique characteristics distinguishing it from previous programs at the time of its development. First, the length of the period covered (1957-1996) contains what is believed to be 40 years of the most reliable data available. Second, this numerical model utilizes an extremely comprehensive observational database that incorporates most of the various forms of atmospheric data collection during the period (Kalnay et al., 1996). Most importantly, this process provides a consistent analysis procedure over previously run data and future input. Future

data sources, such as those from newly developed satellite sensors, are scheduled to be assimilated accordingly.

Satellite data are another important analysis tool. OLR and precipitable water vapor can be helpful in determining regions of active weather and high moisture values. All atmospheric disturbances, however, do not necessarily yield clouds and convection. Most disturbances do show at least some slight anomaly in one field or another. Independently moving areas of high (positive) PW anomalies, found in the TOVS PW satellite data, and their structure are at the focus of this study.

Mackey (1996) studied such positive anomalies around the tropics using three to eight-day filtered PW estimates from TOVS operational satellite observations for 24 three-month seasons. The nonlinear filter used, described by Murakami (1980), operates on the time series of PW at each grid point separately. The filter does not introduce significant signals from the frequencies outside the three to eight-day spectrum and, therefore, the signal produced is believed to be real. Others whom have applied such a time filter to remove synoptic scale information include work by Strager (1989) and Winton (1991).

Figure 1 displays seven particular locations isolated as significant source regions in which the three to eight-day spectrum showed coherent propagation characteristics of positive anomalies in the PW field. The strongest and most consistent filtered signal is found across North Africa, particularly just northwest of the Gulf of Guinea near 12.5°N, over the Sahel Desert, and during the MAM season, particularly in 1988. This season happens to be a period where easterly waves are at a minimum. The anomalies appear to propagate from this region year-round in an *eastward* direction near 7 m/sec. This appears unique since all of the aforementioned studies dealt primarily with system and

disturbances that propagate to the west off the African coast. The PW anomalies exhibit a zonal wavelength of 2,500-3,000 km, unlike the typical *westward* propagating disturbances observed in the region in OLR and in situ observations. Analysis of the filtered data reveals numerous and cyclic cases of positive anomaly development and eastward propagation northwest of the Gulf of Guinea and across the Sahel into east central Africa (near 20°E). This may lead one to believe that the area is a source region for some sort of disturbances associated with the positive PW anomalies unlike those previously found to propagate to the west. Any conclusive interaction between eastward propagating PW anomalies and westward propagating disturbances, such as easterly waves, is unlikely due to minimal development during the season under study.

The decades of research accomplished in and around western Africa have still left many questions unanswered. Especially at the synoptic scale, the evolution and structure of the tropical atmosphere has been an intensely studied topic. As seen in the above mentioned studies, however, much more is known about the origin and structure of westward propagating disturbances found in both composite analysis and numerical model analysis. A strong low and mid level temperature, wind, moisture, and vorticity structure has been determined by a number of methods for westward propagating disturbances. Very little, however, has been found regarding any eastward propagating disturbances significantly far (8°N to 18°N) off the equator, especially in the PW field. This study provides insight into eastward propagating PW anomalies and the atmospheric fields that exhibit unexpected traits for the region in which they exist.

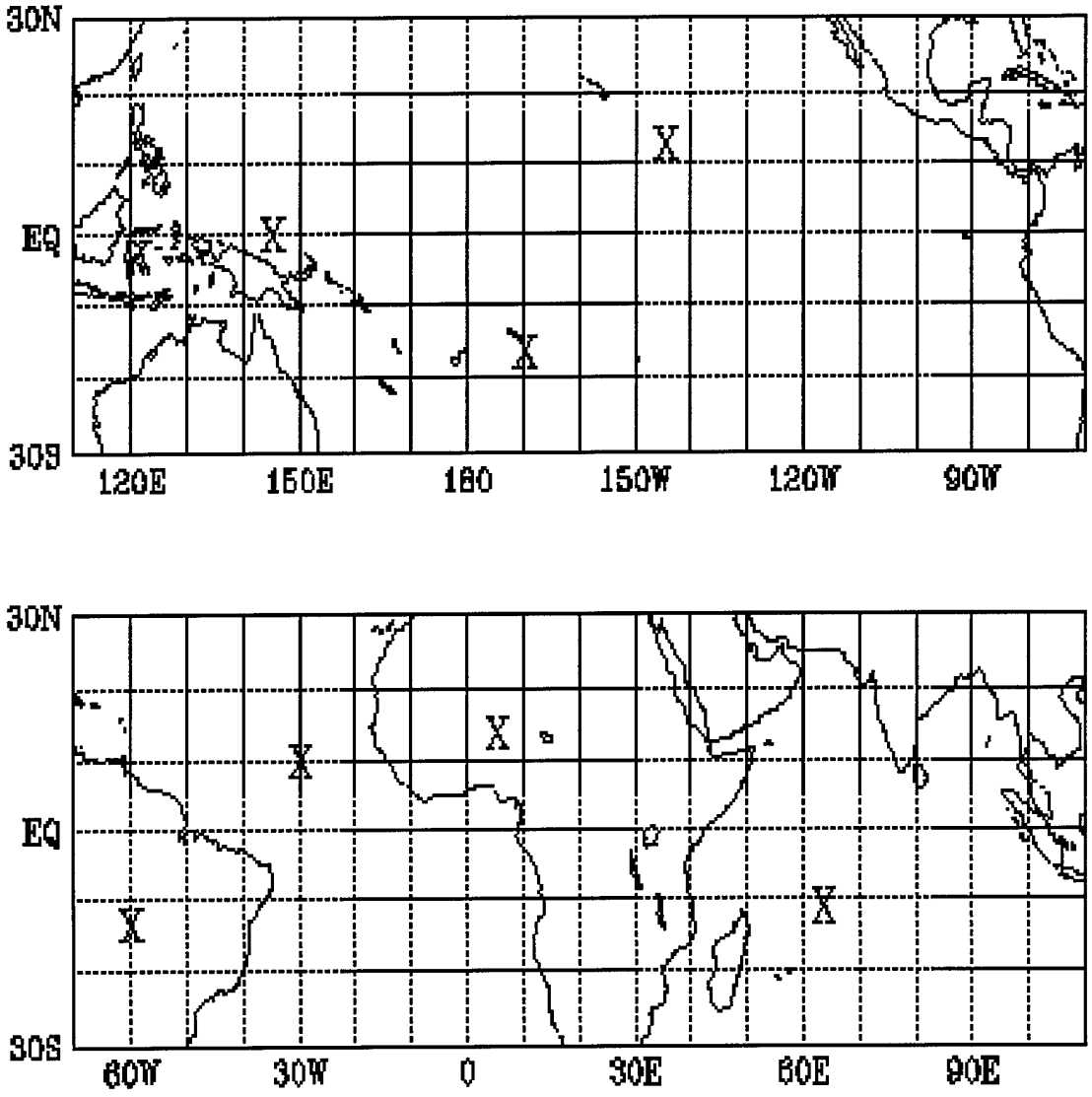

FIG. 1. *Axis*, or regional center, locations of source regions for filtered TOVS-generated positive PW anomalies.

CHAPTER III

APPROACH

A. OBJECTIVES

The primary objective of this research is to document the evolution and structure of eastward propagating positive PW anomalies that organize near the northwestern Gulf of Guinea (0°W-10°W and 8°N-18°N) and maintain their identity into eastern Africa (approx. 20°E-30°E). Daily grids and three- to eight-day filtered TOVS PW imagery are used to locate the anomalies. NCEP/NCAR Reanalysis data provides the model output to explain their propagation characteristics and mechanisms within the actual wind fields and to determine their evolution and structure in other various atmospheric fields. This involves reducing horizontal wind shear with increasing latitude by removing the mean of the longitudinal (U) wind component at each 2.5° latitude band and compositing the background anomalous flow of specific cases over one three-month season. The resulting wind/flow pattern and propagation characteristics are analyzed and compared to theorized tropical waves (Matsuno, 1966).

The second objective involves analyzing various fields in order to determine how they interact with the anomalies. These fields include computed omega, specific humidity, potential vorticity and temperature at 850hPa, 500hPa, and 250hPa. Variables are statistically analyzed at two resolutions and compared to the seasonal and geographic variations across the region of propagation in order to develop an empirical model for the anomalies. This

model provides a simple step by step visual representation of a PW anomaly evolution.

The geographic regime of anomaly propagation is roughly 30° (latitude) by 60° (longitude). Isolating atmospheric variables over this region allows for a more localized statistical analysis.

B. DATA PRODUCTS

The PW dataset, as described by Mackey (1996), was extracted from a much larger dataset covering 24 three-month seasons within the years 1979-1992. The dataset was composed of a combination of TOVS brightness temperature channels which were processed through a regression algorithm, established by Yin (1994), converting it to PW values. The resulting dataset was then verified against collocated raobs collected from around the tropics throughout the calibration period, specifically 1982-1984 and 1987-1990. The resulting strong correlation of the data with that of the raobs provided a reliable source of PW data; the algorithm captures about 73% of the raob PW variance throughout the tropics and about 40% of the local synoptic variance. Schroeder and McGuirk (1996) have subsequently developed a more accurate gridded dataset (2.5° x 2.5°) around the globe from 30°N to 30°S starting at 180°, which was not available for this study.

To avoid the inherent problems of missing data, this study focuses on those seasonal periods and locations with little or no missing data. Prior research by Mackey (1996) shows one of the best three-month periods and locations for strong PW anomalies to be northwest of the Gulf of Guinea (at about 12.5°N) during MAM 1988.

NCEP/NCAR Reanalysis Data incorporates data from an international spectrum of sources. Geophysical Fluid Dynamics Laboratory for ocean reanalysis, the United Kingdom Meteorological Office for SST and global ice data, Japanese Meteorological Agency included special rawinsondes and cloud-track winds and the ECMWF are only a few of the sources from which the entire reanalysis database was compiled (Kalnay et al., 1996).

The model data was downloaded from standard 8mm tapes. John Nielsen-Gammon, of Texas A&M University, developed a program to access grids from the reanalysis' sigma coordinate data and interpolate it into pressure coordinates. Fields are constructed and displayed using GEMPAK analysis software. Additionally, the data have been further divided into separate files of isolated variables for image looping over required geographical regimes. The temperature, specific humidity, potential vorticity, wind components and computed omega values are available at the 850hPa, 500hPa, and 250hPa pressure levels.

C. ANALYSIS STRATEGY

To determine the locations of significant synoptic scale activity within the TOVS PW data, Mackey (1996) began by observing the normal tropical convergence zones. This was accomplished by noting the axis of most frequent 3 to 8 day filtered PW relative maximum and isolating strong data signals within their specific regions through local filtering. Though the filter had its advantages and disadvantages, the signal was determined by Mackey to be strong enough to indicate seasonal and annual cyclic variations within the synoptic scale. Once the regions' "focal point" location was determined, Mackey considered four

factors: location of activity, movement of the nearby tropical convergence zones, size of the region, and regional climatological characteristics. It is important to note that the grid average of PW varied significantly during the 12 years of Mackey's study. PW values varied from a low of approximately 2.6 cm around early 1985, partially due to bad data products, to a high of approximately 3.8 cm in early 1986. During the period of this study, grid average PW values remained relatively constant around 3.3 cm (Fig. 2.).

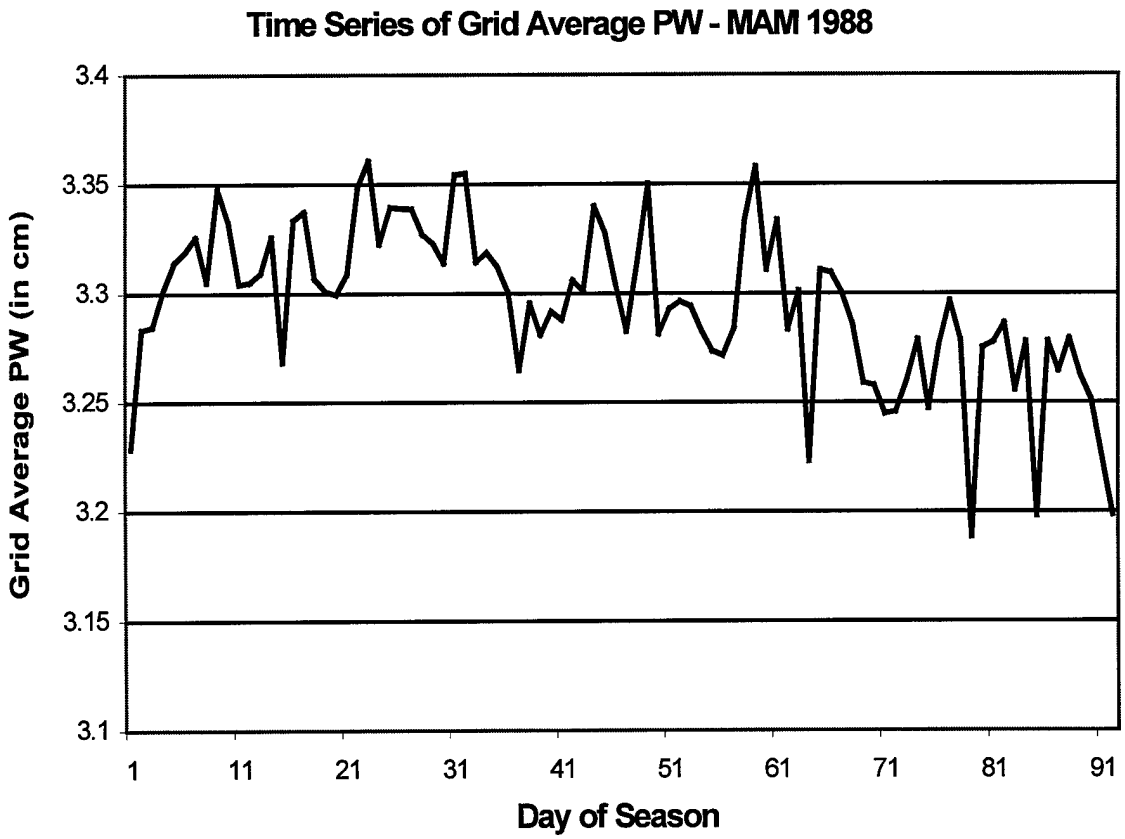

FIG. 2. Time series grid average PW from 30°N to 30°S for MAM 1988 in cm.

Seven positive PW anomaly cases are chosen from the TOVS PW data within the MAM 1988 season. Each case is chosen by way of simply looping and reviewing time filtered and unfiltered PW data throughout the period and finding those positive synoptic anomalies that carried the strongest and most coherent signal. The duration of the isolated signals, on average, appeared to be about five days. Prior to and immediately after this five-day period, both the time-filtered and unfiltered PW signal appeared either weak and/or incoherent compared to other high PW anomalies (propagating or stationary). Once a five-day period was chosen, referred to as the disturbance's "life cycle", the period is broken down into three specific days: initiation day (day 1), peak day (day 3), and dissipating day (day 5). The results are discussed focusing on each of these three days. In some cases, especially in the actual wind field, the days prior to the initiation day are also necessary to discuss. Samples of the filtered and unfiltered PW frames are provided in future chapters where applicable.

The actual wind field at each available level is composited using all applicable cases of the case study. Applicable cases are those that retain a strong coherent PW signal and follow similar paths of propagation. Composites are also made of the background actual wind field with the mean U component at each 2.5° latitude band removed. This reduces wind shear with increasing latitude, especially at the upper levels. Results of these composites allow for a mean structure to be determined.

The NCEP/NCAR analysis are verified against known large scale atmospheric features by reviewing the 92-day (MAM) mean state of the atmospheric variables at each level. Finding these large scale features provides confidence in the data when applied to the PW anomaly analysis. The mean

values also show maximums and minimums within the field of a particular atmospheric field.

Interaction with, and structure of, atmospheric variables is accomplished by first producing a descriptive statistical analysis of the variables at each level. Localized statistics for the region of anomaly propagation is used to determine deviations from the mean state. Variables found statistically significant (α approximately 0.90) when correlated with TOVS PW values are also discussed in relation to the PW anomalies and actual wind field structure. These findings allow for the development of a simplistic empirical model of the evolution and structure of the TOVS PW anomalies that develop north of equatorial Africa.

CHAPTER IV

CASE STUDY RESULTS

A. WIND FIELD COMPOSITE ANALYSIS RESULTS

The seven cases chosen for this case study each carried some distinct and some shared characteristics throughout their 5-day duration. Table 1 provides a list of case initiation and dissipation dates for each of the anomalies involved in this case study. Each anomaly may have existed up to one day prior to or after the listed dates, though with a much weaker and incoherent signal.

Table. 1. Case initiation and dissipation dates for positive PW anomalies.

Case #	Initiation Date	Dissipation Date
1	3 March 1988	7 March 1988
2	8 March 1988	12 March 1988
3*	24 March 1988	28 March 1988
4	14 April 1988	18 April 1988
5	23 April 1988	27 April 1988
6	12 May 1988	16 May 1988
7	25 May 1988	29 May 1988

* outlier case

The centers of six of the seven cases were first noted as isolated and coherent anomalies within the same 10° X 10° generation region northwest of the Gulf of Guinea (8°N to 18°N and 10°W to 0°). The remaining anomaly (case #3) developed about 5° to the southeast of this region, near 10°N, 5°E. This particular case is subsequently ignored in both wind field composites due to the isolation of its development location. Figure 3 displays the local grid region in which the anomalies develop, propagate and dissipate over the duration of approximately five days. The geographic center of the filtered PW signal is used to mark the center of the entire anomaly, most of which developed north of 10°N.

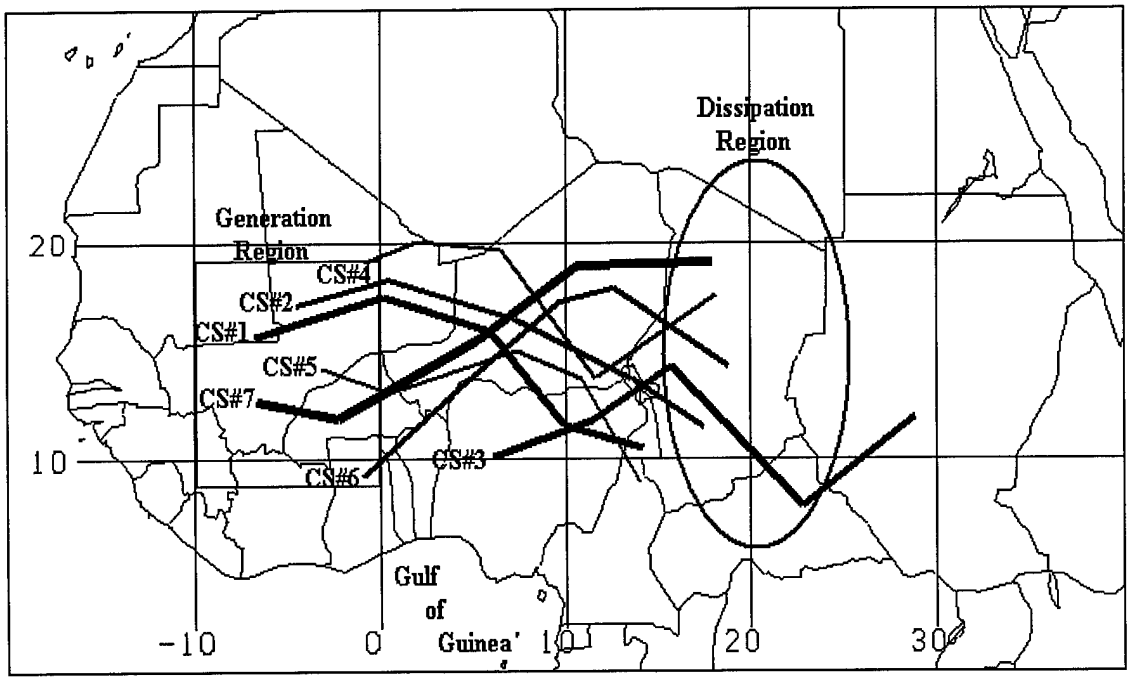

FIG. 3. Local grid region in which seven cases initiated, propagated and dissipated during MAM 1988. Approximate initiation and dissipation regions are marked. Individual cases are annotated by a 'CS#' followed by their designated number in order of appearance.

Throughout the 5-day period, most of the anomalies remained within the same 10° latitudinal band as they propagated east. The apparent "wobble" in the course taken by each system is due mostly to broadening of the signal in time. Instead of a perfectly symmetric and coherent filtered and unfiltered PW signal, the signal occasionally becomes latitudinally elongated, making it necessary to use both the filtered and unfiltered signatures to approximate the geographic center. Additionally, through the course of the three months of data, the strength and coherence of the PW signal, both filtered and unfiltered, varies only slightly as the season progressed.

Analysis of two-dimensional flow at several levels allows for an understanding of the mean flow and its affects on advection. This study's local grid area spans from the equator into the southernmost reaches of the midlatitudes (30°N). Significant variability in latitude yields two extreme mean wind characteristics across the region. Near 30°N, during the MAM season, the southern influence of the midlatitude jet can occasionally dip into the region and provide strong westerlies across the northern Sahara. At this latitude, upper level flow is strongly influenced by its geostrophic components, including pressure gradients and the coriolis parameter.

Closer to the equator, however, upper level flow is mostly under the influence of pressure gradients and virtually no coriolis force. Tropical upper level temperature gradients are much more relaxed than those of the mid-latitudes, reducing the development of cold core cyclones near the equator. Intense pressure gradients, therefore, are seldom found here. Weak pressure gradients then allows for generally weak flow across the region and, in turn, provide the second of the two extremes in the mean wind field over the local grid region.

The latitudinal extent of the anomalies alone can provide significant variability in wind flow across any one case. The PW signature, by peak day, appeared to span nearly 20° of latitude, placing the northern portion within strong westerlies and the southern portion within relatively calm conditions.

To remove some of this latitudinal shear, the mean value of the U component (longitudinal) is computed, subtracted from the U components of applicable cases, and the resultant winds analyzed at 2.5° intervals. Composites of six of these resultants are then developed. Removing this mean flow within the composites reveals the local anomalous wind pattern within this background flow. The representation of this anomalous wind field is furthermore referred to as the "reduced-shear" field.

Though each PW anomaly case spanned approximately five days, the reduced-shear field for two days prior to each initiation day is also necessary for review since the composite studies revealed a northeasterly surge of moisture originating on a particular day. Studying this background flow during the days prior provides insight into understanding why PW anomaly initiation takes place.

Figure 4 shows composites of the actual winds for six cases at 250hPa, 500hPa and 850hPa for *two days prior* to initiation day. Important features found within the six case composite may include closed circulations, troughs, ridges and advective wind patterns. Anomalous onshore flow, too, may provide moisture advection from the deeper tropics or from convective processes into the PW anomaly domain.

At 250hPa, a well-defined positively tilted trough, extending south to at least 10°N, is approaching from the west with strong west southwest flow ahead of it. Winds near the coast of northwest the Gulf of Guinea are offshore, inhibiting moisture advection from the deeper tropics. Most of the cases

revealed nearly mean PW values or negative PW anomalies two days prior to each of the case initiation days within the generation region.

At 500hPa, the trough is hardly distinguishable from the southwest flow beneath the 250hPa trough. Here, too, the coastal winds near the northwest Gulf of Guinea are offshore. Neither of the two upper level composites reveal any northward advection from the Gulf at two days prior to initiation day.

Near the lowest level, 850hPa, flow is very weak and almost non-directional. This is found true throughout the entire composite series in both the actual wind field and the background flow. 850hPa appears to offer no significant onshore advective pattern at any time and is considered unimportant regarding horizontal advection during this study. Figure 4c. is one example of this non-advecting field. No further 850hPa wind or reduced-shear field diagrams are presented due to this lack of structure at this level.

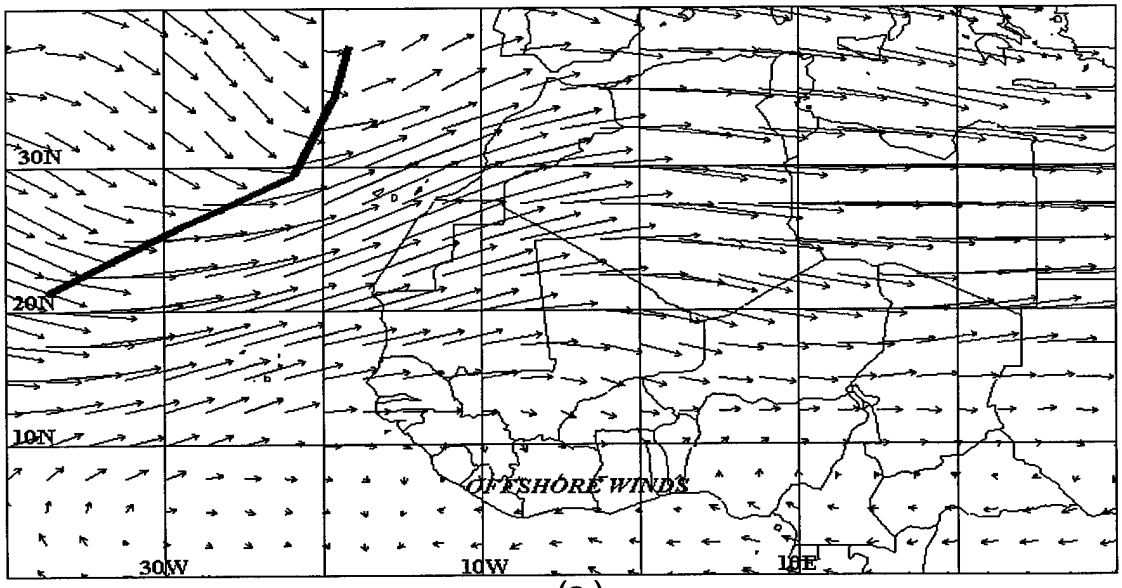

(a.)

Fig. 4a. Six case composite of the 250hPa actual wind field for two days prior to initiation day. 5° long wind arrow approximately 15 m/sec. Heavy line indicates trough axis.

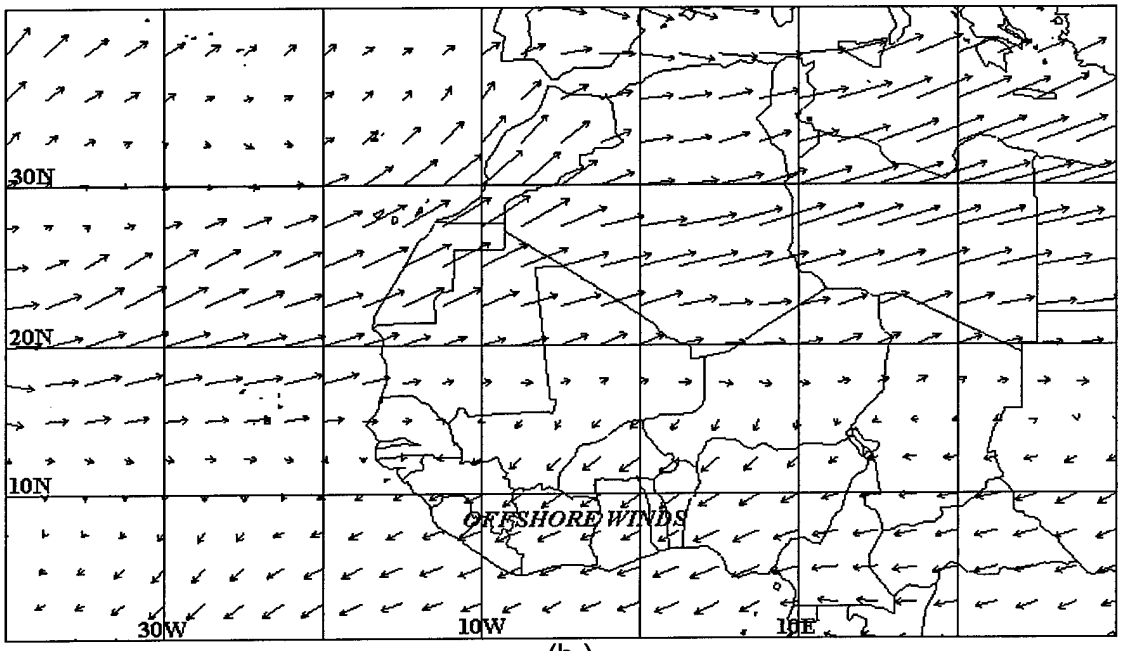

(b.)

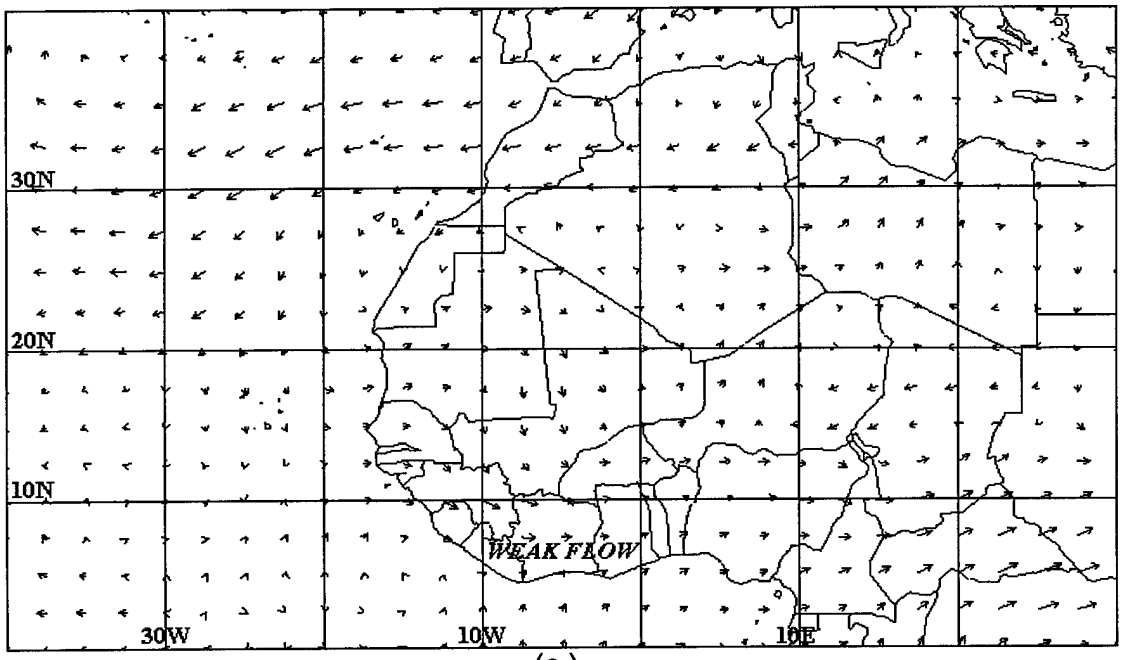

(c.)

Fig.4. Six case composites of the b.) 500hPa and, c.) 850hPa actual wind field for two days prior to initiation day. 5° long wind arrow approximately 15 m/sec.

Table 2 provides a list of the approximate mean latitudinal winds removed (here at every 10°) from the actual U (zonal) components to produce the reduced shear flow. Significant case days include two days prior to initiation day through dissipation day. Positive values indicate eastward flow.

Figure 5 is a graphical depiction of the zonal wind values removed for each 10° latitude band at both 250hPa and 500hPa. Bar values to the right of the zero line indicates easterlies, left indicates westerlies. The bottom of the four bars at each latitude is two days prior, increasing in time to the top bar, or dissipation day.

Table 2. List of mean U (zonal) components subtracted from actual flow, here at 10° increments, to display reduced shear flow. U component wind values are measured in m/sec.

Case Day	Level	40N	30N	20N	10N	Equator
Initiation Day-2	250	15.5	34	26	6	-4.5
	500	7	14	11	-4	-5
Initiation Day	250	16	33	24	4	-3
	500	7	14	11	-3.5	-7
Peak Day	250	15.5	35	25	4	-4
	500	8	14.5	11	-5	-6.5
Dissipation. Day	250	16	33	23	2.5	-2.5
	500	5.5	13	9	-4	-7.5

Mean Zonal Winds Removed for Reduced Shear Composites

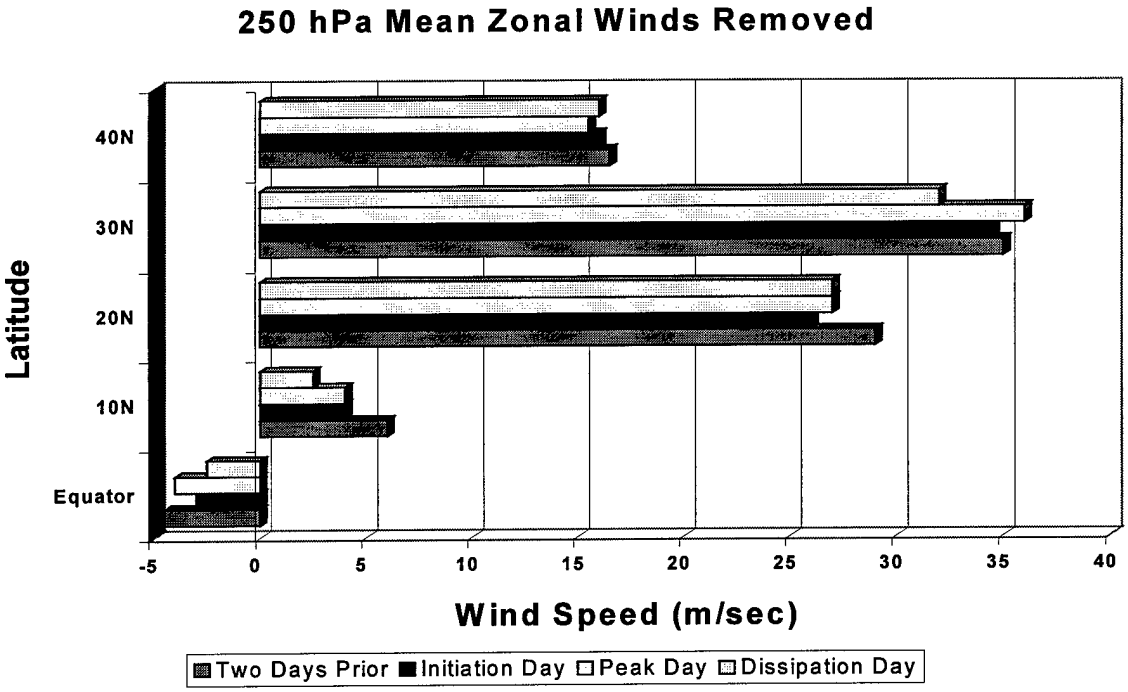

(a.)

(b.)

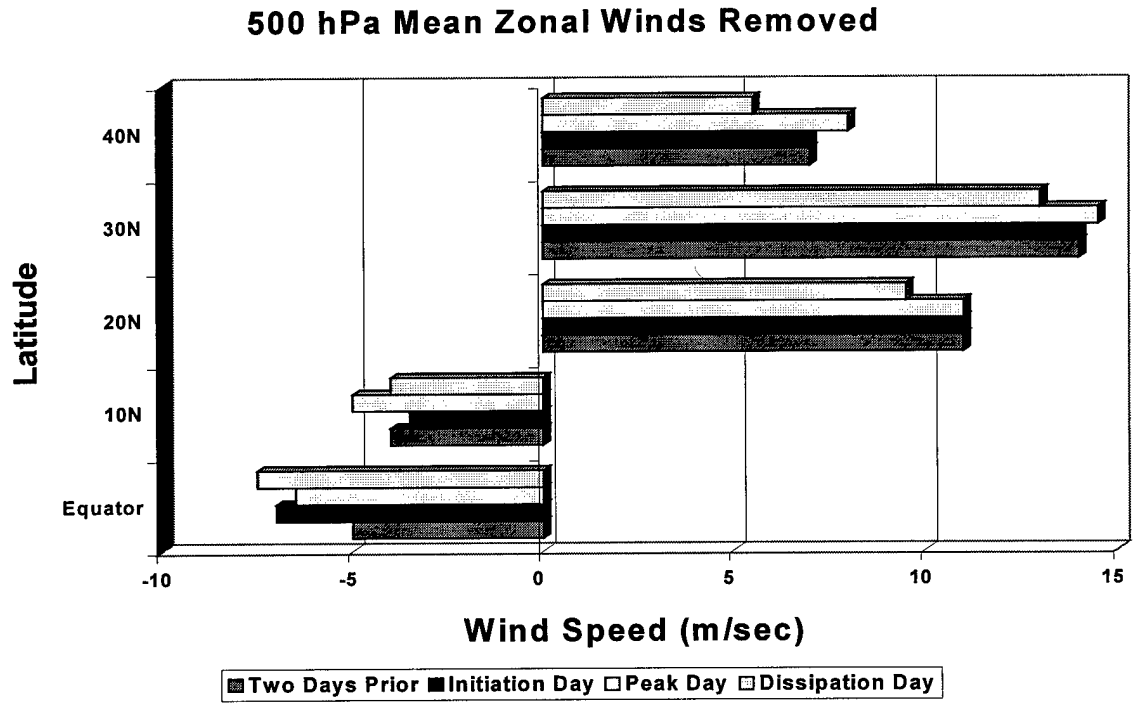

Fig. 5. Graphical depiction of the mean zonal winds removed for reduced shear compositing at a.) 250hPa and, b.) 500hPa.

The 250hPa reduced shear flow two days prior to initiation day reveals a closed cyclone and anticyclone system, approximately 30° (3,000km) apart, located at about 20°N. The same is also true at 500hPa, except the anticyclone in not yet evident. A weak region of diverging winds, however, is centered beneath the 250hPa anticyclone.

Figure 6 shows the two levels and the southwesterly flow between the two circulations. The northerly advective flow remains about the same as the actual wind composites since the V wind component is not adjusted. Decreasing the zonal component yields a more poleward vector in the winds field, and increasing the zonal component lessens the poleward vector. Latitudinal advection rates, therefore, remains unchanged between the actual wind field and the reduced shear wind field.

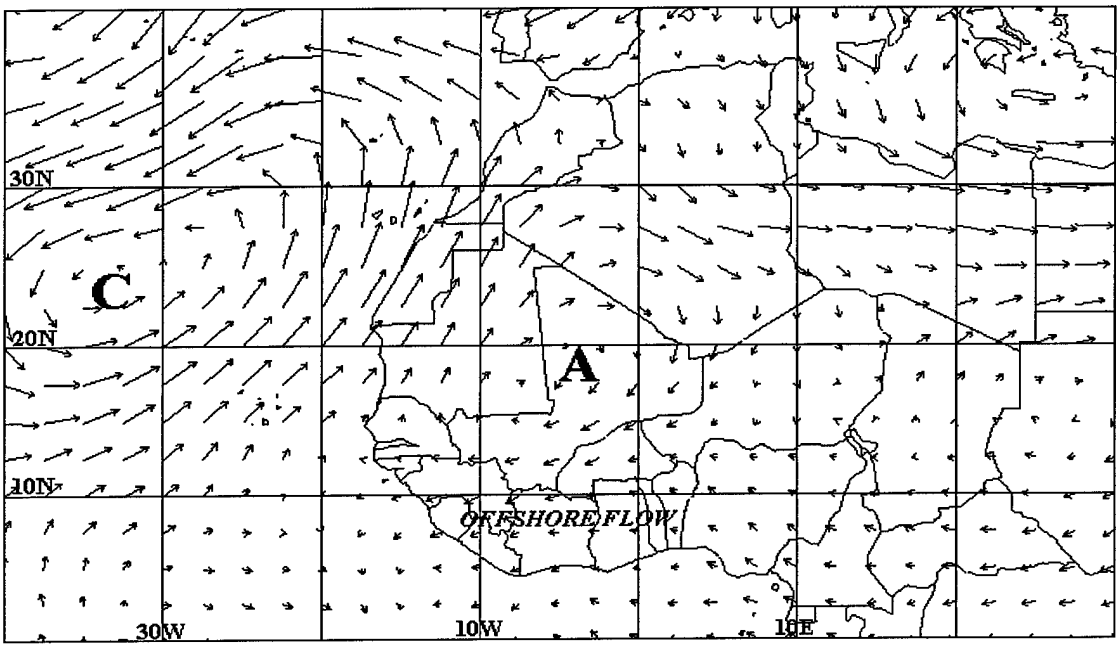

(a.)

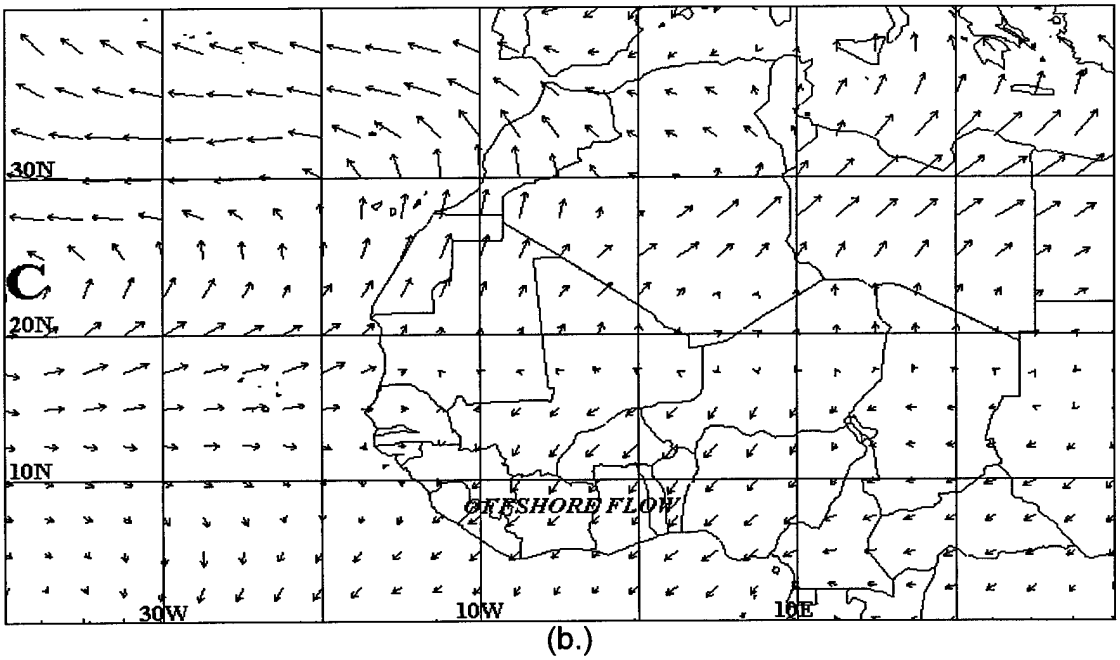

(b.)

Fig. 6. Six case composites of the a.) 250hPa and, b.) 500hPa reduced-shear field (see text) for two days prior to initiation day. 5° long wind arrow approximately 15 m/sec.

Near initiation day, a new pattern begins to develop. Figure 7 displays the six case composited actual wind fields at both upper levels. The 250hPa composite reveals the trough has propagated to just west of the west African coastline. The wind pattern ahead of the trough has increased its southerly component and become more southwestward. Additionally, the trough has developed further to the south.

The coastal flow has turned onshore across the entire extent of the Gulf of Guinea northern coastline, with southerly flow almost to the equator. Higher moisture values and associated variables near the coastline, due to convective enhancement or advected higher mean values from the deeper tropics, could be advected northward and into the source region of the TOVS positive PW anomalies.

At 500hPa, the trough is much more evident and the flow has become increasingly similar to that of the 250hPa level, though the trough axis is slightly more vertical. The flow near the shoreline shows no significant northerly advection with relation to the shoreline, compared to two days prior and the 250hPa flow on initiation day.

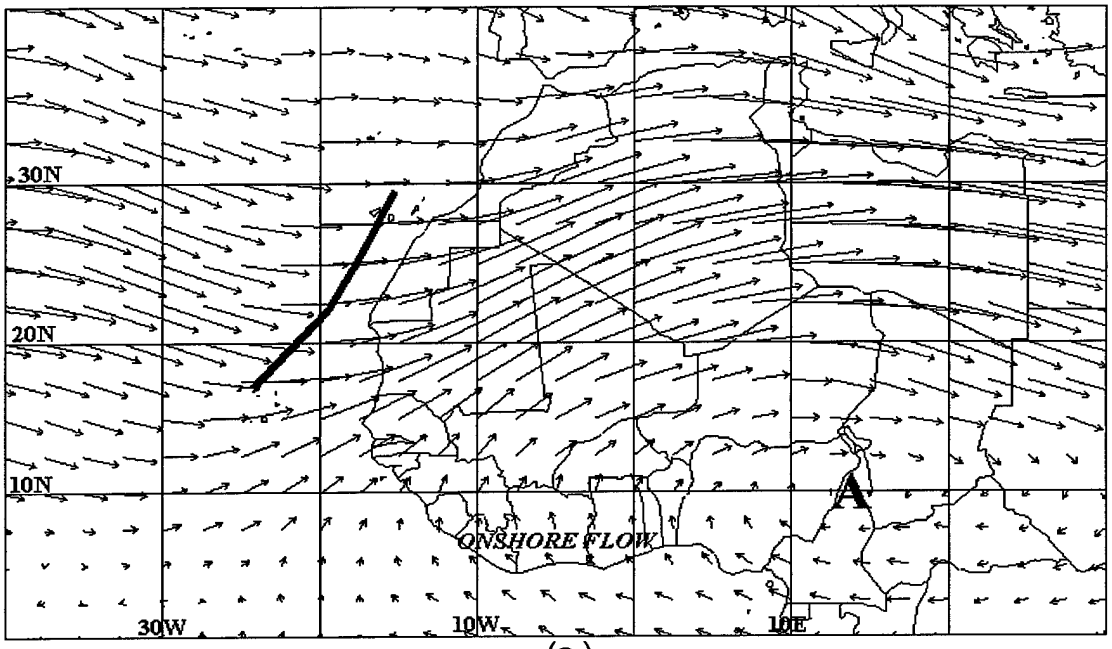

(a.)

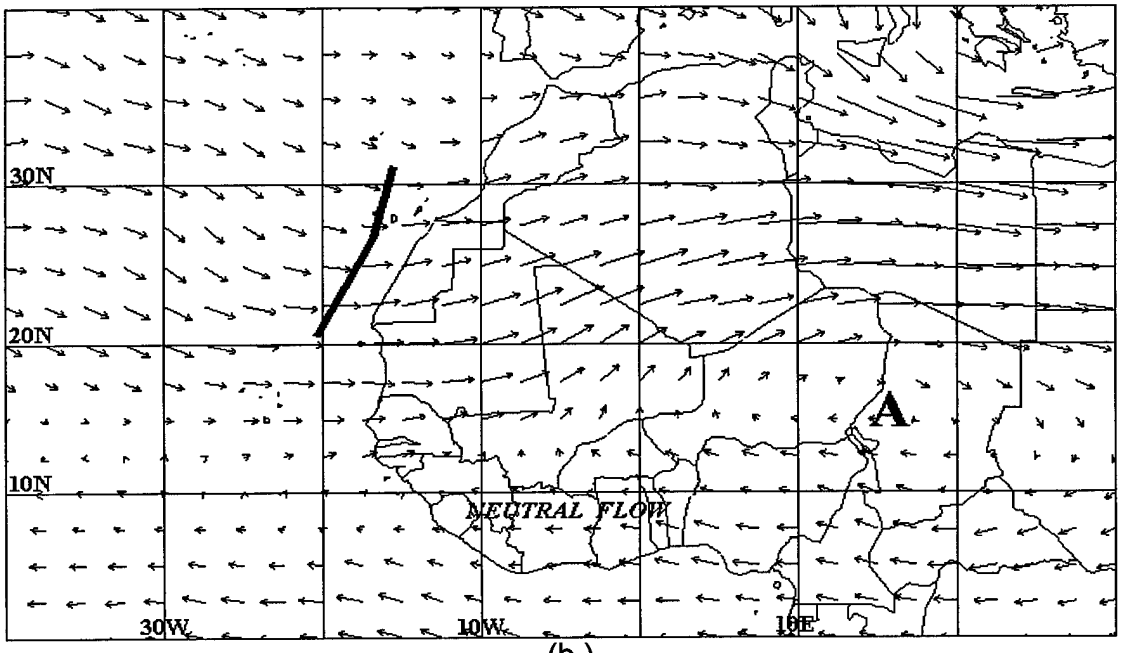

(b.)

Fig. 7. Six case composites of the a.) 250hPa and, b.) 500hPa actual wind field for initiation day. 5° long wind arrow approximately 15 m/sec. Heavy line indicates trough axis.

Compositing the initiation day reduced-shear flow reveals the same cyclone - anticyclone pattern as those found two days prior to initiation day at 250hPa. Figure 8 displays the composite reduced-shear fields for initiation day. The cyclone has now moved to within 5° of the west African coastline, and has retained a significant cusp-like structure between itself and the associated anticyclone found over central Niger. The flow near the Gulf of Guinea coastline has again turned onshore, providing support for moisture advection. The same pattern has become evident at 500hPa as well, though with weaker flow. The cyclone at this level appears slightly further east than at 250hPa.

The southwestern extent of the structure at both levels allows for higher tropical moisture values to be readily tapped. Moisture that may not normally be associated with the generation grid area becomes available and may advect into the region. Even at only 7 m/sec, anomalous moisture could advect nearly 1,200 km during a 48-hour period, easily over 10° of latitude.

Additional moisture may originate from a number of sources. Mean moisture values at the upper levels, much higher over the Gulf of Guinea and near the Atlantic ITCZ, may be advected into the PW anomaly. Values as high as 0.28 g/kg at 250hPa and 2.25 g/kg at 500hPa represent the seasonal mean for the region. Additionally, this region's current low convective activity, such as MCS development (Devlin, 1995), increases throughout the season. Convection and/or enhanced vertical motion may also contribute to the substantial moisture abundance to the upper levels. The convection itself, however, may not be a byproduct of the anomalous wind field. Rather, increased southerly flow from the cusp-like structrue causing the anomalies may increase moisture advection into the convective region enhancing the convection and further moistening the upper levels.

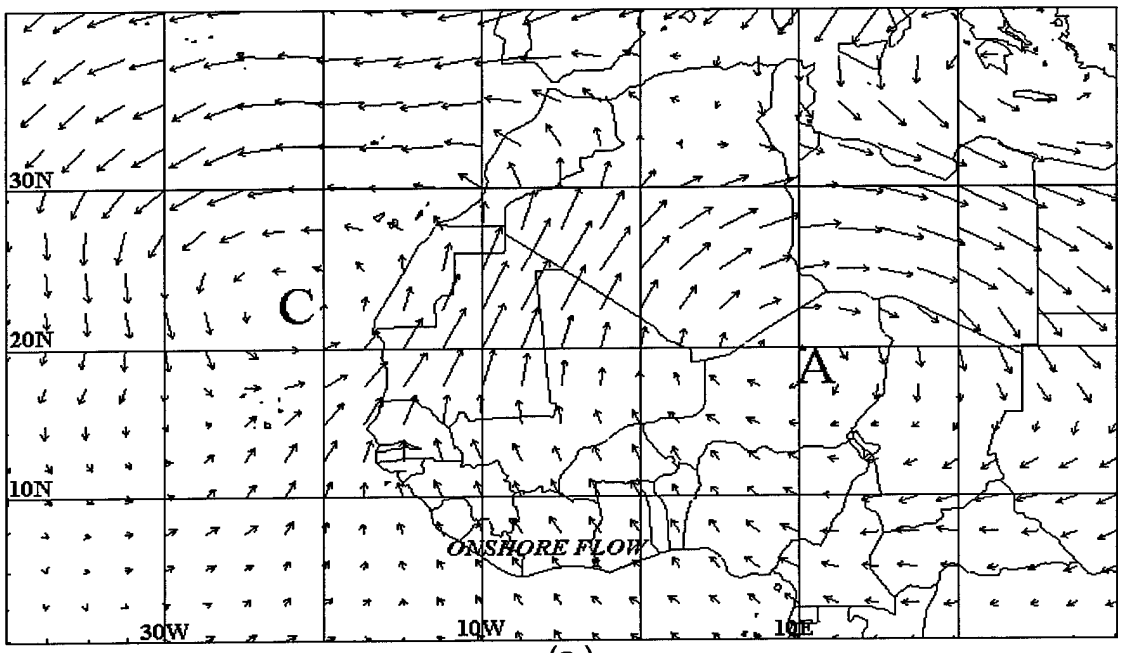

(a.)

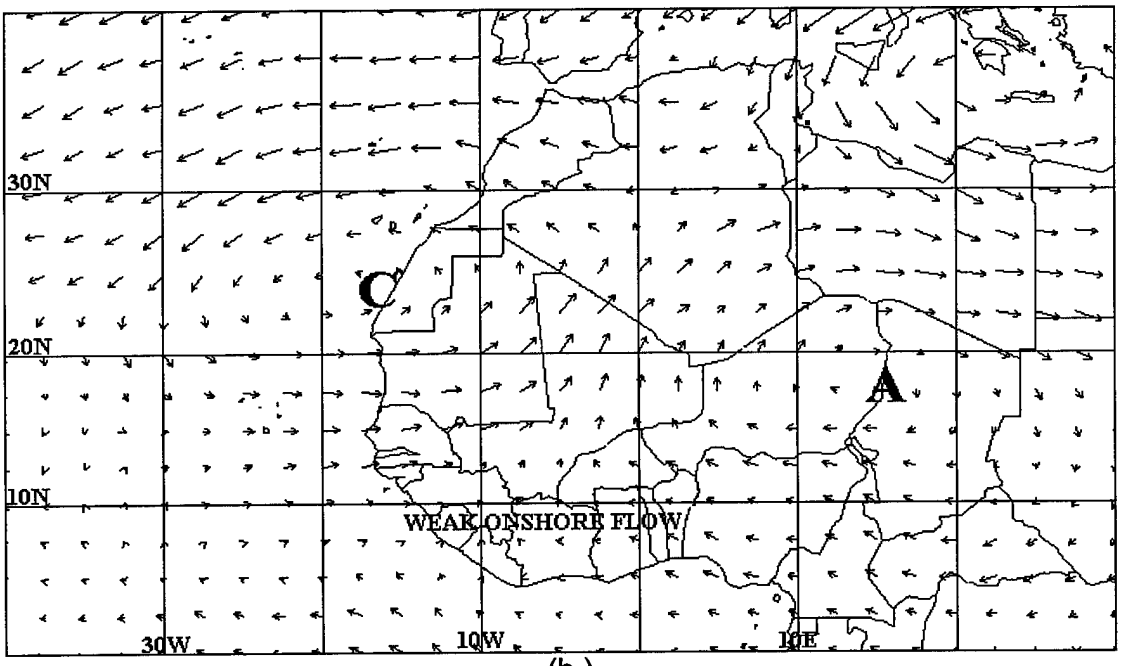

(b.)

Fig. 8. Six case composites of the a.) 250hPa and, b.) 500hPa reduced-shear field for initiation day. 5° long wind arrow approximately 15 m/sec.

These higher moisture values may help explain the positive PW anomalies detected by the TOVS sensor. Since the cusp-like structure advects moisture into the region at a synoptic scale, filtering, such as the work accomplished by Mackey (1996), can locate a positive PW signal within the PW field.

Two days later, around peak day, the trough at both 250hPa and 500hPa moves just east of 0° and begins to pull back towards the north. Figure 9 displays the composite actual wind fields for peak day. The winds ahead of the trough have turned back more eastward, and the onshore flow near the north coast of the Gulf of Guinea has weakened at 250hPa and become offshore at 500hPa. This indicates a significant lessening of moisture advection into the PW anomaly from the higher moisture values to the south.

Composites of the reduced-shear fields on peak day reveal similar results to that of the actual wind fields. Figure 10 displays the composite reduced-shear field for peak day. The cyclone at both 250hPa and 500hPa begins to pull back towards the north. The 500hPa cyclone, however, remains about 4° further south than that of the 250hPa. Flow near the northern coast of the Gulf of Guinea has weakened significantly at 250hPa, and become offshore at 500hPa. Additionally, the appearance of weaker flow and a tighter circulation around the cyclone indicates the system has filled slightly.

Both peak day composites reflect less and less advection out of the Gulf of Guinea and into the PW anomaly. The TOVS filtered and unfiltered, in turn, reflect a degrading signal during the two following days.

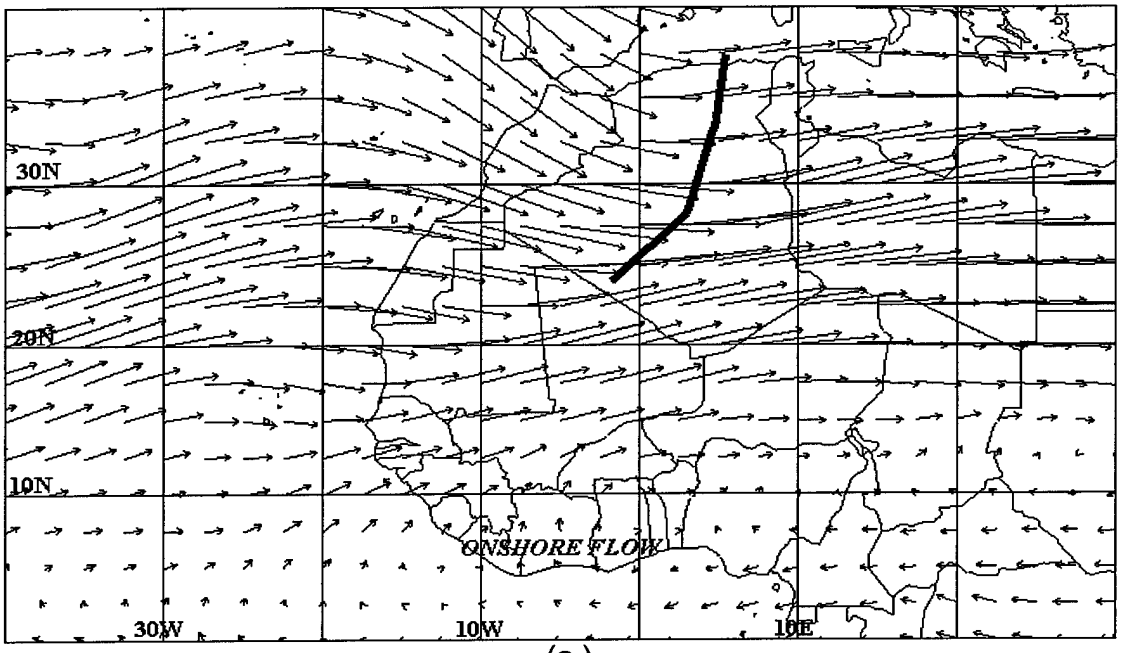

(a.)

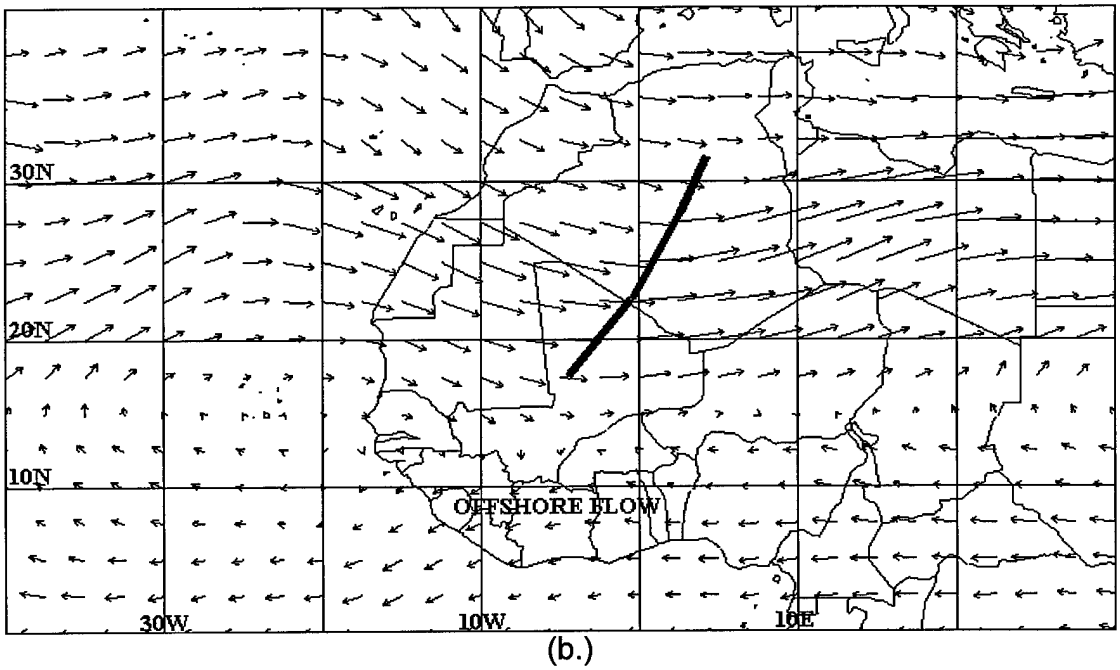

(b.)

Fig. 9. Six case composites of the a.)250hPa and, b.) 500hPa actual wind field for peak day. 5° long wind arrow approximately 15 m/sec. Heavy line indicates trough axis.

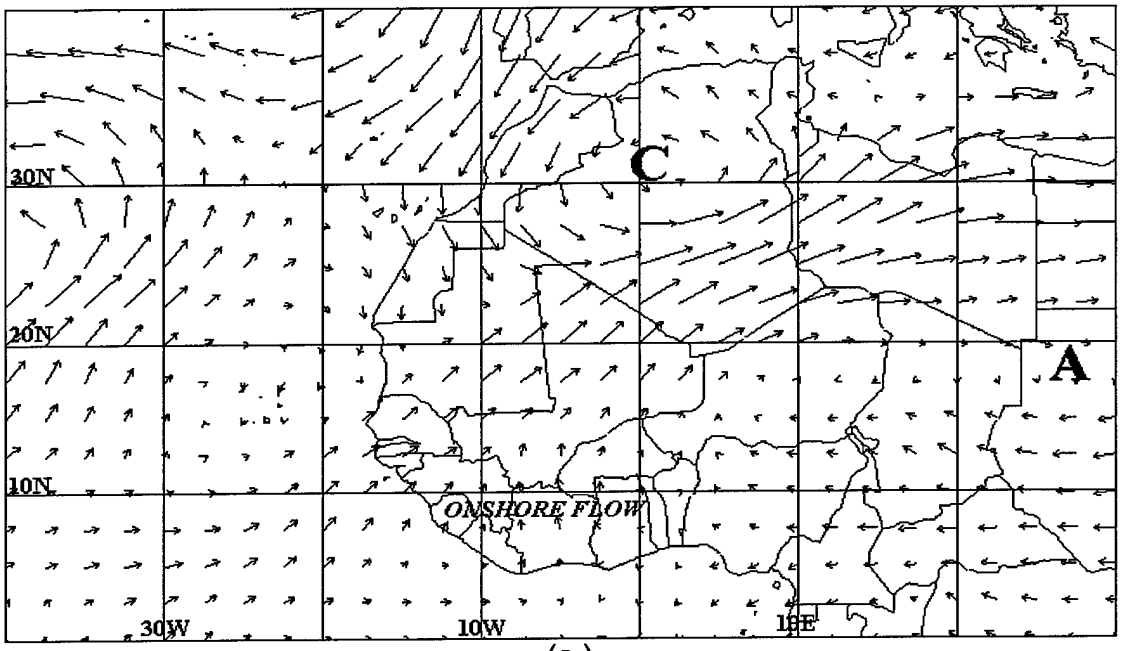

(a.)

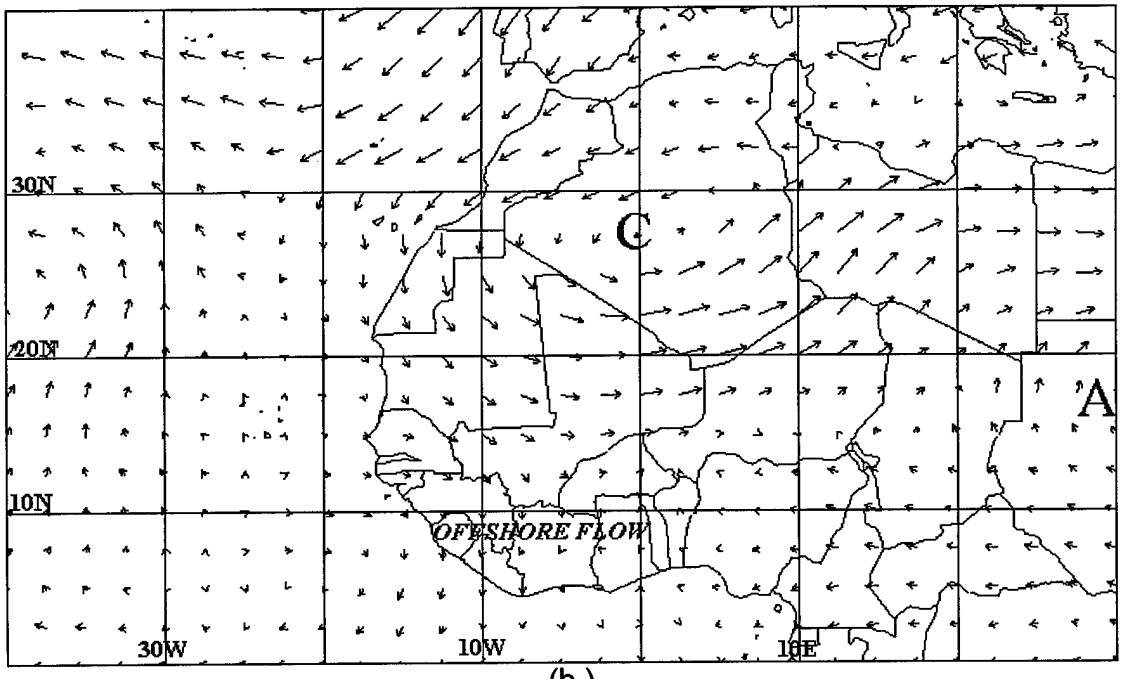

(b.)

Fig. 10. Six case composites of the a.) 250hPa and b.) 500hPa reduced-shear field for peak day. 5° long wind arrow approximately 15 m/sec.

Composites of the actual wind field on the fifth day, or dissipation day, provide evidence of continued lack of advective support for the PW anomaly. Figure 11 displays the composite actual wind field for dissipation day. The southern extent of the trough at both 250hPa and 500hPa has propagated north to near 30°N and moved east to about 20°E. The cusp-like feature has moved mostly out of the local grid. Any properties remaining around the PW anomalies themselves are either only remnant or have become indistinguishable from local PW maximums. Flow near the northern coast of the Gulf of Guinea is either neutral or offshore at both levels, with mostly zonal flow across the entire region of anomaly propagation.

Composites of the reduced-shear field yield very similar results, showing the cyclone moving off to the east-northeast, and the anticyclone out of the local grid. Figure 12 displays the composite reduced-shear field for dissipation day. Additionally, the next trough/cyclone system can be found approaching the west African coast near 20°W, 20°N.

In order to provide a clearer view of how the PW field responds to this propagating pattern, including the cusp-like structure, a sample is displayed in Fig. 13. These are samples of unfiltered TOVS-initiated PW frames, including initiation day, peak day, and dissipation day. This particular case (case #5) exhibited one of the strongest and most coherent signals in both the unfiltered and filtered PW field. Notice the beginnings of atmospheric moisture surging north on initiation day, retaining a sound profile on peak day, and all but disappearing on dissipation day.

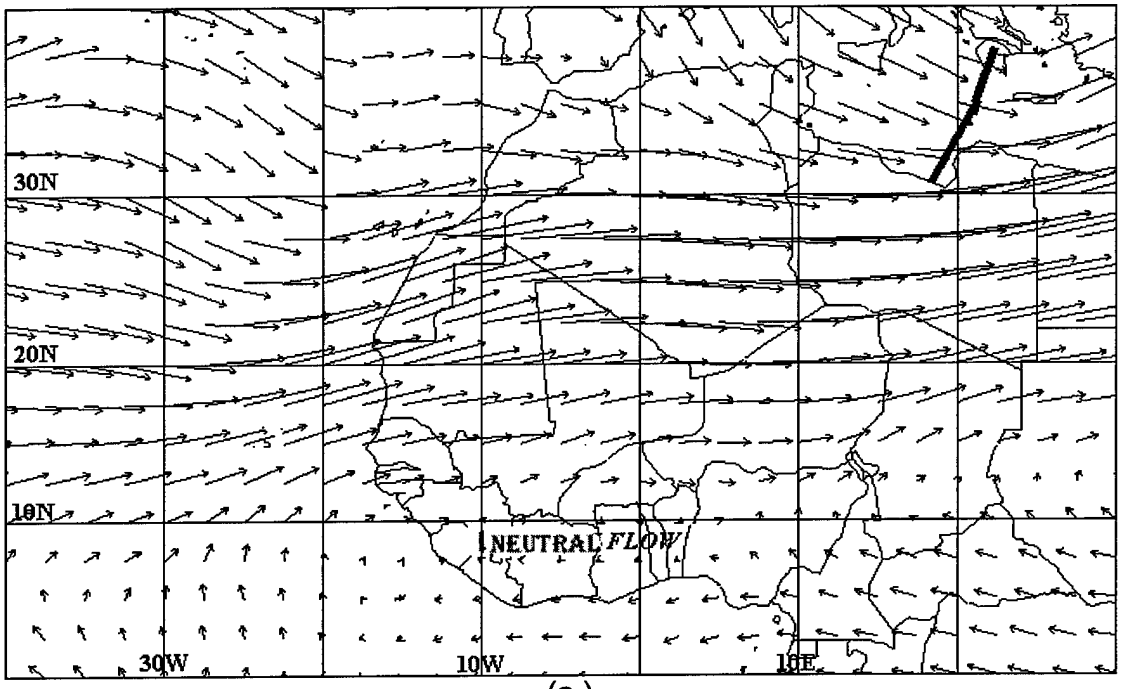

(a.)

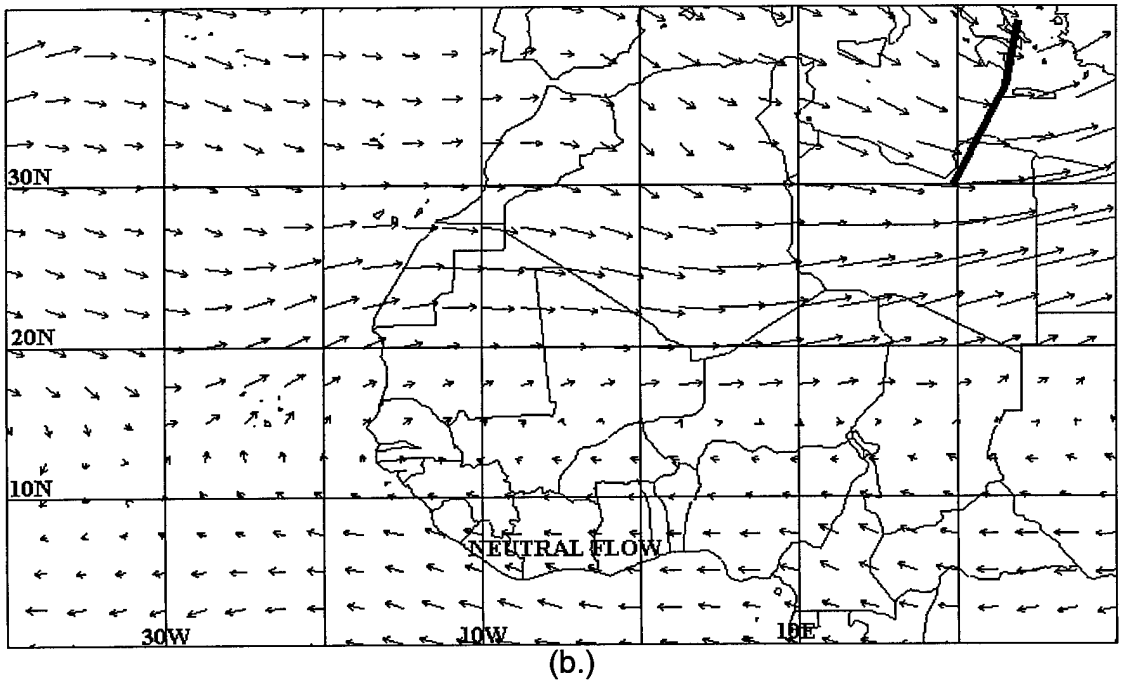

(b.)

Fig. 11. Six case composites of the a.) 250hPa and, b.) 500hPa actual wind field for dissipation day. 5° long wind arrow approximately 15 m/sec. Heavy line indicates trough axis.

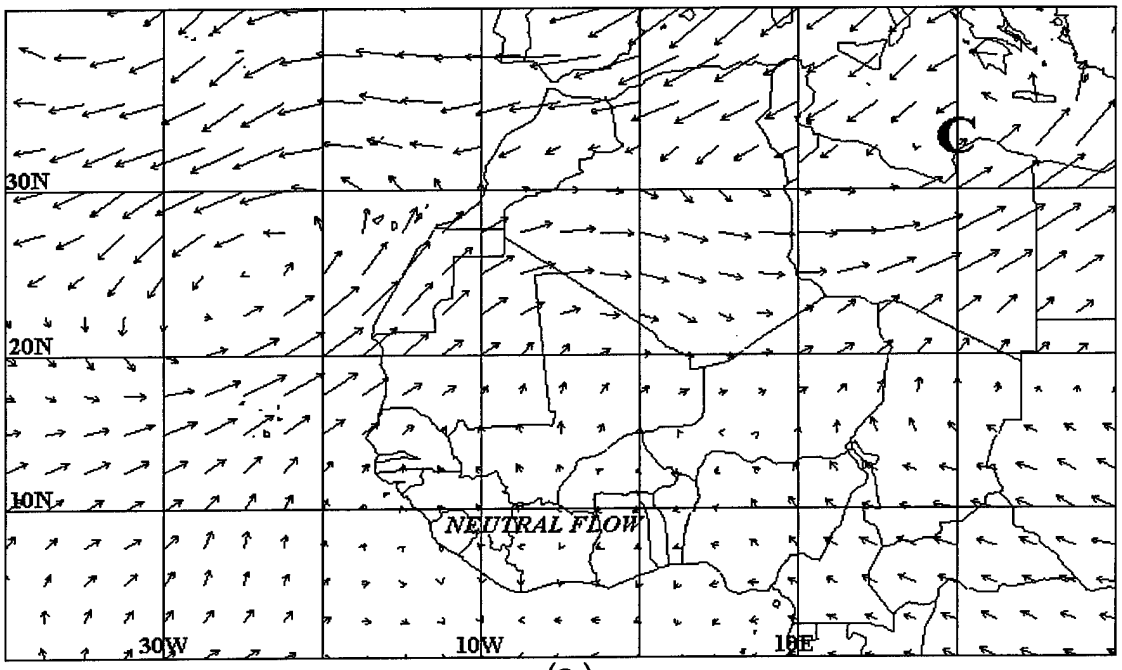

(a.)

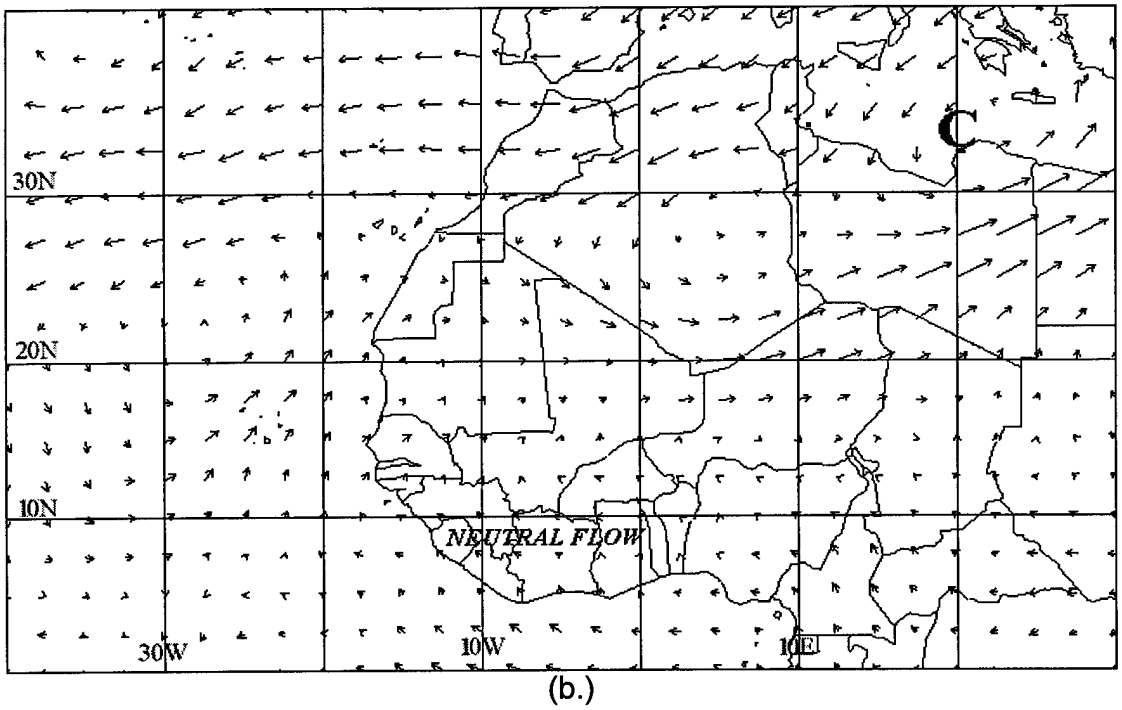

(b.)

Fig. 12. Six case composites of the a.) 250hPa and, b.) 500hPa reduced-shear field for dissipation day. 5° long wind arrow approximately 15 m/sec.

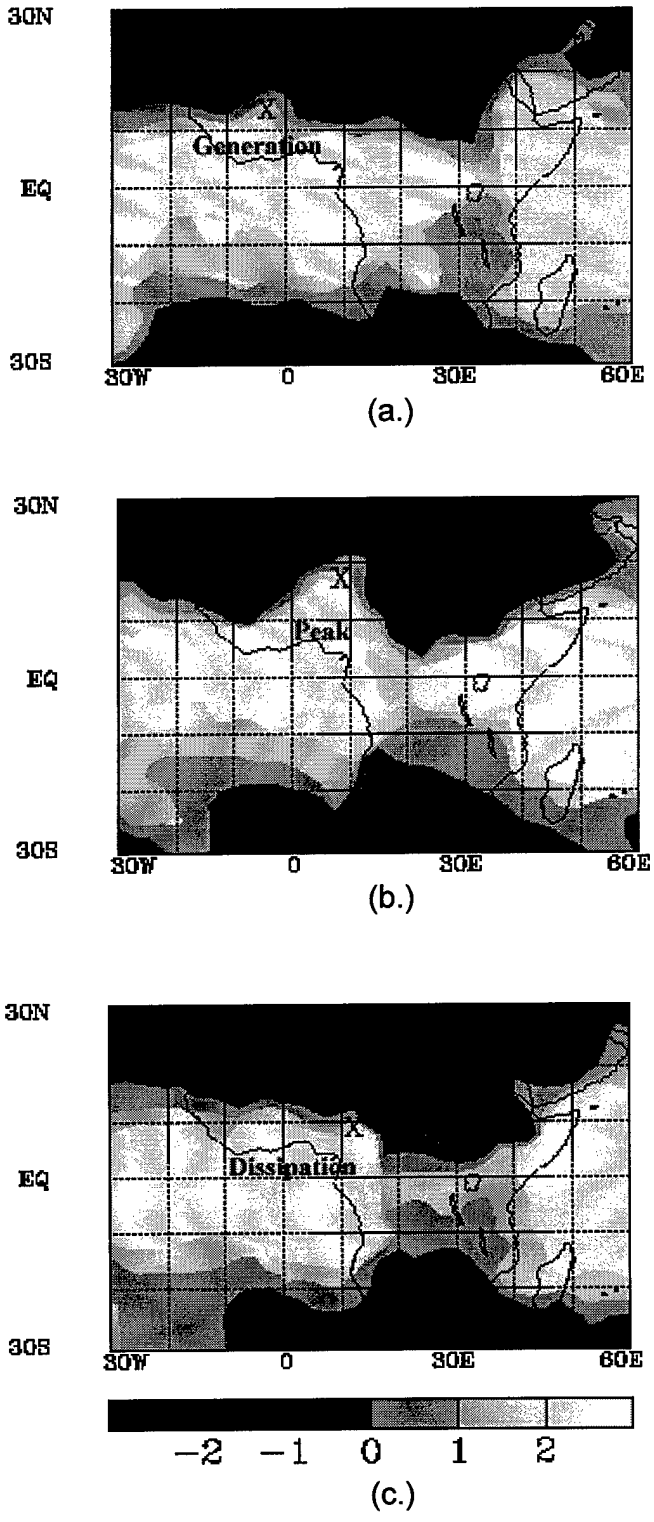

FIG. 13a.-c. a.) Initiation day, b.) peak day, and c.) dissipation day for the sample case PW field (cm). An 'X' indicates the local center of the anomaly. PW values are centered on a mean of zero.

Actual and reduced-shear wind field composites during the anomaly's life cycle reveals a similar structure at two upper levels of the atmosphere. The coherent structure and propagation characteristics exhibited by the anomalous, or reduced-shear, wind field yields evidence of a propagating wave. Table 3 provides composite wave characteristics found at 250hPa, 500hPa and their average for this case study (valid at 20°N). This latitude is the average latitude of the cyclone/anticyclone system for the seven day duration. These values were, therefore, approximated and calculated by average distance measurements from the composite structures. Wavelength, wavenumber and approximated speed are three examples of these measurements. Calculated Rossby Wave speed (at 20°N) is determined by $c = U_{mean} - \beta/k^2$, where $k = 2\pi/\text{wavelength}(L_x)$. The mean zonal speed is also approximated by averages of all seven cases at 5° intervals.

Table 3. Wave characteristics for 250hPa, 500hPa, and the average of the two levels.

Level	Wave Length (l)	Wave Number*	Measured Speed	Calculated Rossby Wave Speed (c)20N	Mean Zonal Speed (U) **
250hPa	5,600 km	6.7	10 m/sec	7 m/sec	24 m/sec
500hPa	6,600 km	5.7	14m/sec	-14 m/sec	10 m/sec
Avg.	6,100 km	6	12 m/sec	-4 m /sec	17 m/sec

*** based on 20N** **** Doppler shifted**

COMPOSITED WAVE CHARACTERISTICS OF CASE STUDY MAM 1988

Since this study is limited to strictly two upper levels, it is impossible to determine the level in which the maximum power of the wave exists. The composites reveal a more pronounced structure at 250hPa than at 500hPa, however, leading one to believe a wave power maximum closer to 250hPa. It may be assumed that the wave maximum exists in the upper levels (above 500hPa) and at a synoptic scale.

The averaged values from Table 3 show the wave propagates to the east at +12 m/sec. The mean zonal wind, based on 20°N, is also to the east at +17 m/sec. The difference between these two values yields –5 m/sec. The appropriate speed of a non-divergent Rossby Wave at 20°N, using the wavelength approximated in this case study, is –4 m/sec, or westward at 4 m/sec. These two values are very similar and are most closely approximated to the wind pattern of a Rossby Wave near 20°N propagating west at 4 m/sec within a higher easterly zonal wind.

There are numerous variations of each type of atmospheric waves throughout the tropics. Identifying this wave as a particular tropical mode involves determining such factors as appropriate direction of propagation (east/west), distance from the equator, wavenumber and specific radius of deformation (R). Takayabu (1994) discusses nine variations of waves at k=1 and displays their horizontal wind and divergence fields. As the mode (0, 1, 2, 3) assigned to each field increases, the horizontal pattern associated with each type of wave increases in distance north or south of the equator.

First, the doppler-shifted average speed of this wave is westward at approximately 4 m/sec. Secondly, the horizontal wind field involves a synoptic scale cyclonic and anticyclonic circulation. These characteristics, in turn, are found to be typical of a Rossby Wave, in this case, located approximately 2,200

km north of the equator (0° to 20°N). Since Rossby Waves are not dynamically isolated to one latitude band, but rather to the varying vorticity field, the wave may propagate in changing latitude, as is found within this particular case study. The latitude of 20°N is an average for the composited seven days discussed in this study.

The following section provides confidence to the NCEP/NCAR by verifying seasonal means with large scale atmospheric structures found throughout the tropics. These values interact closely with the composited wind structure already discussed in this section.

B. ATMOSPHERIC VARIABLES

As with any analysis, the data being initiated must first be validated with known tropical atmospheric features. Large-scale moisture features found throughout the tropics, for example, would be extremely difficult to analyze correctly with a gridded dataset containing poorly measured data at 2.5° resolution. Locating these features, therefore, provides reassurance of quality data within the NCEP/NCAR analysis' output.

Additionally, the computed seasonal means graphically display where high values, such as abundant moisture sources, exist at each level. Extremely dry seasonal conditions, for example, may become excessively moist over a matter of a few hundred kilometers. This is important when considering advection of properties across zonal boundaries and into regions otherwise void of these particular high values. Also, deviations from this variable mean state may indicate the development of anomalous structures.

Convergence zones in the South Pacific, North Atlantic, and Indian Oceans; large subtropical highs in the southeast Pacific ocean and southern Atlantic ocean; and large land-bound convectively active regions, like the Congo and Amazon Basin, are examples of large scale features found in the moisture field. High moisture values at most tropospheric levels should be found within convergence zones and convectively active regions. Conversely, low moisture values should be found within the vicinity of large areas of subsidence, including over large deserts like the Sahara.

Figure 14 displays the mean state for MAM 1988 specific humidity provided by the NCEP/NCAR analysis at 250hPa, 500hPa, and 850hPa. The high moisture values reflect regions where significant convergence and/or convective activity bring ample moisture to the upper reaches of the troposphere, and occasionally into the stratosphere. The highest moisture values at all levels appear to straddle the equator, yet with varying distance. This distance depends mostly on larger scale patterns of subsidence, convergence, and convection. The average located on each figure is the average of the variable for the local grid region, 20°W to 60°E and the equator to 30°N, not for the tropics as a whole.

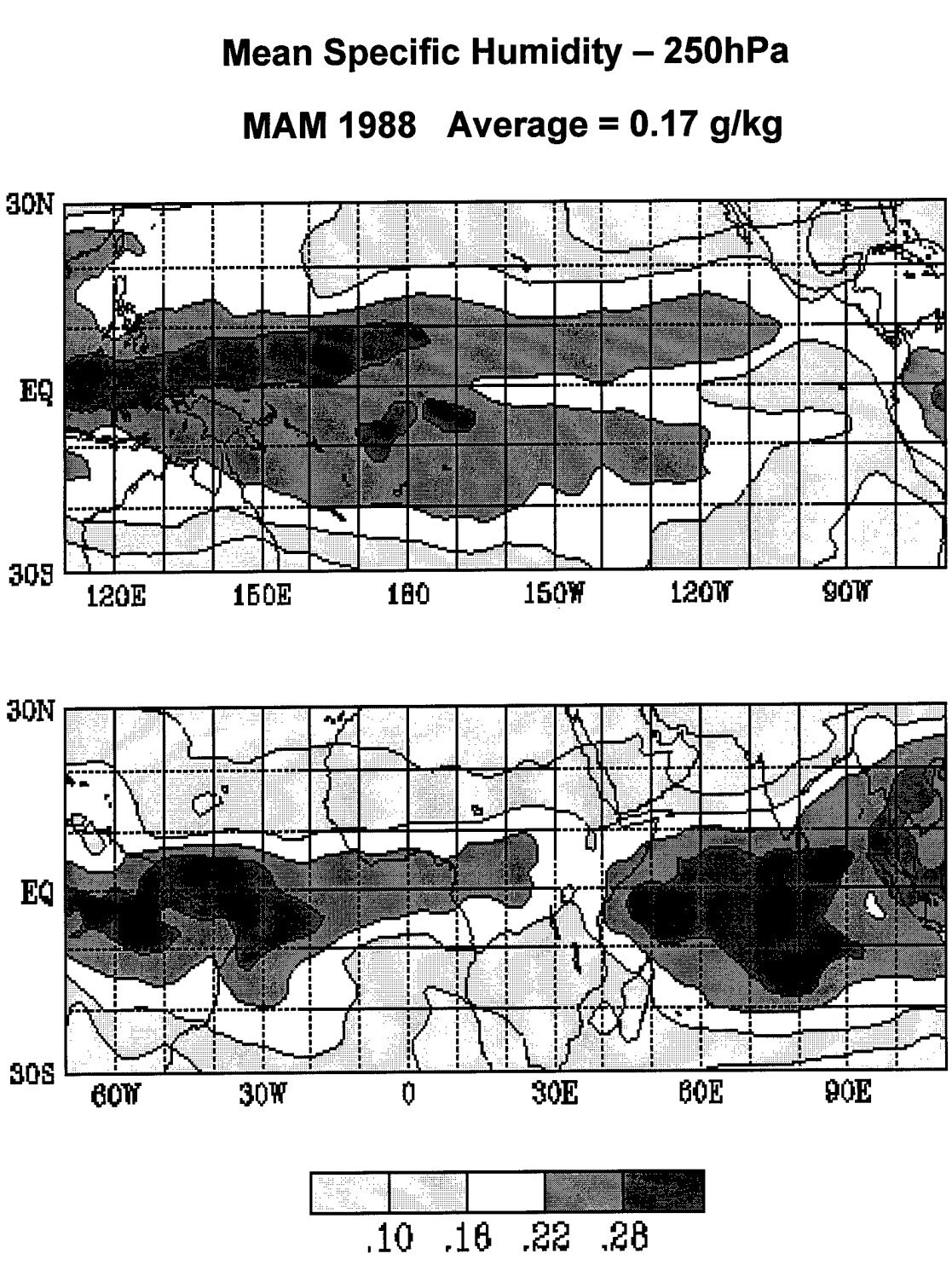

FIG. 14a. Mean specific humidity (g/kg) values for 250hPa from 30°N to 30°S. Specific humidity maxima correspond to the convergence zone regions across the Pacific, Atlantic, and Indian Oceans. Large areas of subsidence are found across northern Africa, the southern Atlantic Ocean, and the southeast Pacific Ocean with low specific humidity. Near the Gulf of Guinea, the maximum mean values possible are approximately 0.28 g/kg bordering the coastline.

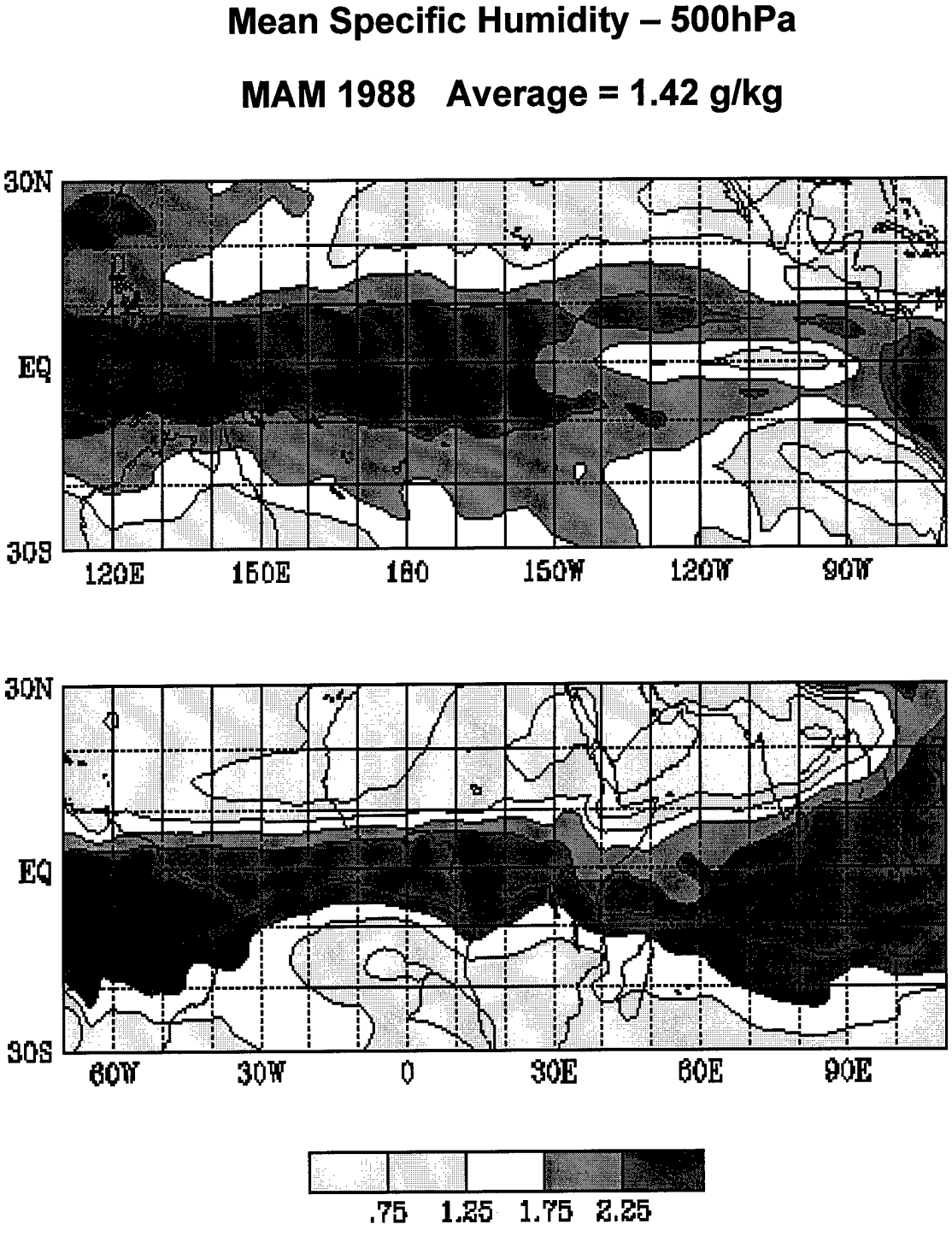

FIG. 14b. Same as Fig 14a, except for 500hPa. Near the Gulf of Guinea, the maximum mean values possible reach 2.25 g/kg inland, and beyond 2.25 g/kg over the Gulf. Notice the extremely dry conditions stretching west of northern Africa.

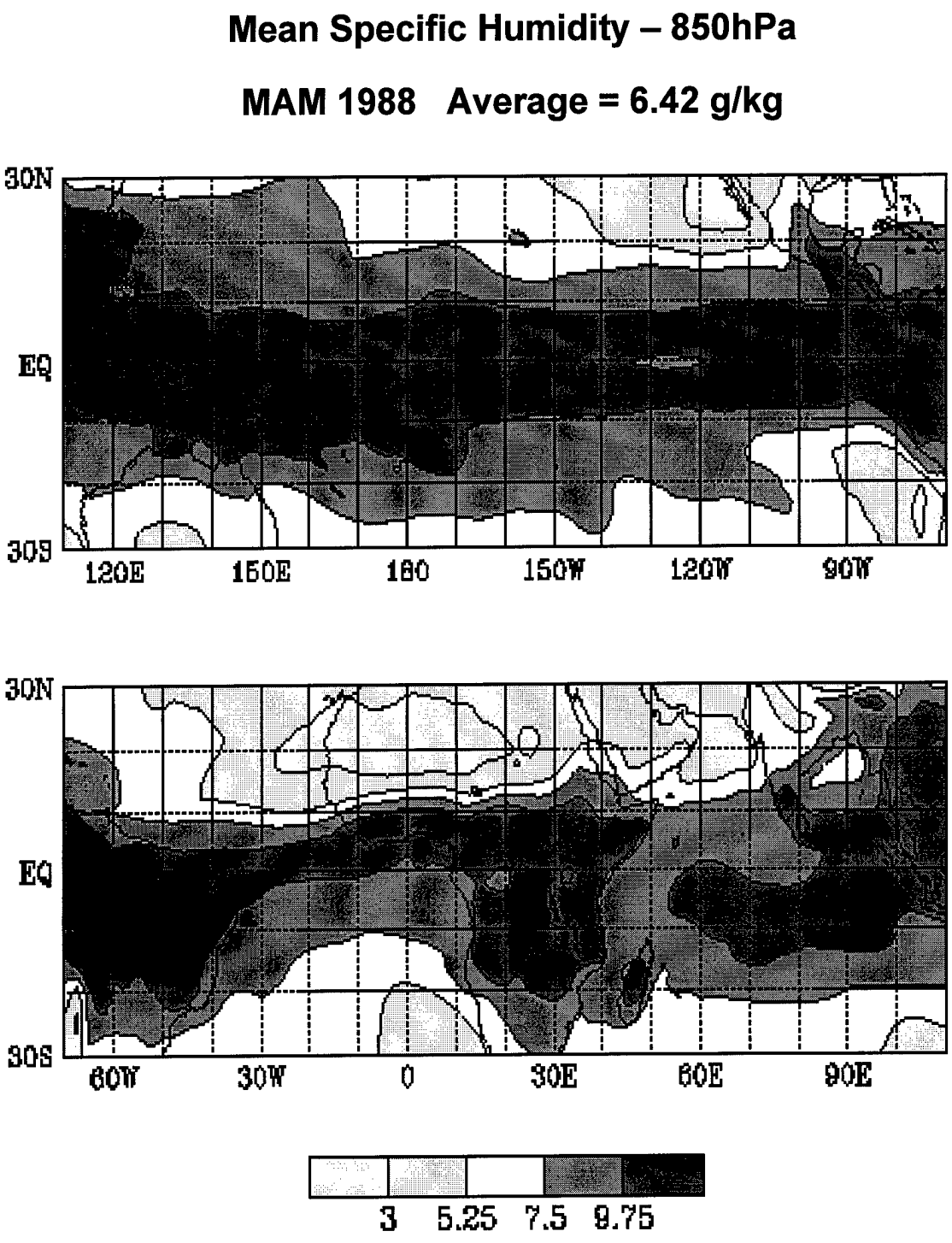

FIG. 14c. Same as Fig 14a, except for 850hPa. Abundant moisture, over 9.75 g/kg, exist well inland of the Gulf of Guinea and within the local convergence region, from 5°N to 12°N.

It is important to observe in these figures the maximum mean values that exist within the region in which the northward advecting cusp-like structure propagates. At 250hPa, the maximum mean values approach 0.28 g/kg near the northern coast of the Gulf of Guinea. If PW anomaly structure reveals greater moisture values at this level advecting out of the region from the south, then the abundant moisture found within the PW anomaly could not be solely advecting in from a region with simply a higher mean. The moisture, rather, must also originate from another source.

Moisture sources may include upward vertical motion, such as convergence zones, that carry additional moisture up from other levels. Convective processes also may assist in moistening the level during the anomaly's lifetime. Though similar to simple vertical motions, regular convective processes, such as those found within the Atlantic ITCZ, quickly and constantly entrain very high amounts of moisture into the upper levels. Lastly, a combination of the two processes may provide the increase. As convection moistens most levels, the southerly flow at 250hPa and 500hPa is able to advect high amounts of moisture along with the propagating wave found in the background wind field. As the wave propagates east and the moisture source is cut off, moist air entrains with the drier air to the east without the constant inflow of additional moisture. This, in turn, causes the PW signal, a measure of the amount of atmospheric moisture, to begin to weaken. In time, the moisture entrains to below the mean moisture levels, and anomalous moisture values (PW anomalies) are no longer associated with the propagating wave over the grid region.

Temperature gradients should also follow suit where, for example, there are steep or shallow gradients expected. At upper levels throughout the tropics

(250hPa and 500hPa), temperatures generally cool with northward or southward progression from the equator, more rapidly in the midlatitudes than in the tropics. The same generally holds true at lower levels (850hPa), unless a large topographic feature influences a region.

Western Africa is one such region in that the Sahara Desert extends across its northern portion and cooler air from the Gulf of Guinea influences the vegetation that lie across the southern portion close to the equator. These topographic features create a localized reversal in the expected temperature gradients with warming as one moves north out of the Gulf of Guinea towards 25°N. The sharp contrast in temperature at 850hPa is similar to that of the moisture field seen in Fig. 14c. Figures 15a.-b. show the mean temperature fields at the two upper levels used in this study. Figure 15c. displays the 850hPa mean temperature field containing the localized reversal of gradient as one moves north from the equator and out of the Gulf of Guinea.

Upper level potential vorticity, a product of static stability and absolute vorticity, also follows an expected pattern. If moving south from the North Pole, planetary vorticity (f) approaches zero at the equator, changing signs to negative once across. Consequently, positive values of potential vorticity increase moving north of the equator towards the poles, and negative values increase moving south. Figure 16 presents graphically the mean state of potential vorticity across the tropics. Since the localized region used in this study runs from the equator north, the average values on the figures are positive.

Potential vorticity values at 850hPa are ignored in this study due to the level's proximity to the boundary layer. Topographic influences within the boundary layer and smaller scale circulation within the lower levels of the

atmosphere cause potential vorticity measurements to be less helpful compared to these at upper levels at the synoptic scale.

Omega values, or vertical velocities, are the least accurate of the variables analyzed in this study since they are not actually measured. Omega values, rather, are computed as a product of the divergence (wind) field within the NCEP/NCAR analysis. Descriptive statistical analysis, discussed in Chapter IV, section C, revealed insignificant correlation between computed omega values and the positive PW anomalies at both 250hPa and 500hPa for both statistical analysis' resolutions. There was, however, a marginally significant correlation coefficient found between computed 850hPa omega values and the positive PW anomalies.

Since upward vertical motions (negative values) are usually the result of convergence, convection, or mechanical lifting, the mean state of the 850hPa omega values should reflect those regions in which there is steady upward motion. Figure 17, the mean state of computed omega values for MAM 1988, clearly reveals the upward vertical motions associated with significant convergence zones found north and south of the equator in the Pacific and Indian Oceans. Additional convergence zones are found across the Ivory Coast into Central Africa, spanning almost the entire length of the southern half of this study's local grid. Downward vertical motions (positive values) are found mostly within the subtropics, especially over Africa, where the downward portions of the Hadley Cell and semi-permanent subtropical highs are found. The entire span of local grid's northern half is within this mean subsiding regime.

Mean Temperatures (°C) – 250hPa

MAM 1988

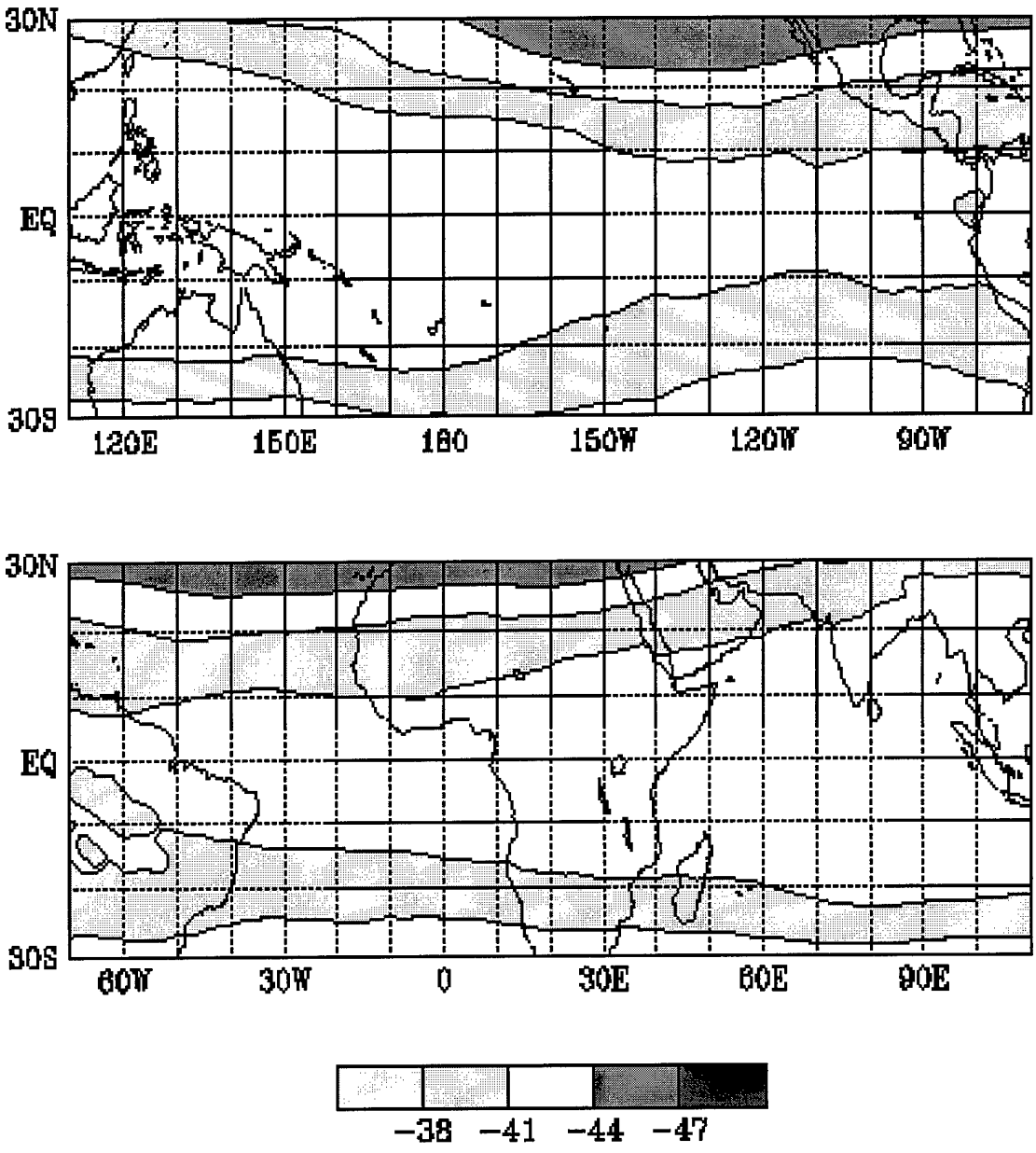

FIG 15a. 250hPa mean temperature field (°C) distribution from 30°N to 30°S.

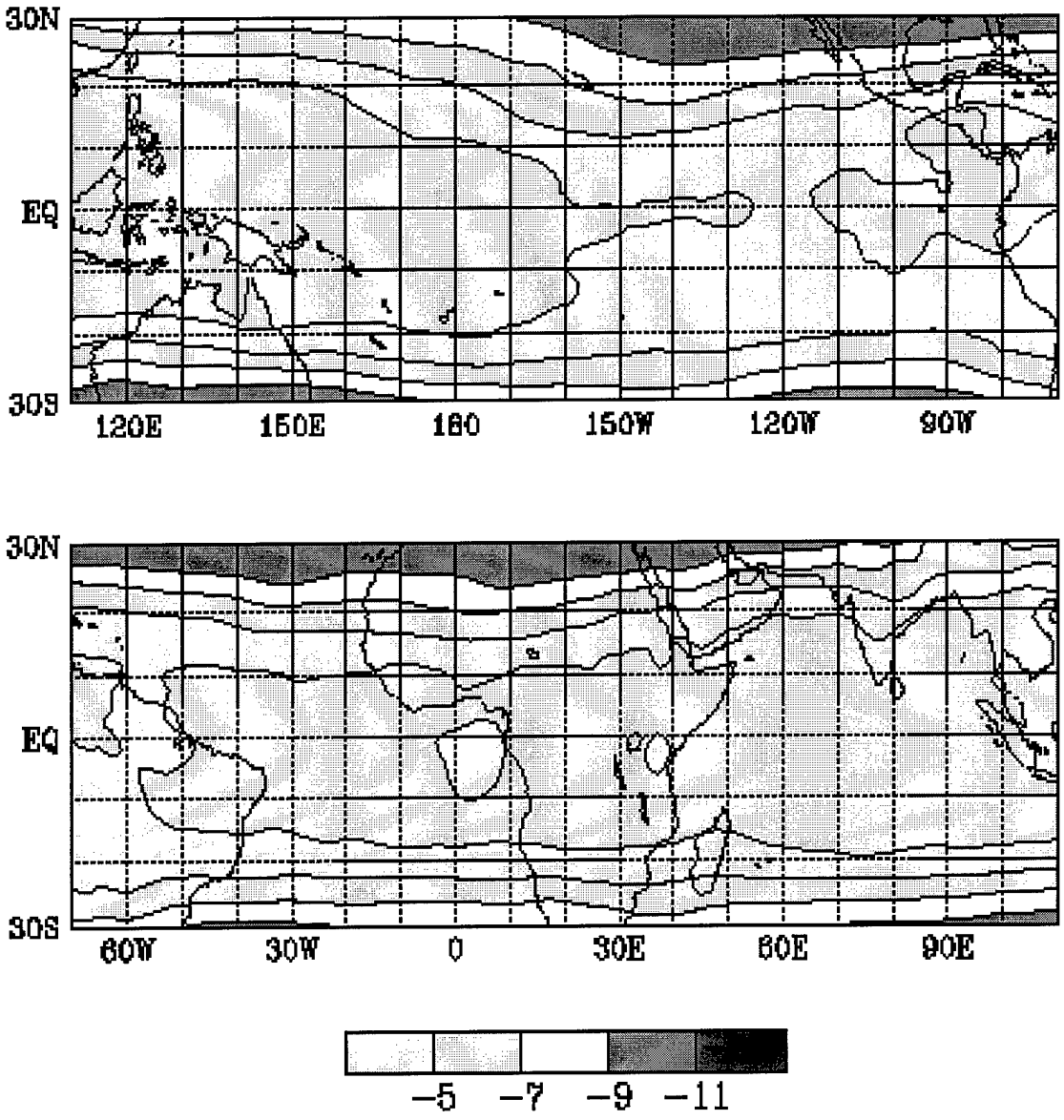

FIG. 15b. Same as Fig. 15a, except for 500hPa.

Mean Temperatures (°C) – 850hPa

MAM 1988

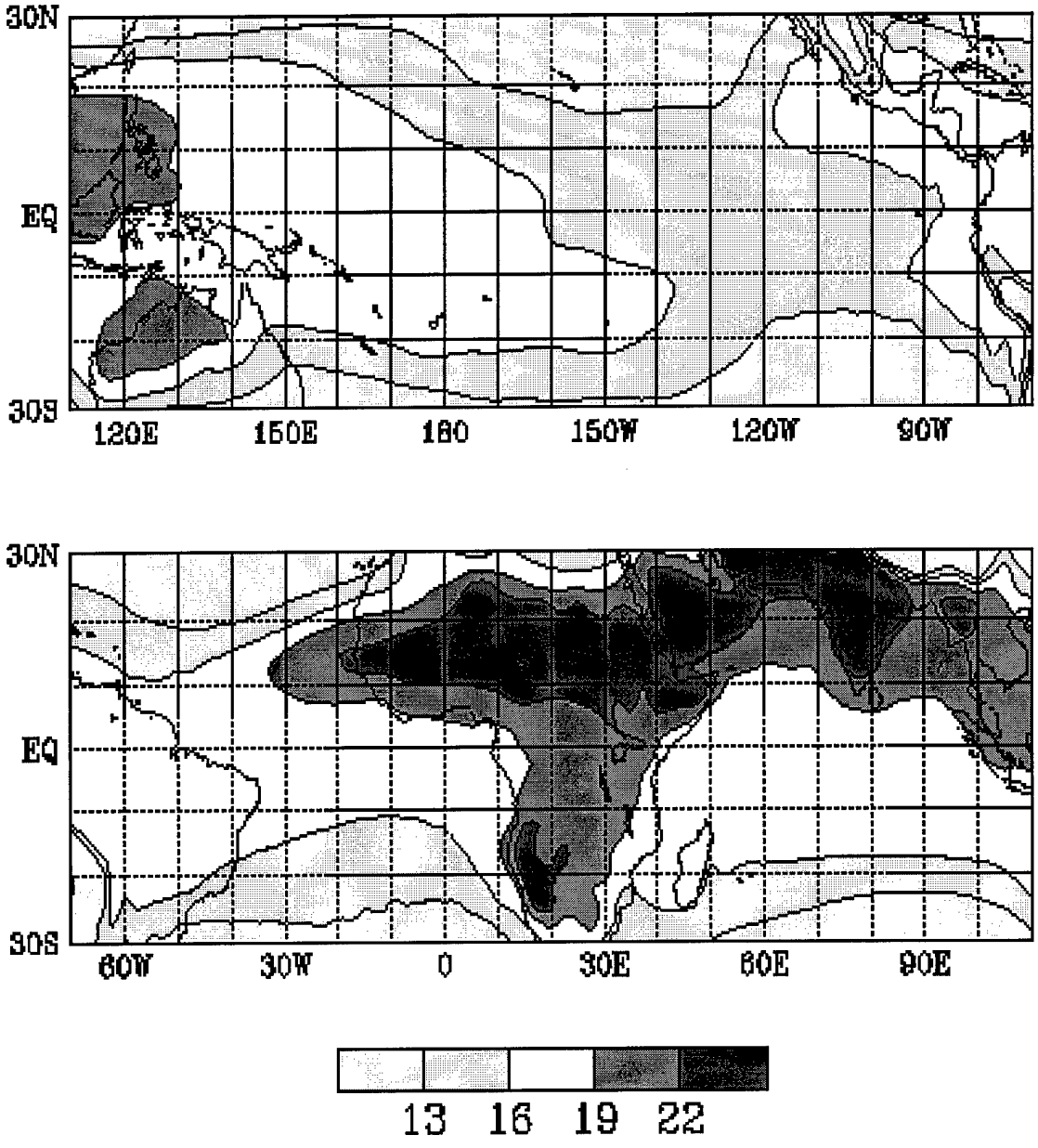

FIG. 15c. Same as 15a, except for 850hPa. Note the increase in temperature moving north from the equator at 0° in Africa.

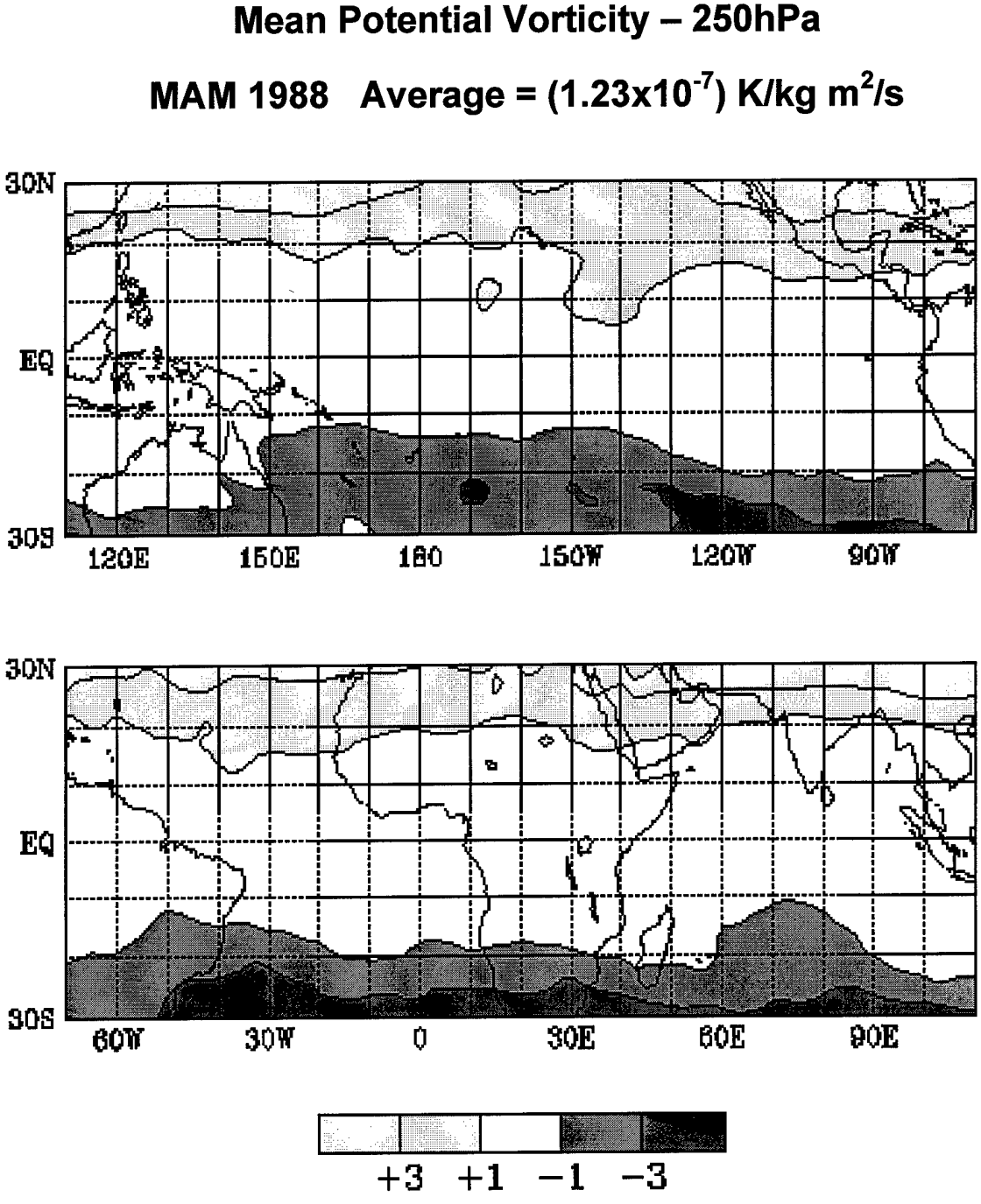

FIG. 16a. 250hPa mean potential vorticity (10^{-7} K/kg m^2/s) field from 30°N to 30°S.

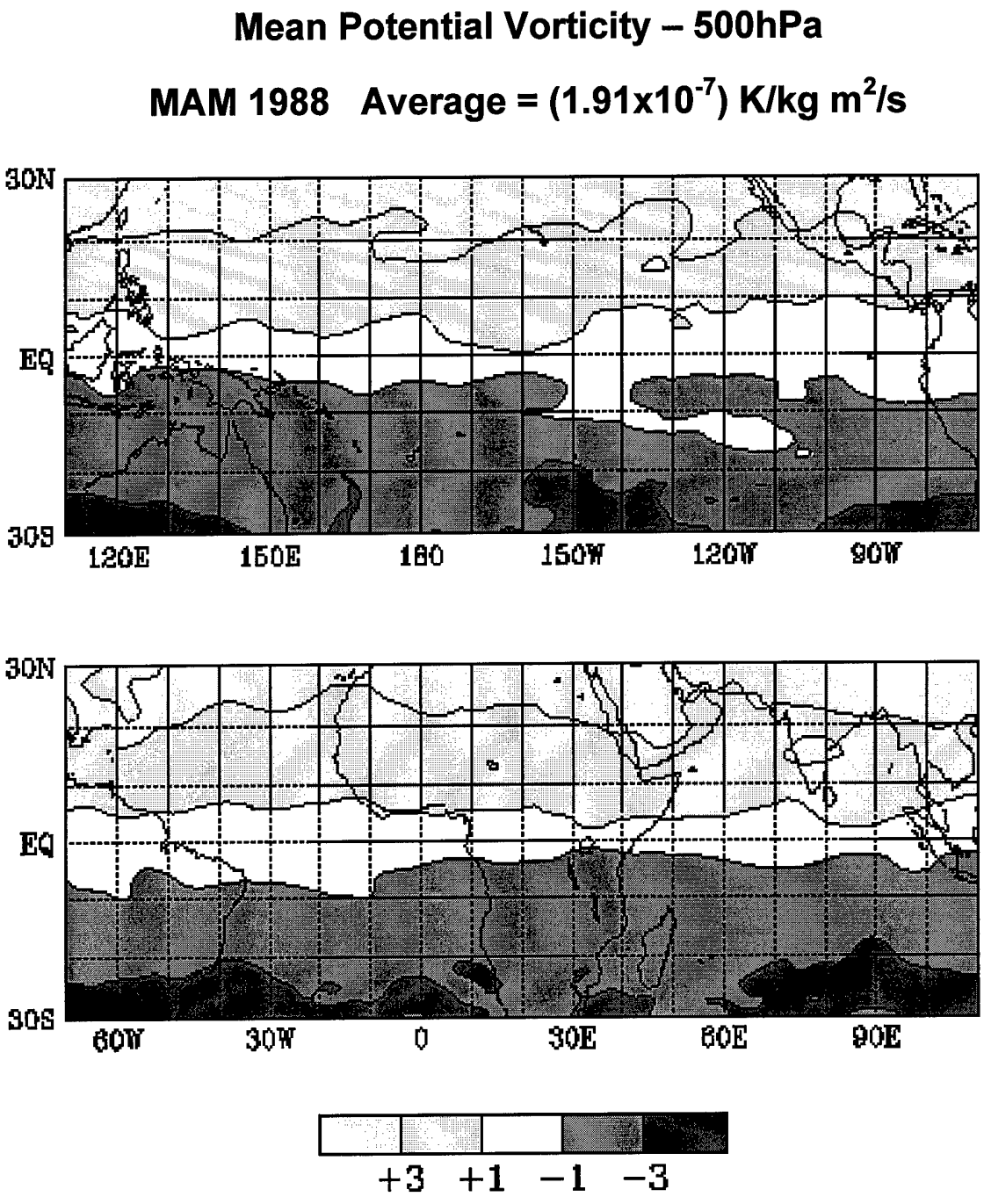

FIG. 16b. Same as Fig. 16a, except for 500hPa.

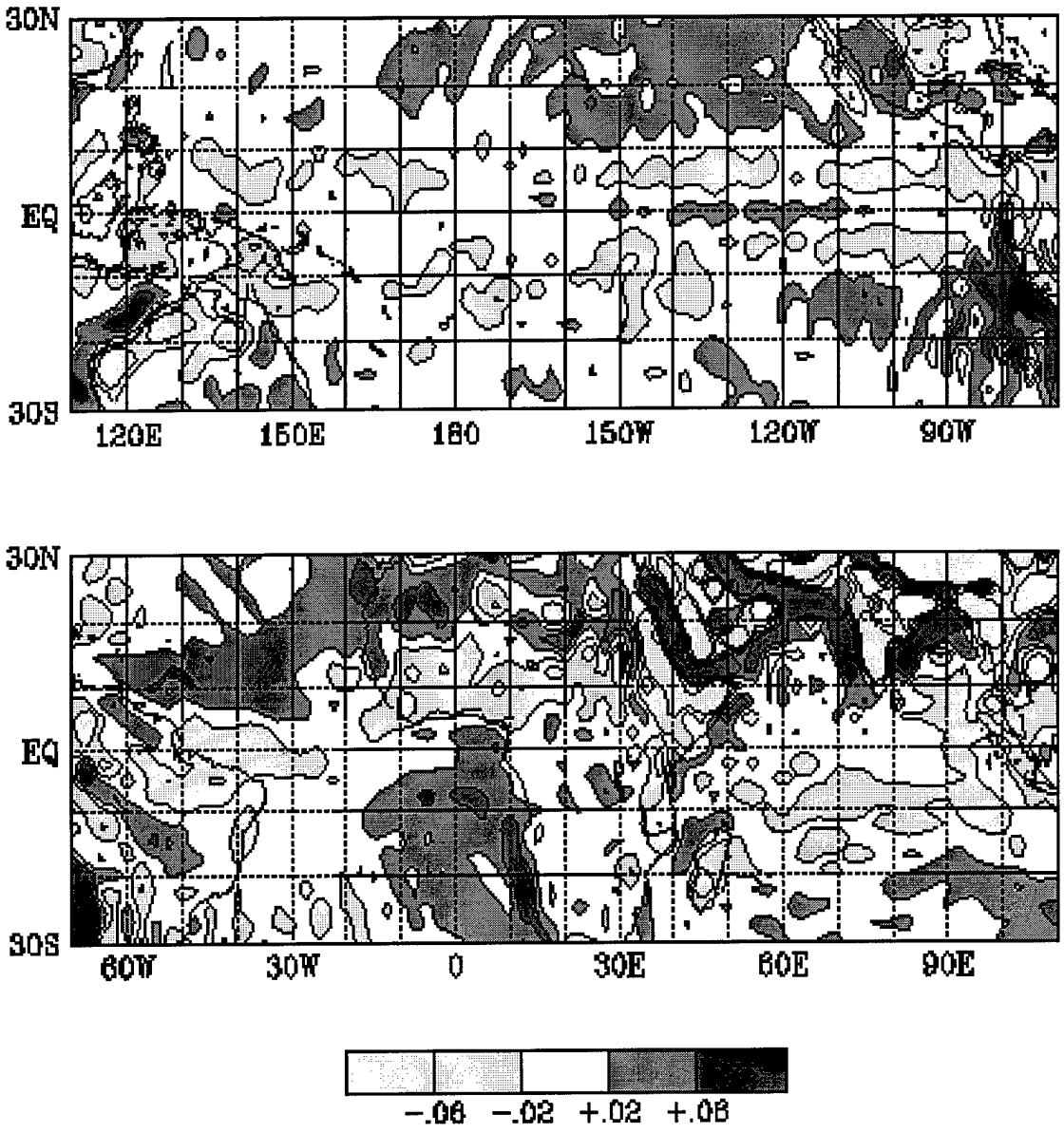

FIG. 17. 850hPa computed omega values (x 10^{-2} hPa/sec) from 30°N to 30°S.

C. DESCRIPTIVE STATISTICAL ANALYSIS RESULTS

Descriptive statistical analysis is extremely important when correlating atmospheric variables of large data arrays. Atmospheric variables that do not appear to visually correlate during analysis of composites may still prove to be significant statistically and, therefore, should not be ignored. Spatial and temporal relationships between variables may be highlighted using this method of analysis.

This study utilizes a spatial grid of 13 X 25 grid points at 2.5° spatial increments over 92 days. This produces a total of 29,900 data points of each NCEP/NCAR atmospheric variable to correlate with values from TOVS-initiated PW field. Table 4a provides a summary of the resulting statistical analysis between variables at three atmospheric levels (except PV) and TOVS-generated PW values. Statistical analysis of such a large number of data points creates large degrees of freedom and, therefore, a very small confidence interval for the correlation coefficient.

Temporal independence can be assured by using a seven day time interval for the NCEP/NCAR atmospheric variables, providing a conservative estimate of the degrees of freedom for statistics. Additionally, though the wavelength of the waves associated with the anomalies is nearly 6,000km, the actual PW anomalies themselves are seldom over 1200km in length. Therefore, to establish additional proof of significance, separate seven-day sampling of the 92 days at 10° spatial increments is accomplished to provide the best temporal and spatial independence possible within the limited datasets. This method produces only 390 data points, and yields a confidence interval of +/-0.05 for the

correlation coefficients. Table 4b provides the summary of statistical analysis results for this reduced dataset.

During this study, computed omega values at 850hPa were found to have a correlation coefficient of only -0.113 with PW, about 1.3% of the PW variance for the first analysis. The second analysis revealed a correlation coefficient of -0.108, still within the confidence interval from zero, and still statistically significant. This indicates a negative linear relationship between the two variables. At about 1.3% of the locations across the grid and over the 92 day duration, locations of upward vertical motion found at 850hPa, strictly based on the NCEP/NCAR numerical model data, will yield higher PW values as well. This provides additional insight as to what provides moisture to the positive PW anomalies found across the region.

TABLE. 4a. Descriptive statistical analysis results for NCEP/NCAR numerical model data versus TOVS PW data at 2.5° spatial resolution.

Variable	Level (hPa)	Mean	Variance	Standard Deviation	Correlation Coefficient	% variance associated
Specific Humidity (g/kg)	250	0.146	0.0198	0.14	0.386	15
	500	1.243	1.095	1.046	0.575	33
	850	6.416	16.05	4.006	0.693	48
Potential Vorticity (K/kg m^2/sec) x 10^{-7}	250	1.23	11.07	3.33	-0.239	5.5
	500	1.91	3.08	1.76	-0.36	13
Computed Omega (hPa/sec) x 10^{-3}	250	0.0102	0.0027	0.052	-0.013	<1
	500	0.003	0.00016	0.013	-0.038	<1
	850	-0.00008	0.00013	-0.112	-0.113	1.3
Temperature (°C)	250	-42.55	11.86	3.44	0.58	34
	500	-7.40	13.02	3.61	0.604	37
	850	20.68	25.18	5.02	0.047	<1
TOVS-generated PW (cm)	sfc-0	2.55	1.12	1.06	****	****

Reanalysis Model Variables Compared to TOVS PW 2.5° Grid Interval

(Localized Grid: 0°, 20°W X 30°N, 40°E) 92 Days

Table 4b. Same as table 4a., except at 7 day temporal interval and 10° spatial interval. **Boldly** indicated correlation coefficients indicate statistical significance is found at both resolutions.

Variable	Level (hPa)	Mean	Variance	Standard Deviation	Correlation Coefficient	% variance associated.
Specific Humidity	250	0.124	0.018	0.135	**0.355**	13
(g/kg)	500	1.28	1.1	1.05	**0.294**	9
	850	6.61	15.6	3.95	**0.621**	39
Potential Vorticity	250	1.52	16.06	4.01	**-0.362**	13
(K/kg m^2/sec) x 10^{-7}	500	1.9	4.11	2.03	**-0.551**	30
Computed Omega	250	0.11	0.27	0.52	-0.104	1.1
(mb/sec) x 10^{-3}	500	0.033	0.016	0.125	-0.161	2.6
	850	0.0045	0.0139	0.118	**-0.108**	1.2
Temperature (°C)	250	-43.1	16.1	4	**0.538**	29
	500	-7.7	18.1	4.3	**0.704**	50
	850	19.5	27.2	5.2	**-0.252**	6.4
TOVS-generated PW (cm)	sfc ---> 0	2.56	1.13	1.06	****	****

Reanalysis Model Variables Compared to TOVS PW 10° Grid Interval

(Localized Grid: 0°, 20°W X 30°N, 40°E) 7 Day Interval

Only variables and specific levels that are found statistically significant at both resolutions are analyzed. Graphical representations of mean standard deviations are developed to distinguish "noise" from significant variable anomalies found within each field in relation to the PW anomalies. For example, a temperature anomaly of +2°C above the local mean may have no significance if the region's standard deviation is +6°C. Conversely, if a temperature anomaly of +12°C (2 standard deviations) is found correlating in time and space with the

PW anomaly, then it becomes apparent that a temperature anomaly *is* significant and possibly related to the PW anomaly structure. Figure 18 reveals the spatial pattern of the temporal standard deviations of significantly correlated variables across the local grid region and its symmetric equivalent south of the equator.

An important feature to note is the location of the mean maximums and the location of the standard deviation maximums. The axis of the convergence zone across northern Africa is near 10°N (see fig. 17), south of the axis of higher temporal standard deviations, near 14°N (see fig. 18a). The offsetting is because the mean omega values are near zero, between the mean positive and mean negative halves of the local grid, just north of the convergence zone and where the most variability in the omega field occurs. Other regions around the tropics where the means omega field is near zero may not retain this correlation, however. These regions may not be conducive to strong vertical motions as those found within convergence zones across this region. Additionally, note the analysis over the water begins to lose definition off the west African coastline. Lack of data to compute omega and associated standard deviations may causes a poor analysis and, therefore, the incoherent structure.

Specific humidity standard deviations are highest where there are pockets of high moisture values, much like those found in Fig. 14, peaking near the equator at 250hPa, and sloping northward down to 850hPa (Fig. 18b.-d.). This indicates greater variability within convergence zones at a lower level of analysis. At lower levels, most of the available moisture is brought up from the surface via these convergence regions allowing for greater moisture values. It is also interesting to note the different locations of the specific humidity axis at each level versus the location of the appropriate standard deviation axis.

Especially at 500hPa and 850hPa, the zonal axis of maximum mean specific humidity is about 7° south of the maximum standard deviation axis. The maximum standard deviation axis is found roughly over the area of maximum specific humidity gradient, which is very pronounced just south of the Sahara.

The temperature fields, at upper levels, display an increasing gradient moving away from the equator. This is reflected by the zonal increase of standard deviations much the same (Figs. 18e.-f.). The greatest standard deviation gradient is found approximately where the greatest temperature gradient is located, near 20°N. Closer to the equator, the gradient relaxes and the lowest standard deviations are found. This reflects the almost isothermal conditions that exist at this level near the equator.

Potential vorticity also rapidly increases in value and gradient when moving away from the equator. This, too, is found in the distribution of the mean standard deviations, though not as clearly as in the temperature fields (Figs. 18g.-h.). Close to the equator, coriolis force is near zero, and potential vorticity values remain near zero. These values increase rapidly as they approach the southernmost reaches of the midlatitudes.

The next section discusses the structure of the TOVS-initiated positive PW anomalies as found in the NCEP/NCAR fields, and how they interact with its propagation. Fields used to develop the structure are determined by the statistical analysis.

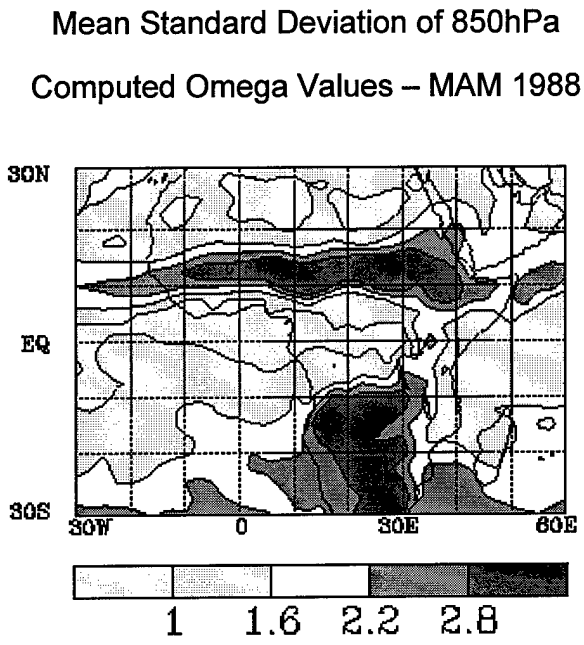

FIG. 18a. Mean standard deviation of computed omega values (hPa (x 10^{-4})/sec) for 850hPa.

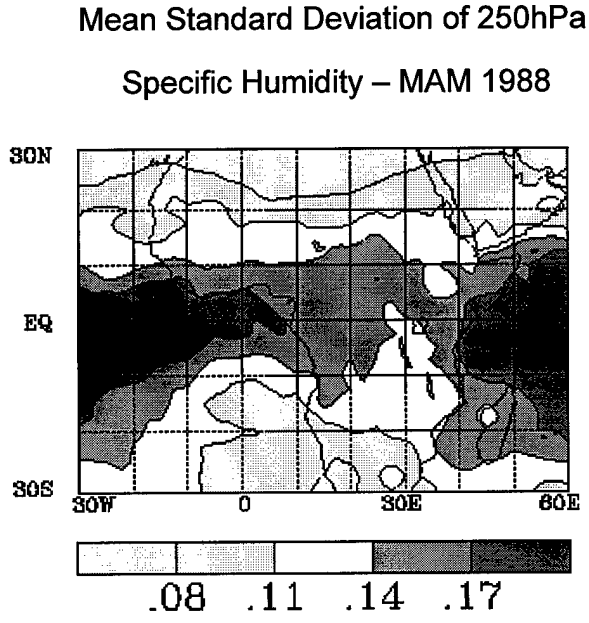

FIG. 18b. Mean standard deviation of specific humidity (g/kg) for 250hPa.

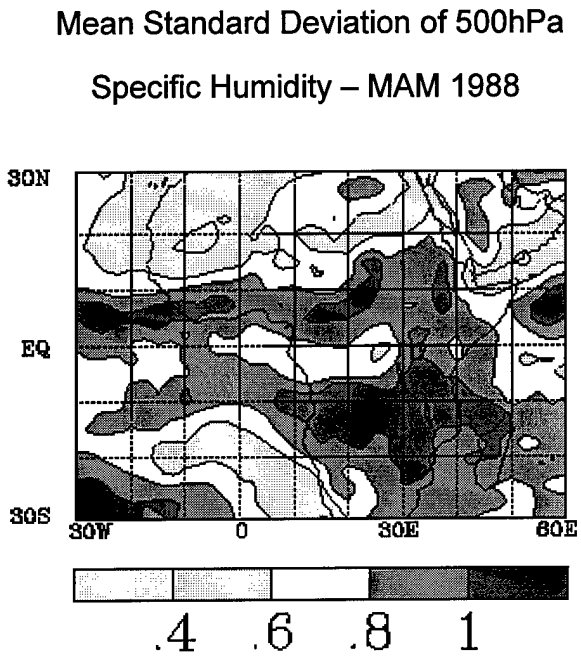

FIG. 18c. Same as Fig. 18b, except for 500hPa.

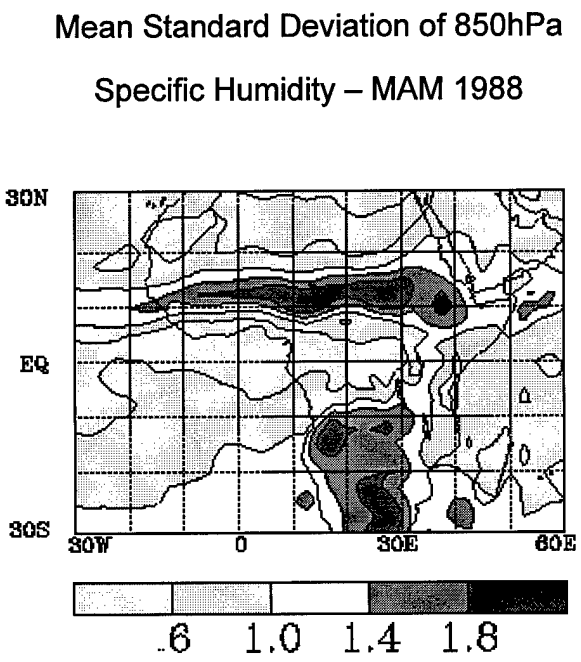

FIG. 18d. Same as Fig. 18b, except for 850hPa.

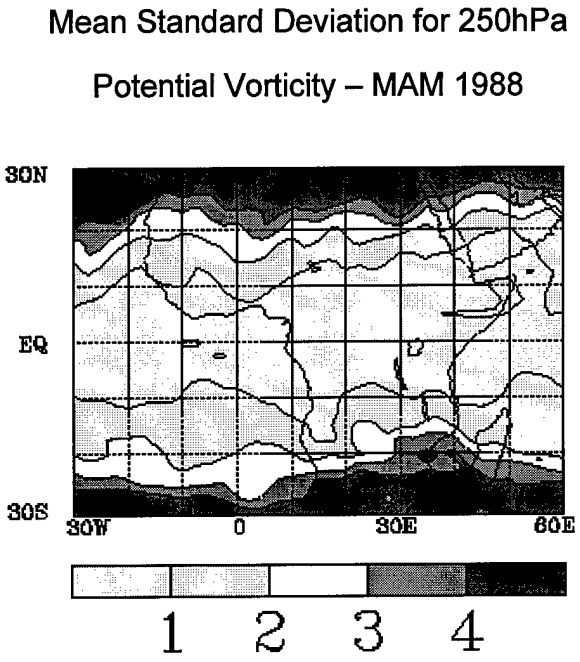

FIG. 18e. Mean standard deviation of potential vorticity ($x10^{-7}$ K/kg m^2/sec) for 250hPa.

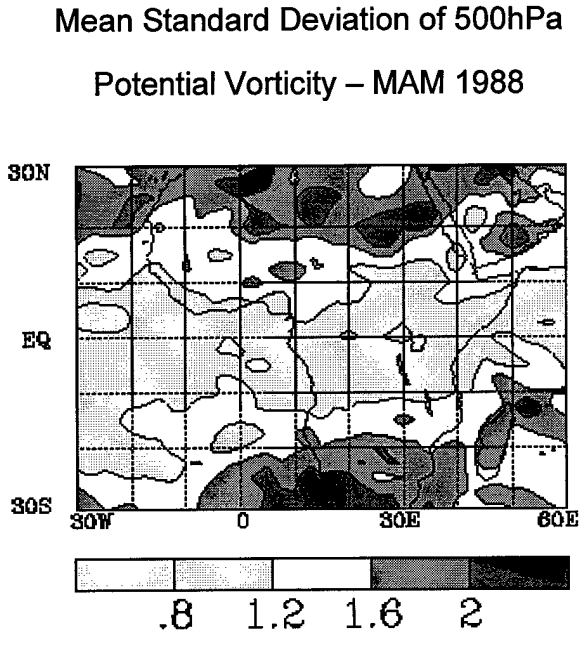

FIG. 18f. Same as Fig. 18e, except for 500hPa.

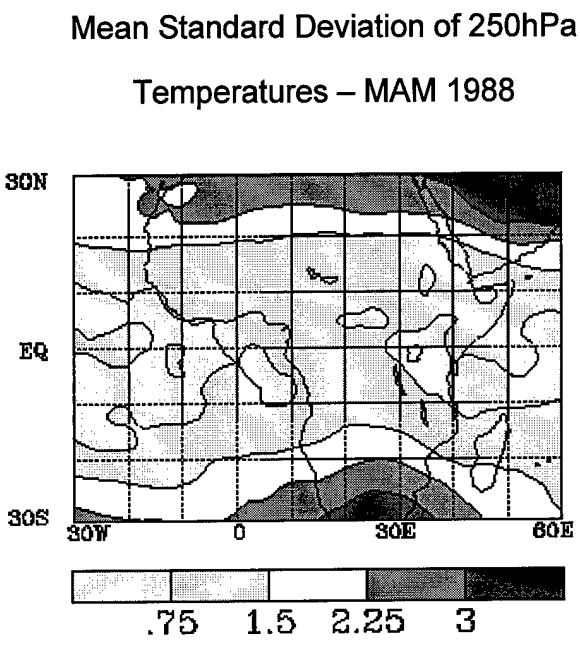

FIG. 18g. Mean standard deviation of temperatures (°C) at 250hPa

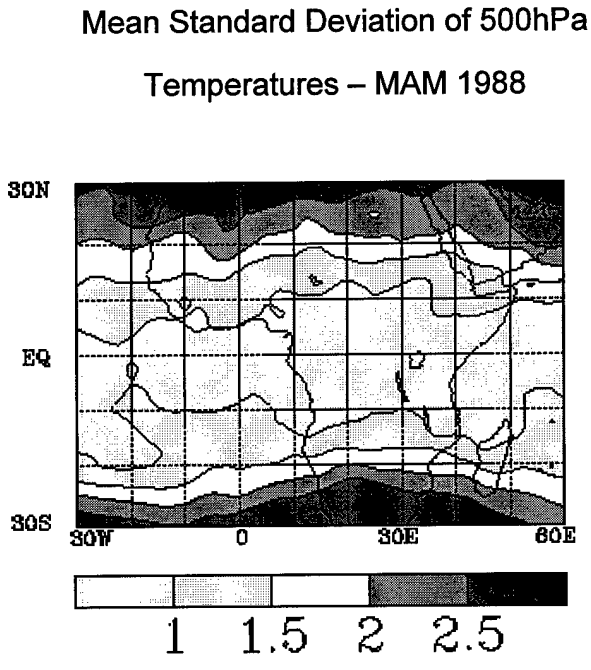

FIG. 18h. Same as Fig. 18g, except for 500hPa.

D. GENERAL STRUCTURE RESULTS

Computed omega values, potential vorticity, temperature, and specific humidity fields are reviewed for all seven cases at the three pressure levels: 250hPa, 500hPa, and 850hPa. As discussed in the prior section, descriptive statistical analysis is used to determine those variables that appear most statistically significant during correlation with the positive PW anomalies. The variables found significant are then used to provide a sample case (case # from table 1) for the PW anomalies.

Initiation day marks the point in which a coherent and defined signal is found in the PW field. The representation of the unfiltered PW field appears as more of a northerly bow, or surge, of high PW values. The filtered data usually appear more symmetric, marking the location of maximum signal strength (averages approximately 12.5°N). The "local center" of a sample case is marked for each variable. This location is essentially the geographic center of an actual anomaly during the MAM 1988 season (covering as much as 10° X 10° in area) that reveals a structure best displaying the common pattern found in each of the cases for a particular atmospheric variable.

Computed omega values are not found statistically significant at 250hPa or 500hPa for both statistical resolutions (see Tables 4a. and 4b.) regarding positive PW variance and, therefore, are not discussed. At 850hPa, however, some significance is found at both statistical resolutions. General values of omega are, therefore, applied to initiation day for a PW anomaly.

Each of the cases exhibited 850hPa negative omega values of approximately -0.0015 to -0.002hPa/sec (-130 to -170hPa/day), generally to the south of the anomaly's center on initiation day. Upward vertical motion may

begin here to be excited by the increasing southerly flow at 500hPa and 250hPa, discussed in section A, associated with the approaching wave. The location of the region of negative omega is to the rear right quadrant of the cusp-like structure, or wind maximum, allowing greater divergence aloft. This slightly lowers the pressure at the upper levels, and upward displacement within the convergence zone increases.

Figure 19 is a representation of the 850hPa computed omega field structure for this day. The 'X' marks the local center of the PW anomaly, though the actual extent of the anomaly may be much greater. In this representation, the PW anomaly center is located within a zonally elongated region of weak upward vertical motions. The omega values correlating with the PW anomalies are approximately one standard deviation from the local mean across the grid area (see Fig. 18a.).

In most cases, the upward vertical motion lay within the seasonal convergence zone. The seasonal convergence zone, as noted by Krishnamurti (1979), slowly propagates northward away from the Guinea coast throughout the MAM season. Low level moisture in proximity to this region of upward vertical motion may provide an additional source of moisture for PW anomaly development. This moisture may then be drawn in by southerly flow aloft (Chapter IV, Section A) and advected northeastward with the propagating wave and associated PW anomaly.

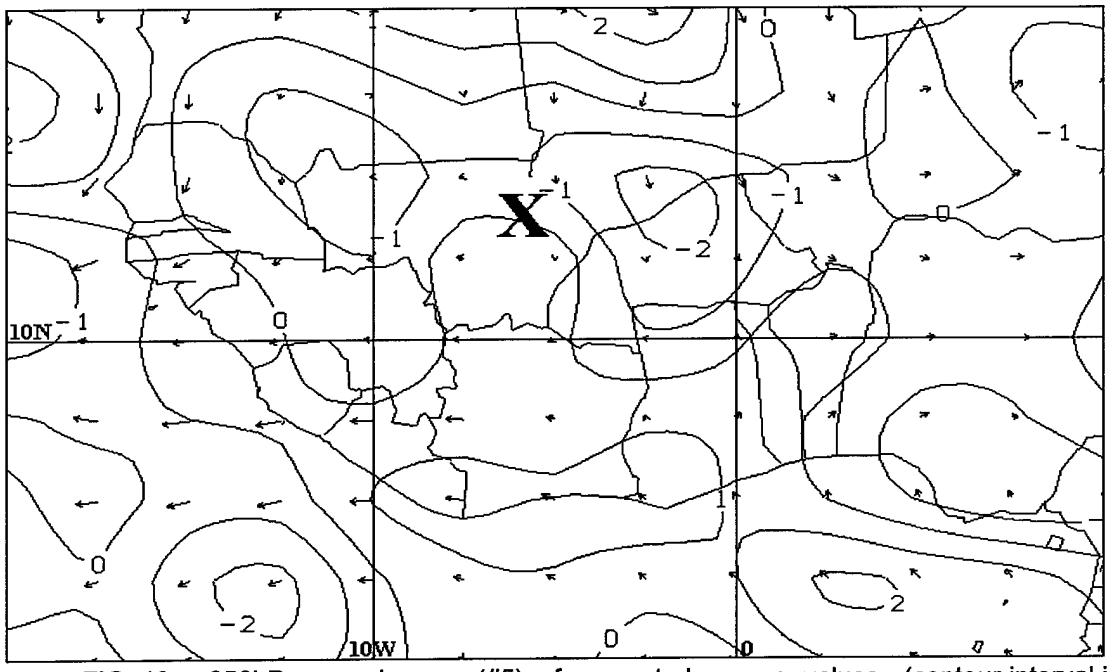

FIG. 19. 850hPa sample case (#5) of computed omega values (contour interval is 1hPa x 10^{-3}/sec) on initiation day for the seven cases in the MAM 1988 season. The local center of the PW anomaly is annotated by an 'X'. 5° long wind arrows are approximately 15 m/sec.

Potential vorticity values are found to have a negative correlation with PW values. Higher PW values should yield lower potential vorticity values across the local grid. At both 500hPa and 250hPa, values of +2 to +10 K/kg m^2/sec are to the east and west of the PW anomaly's center. Directly over the center of the anomalies, however, no values greater than +2 K/kg m^2/sec are found. Figure 20 is a representation of the 250hPa potential vorticity structure on initiation day. The center of the anomaly is found within a local minimum of potential vorticity values. A moderate maximum lays to the east, and a strong maximum well to the west. The region of maximum potential vorticity to the west is associated with the strong upper level trough approaching the west African coast (see Fig. 4a.).

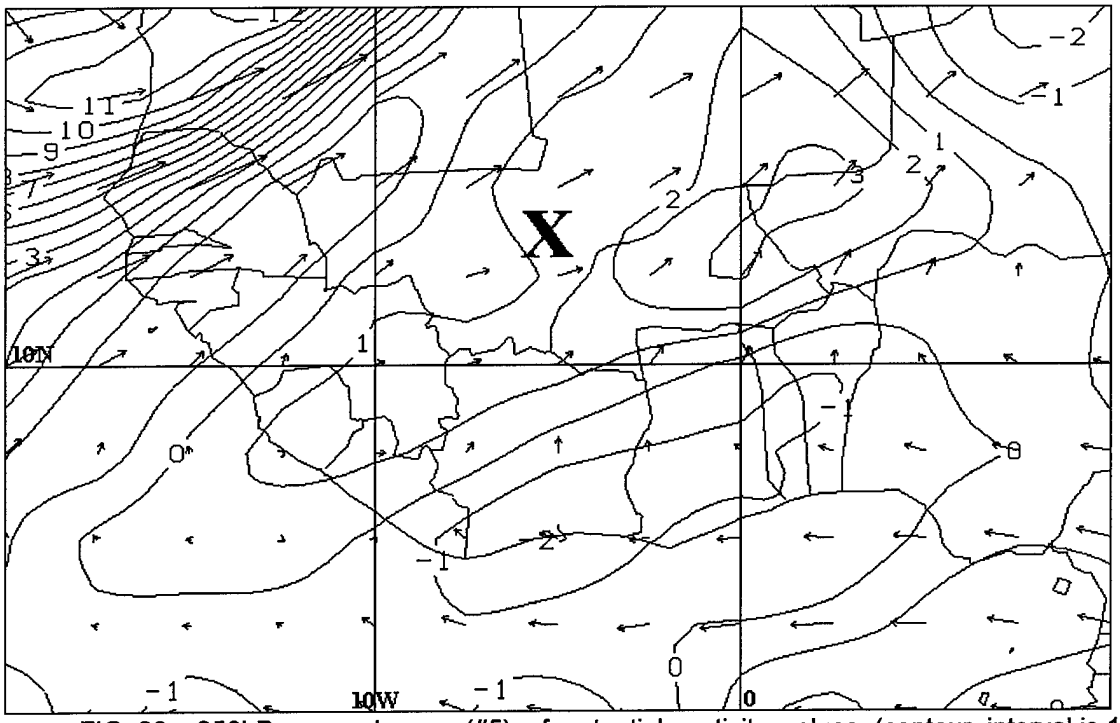

FIG. 20. 250hPa sample case (#5) of potential vorticity values (contour interval is 1 (K/kg m^{-2}/sec) x 10^{-7}) on initiation day for the seven cases in the MAM 1988 season. The local center of the PW anomaly is annotated by an 'X' . 5° long wind arrows are approximately 15 m/sec.

Specific humidity values provided the most pronounced visual correlation between the NCEP/NCAR data and the TOVS-generated PW values. In six of the seven cases, high specific humidity values nearly matched that of the non-filtered PW signature associated with the anomalies. The levels at which the outline-match best occurs are the two upper levels: 500hPa and 250hPa. The 850hPa values, in turn, remain extremely rigid throughout the entire season. A strong zonal gradient bordering the southern Sahara fluctuated only slightly,

though the two upper levels, especially 250hPa, displayed intense northerly advection of moisture associated with each passing PW anomaly.

High moisture values are advected into the center of the PW anomaly from ample moisture existing south of the local area, a region of fluctuating year round convection, on initiation day. Values as moist as 0.5 g/kg at 250hPa and 3.0 g/kg at 500hPa entrain into values lower than 0.1 g/kg at 250hPa and 0.5 g/kg at 500hPa that had persisted the days prior to the anomaly development.

Figure 21 represents the 250hPa and 500hPa specific humidity structure on initiation day. Both levels, especially 250hPa, exhibit a northerly surge of moisture near the anomaly's center. These values, at both levels, are nearly two standard deviations from the mean of the local grid area, revealing a significant moisture structure associated with the TOVS-generated PW anomalies within the NCEP/NCAR data (see Figs. 18b.-c.).

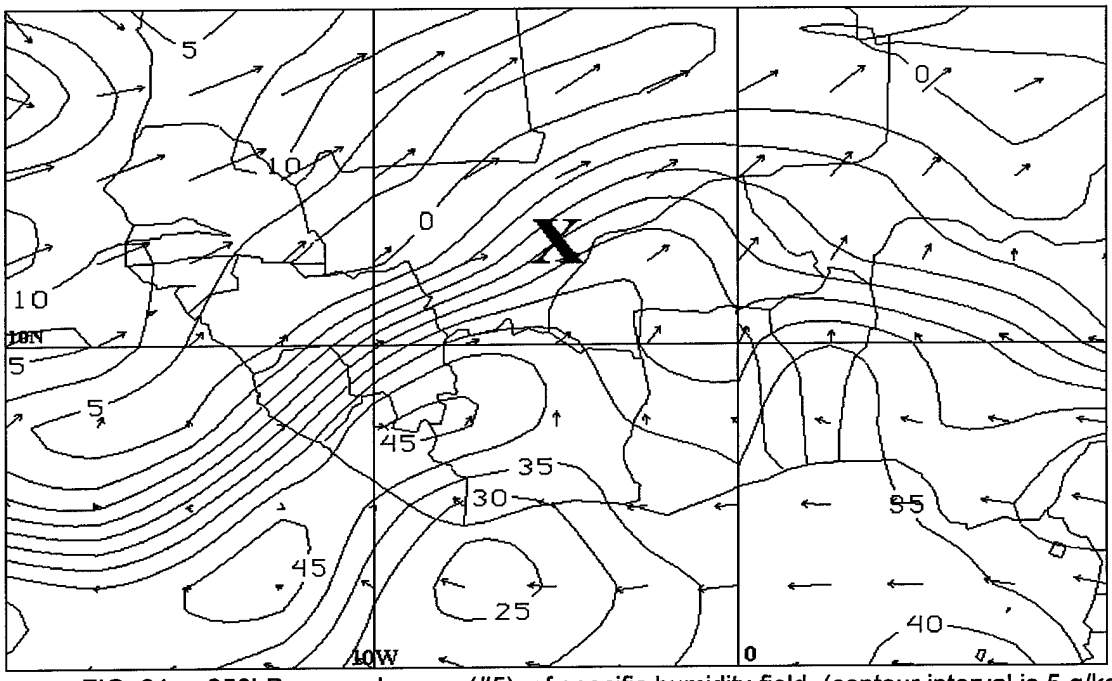

FIG. 21a. 250hPa sample case (#5) of specific humidity field (contour interval is 5 g/kg x 10^{-2}) on initiation day for the seven cases in the MAM 1988 season. The local center of the PW anomaly is annotated by an 'X'. 5° long wind arrows are approximately 15 m/sec. Maximum values approximately 0.45 g/kg. Note: zero isopleth does not indicate sub-zero specific humidity values, rather poor GEMPAK analysis of reanalyzed data.

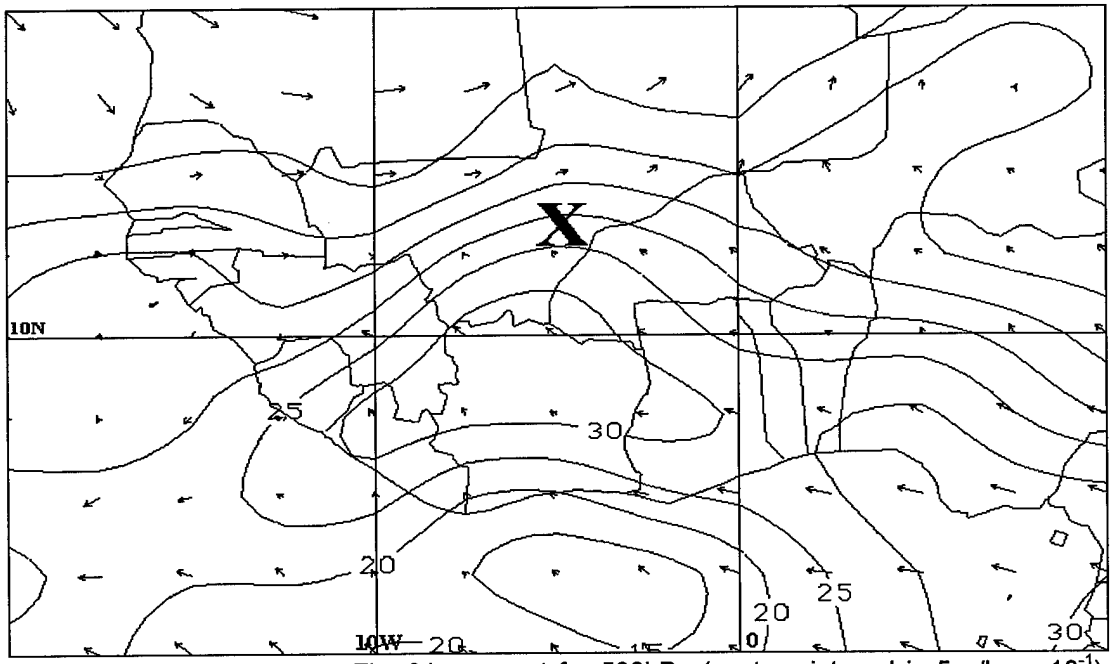

FIG. 21b. Same as Fig. 21a, except for 500hPa (contour interval is 5 g/kg x 10^{-1}) . Maximum values approximately 3.0 g/kg.

Temperatures associated with the cases were considered only at 250hPa and 500hPa. The strong gradients and high temperatures influenced by the nearby desert environment do not allow for adequate temperature anomalies to be found in the analysis at 850hPa. This was also made apparent by the lack of statistical correlation found earlier (see Tables 4a. and 4b.). Across the local grid area, the temperature gradient increases quickly towards the northern and southern extremes, lessening the statistical significance of deviation from the local mean. This variability in latitudinal temperature deviations can be partially overcome by contrasting temperature deviations longitudinally. This allows for a more accurate determination of significant temperature anomalies associated with the PW anomalies.

In most of the cases, warm temperature anomalies, near one standard deviation above the local mean to the east and west (see figs. 18g.-h.) advect along with the higher moisture values of the PW anomalies. Warmer temperatures, in turn, allow for additional moisture to be held by the atmosphere. Since the tropics contain little in the way of large temperature variations at most levels, even a +2°C temperature structure can mark an anomaly in the upper levels. Figure 22 provides a representation of the temperature structure at both 250hPa and 500hPa. Since the PW anomalies extend up to and over 10° in latitudinal extent, an oval is applied to indicate the core extent of the region in which an anomaly develops. Notice the warm pocket across the southern extent of the developing PW anomaly at each level.

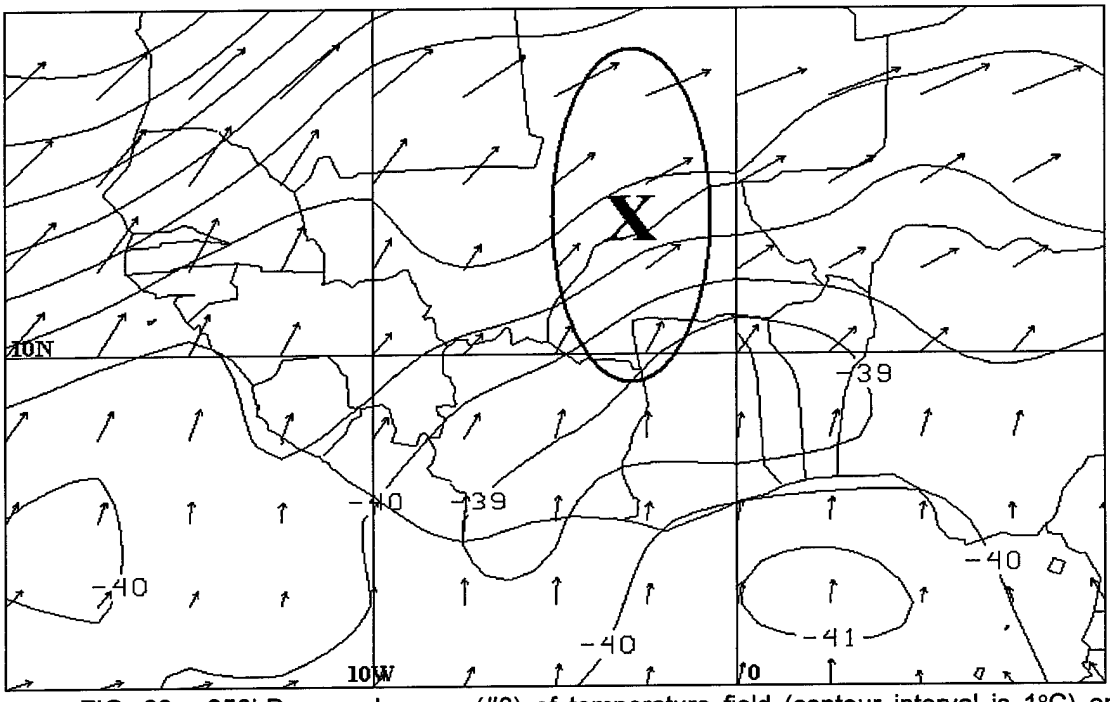

FIG. 22a. 250hPa sample case (#3) of temperature field (contour interval is 1°C) on initiation day for the seven cases in the MAM 1988 season. The local center of the PW anomaly is annotated by an 'X'. The oval indicates the core region of the PW signal. 5° long wind arrows are approximately 15 m/sec.

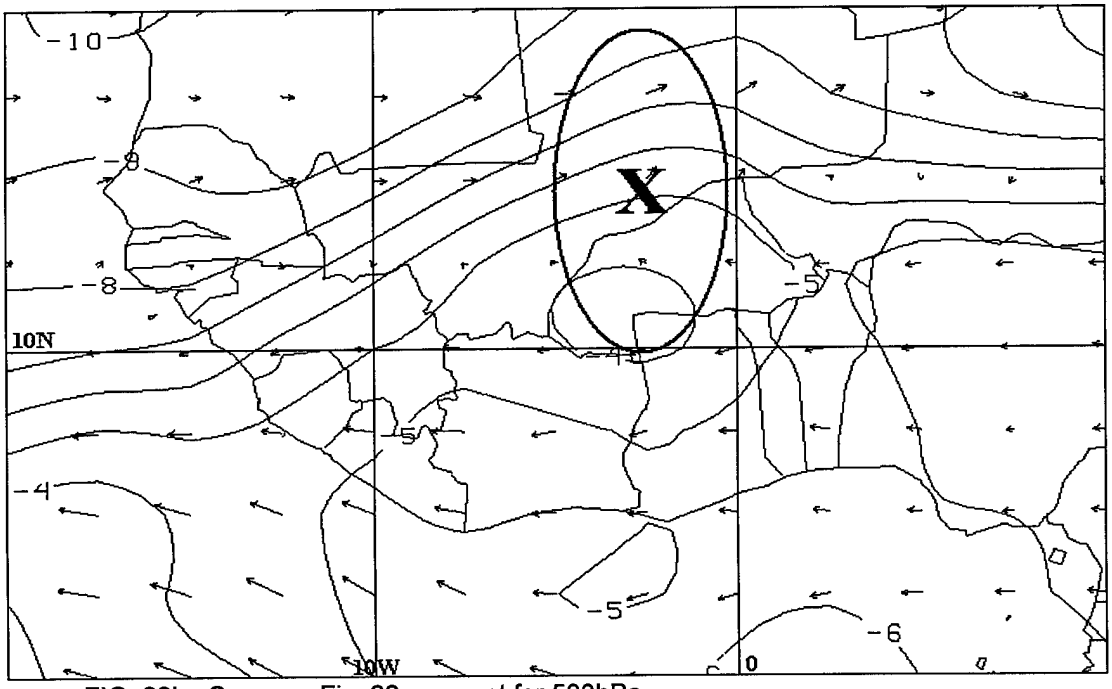

FIG. 22b. Same as Fig. 22a, except for 500hPa.

The third of the five days in the primary life cycle of the PW anomaly is the peak day, usually indicated by the strongest filtered and unfiltered PW signal. By this time, most of the anomalies had moved east to north-central Africa.

Upward vertical motions at 850hPa have strengthened slightly ranging from -0.0015 to nearly -0.003hPa/sec (-130 to -260hPa/day) in some cases, and remain located along the southern portion of the anomaly near the convergence zone. These upward vertical motion values exceed one standard deviation from the local mean, increasing their significance if compared to surrounding noise. Some of the cases begin to develop significant downward vertical motion regions near the northern portion of the anomalies at 850hPa. Figure 23 is a sample case of this almost symmetric rising and sinking of air from the convergence region and into the southern desert region at 850hPa.

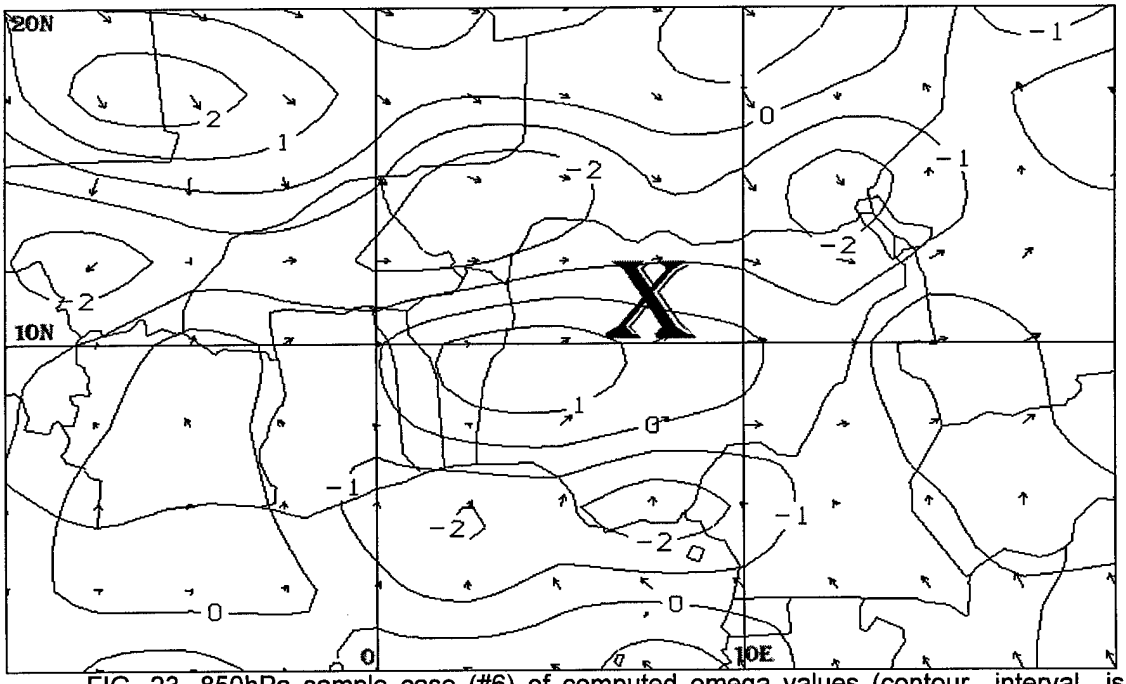

FIG. 23. 850hPa sample case (#6) of computed omega values (contour interval is 1hPa x 10^{-3}/sec) on peak day for seven cases in MAM 1988. An 'X' indicates the local center of the anomalies. 5° long wind arrows are approximately 15 m/sec.

Potential vorticity values immediately surrounding the PW anomalies at both 250hPa and 500hPa broaden and therefore decrease intensity in all except one case. No values greater than +2 K/kg m^2/sec are found within the anomaly's local area for the remaining six. There are still, however, high potential vorticity values across the extreme northern portion of the local grid area associated with the midlatitude jet that continue to push east.

Specific humidity values still outline the unfiltered PW values across most of the cases. The advecting southerly flow proceeds to pull moisture east and north as the wave propagates east. Figure 25 shows all three specific humidity levels for one case. The strongest signal is at 250hPa, though both the 500hPa and 850hPa retain high moisture values as well. Moisture values are still well above the maximum equatorial mean, indicating an additional moisture source exists across the southern portion of the region.

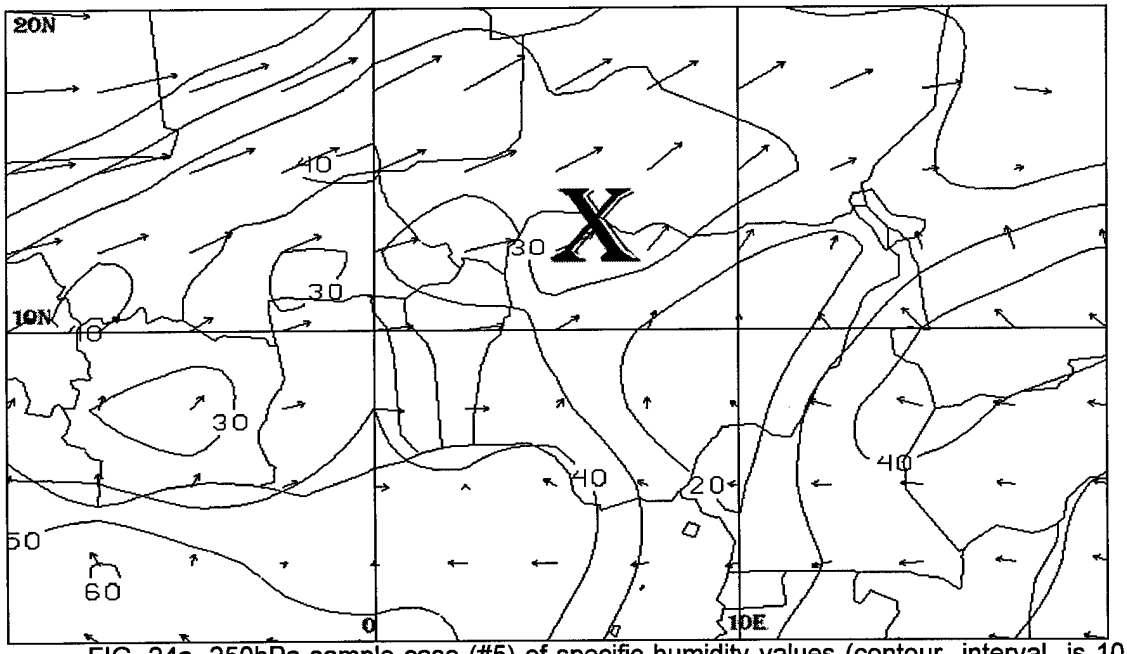

FIG. 24a. 250hPa sample case (#5) of specific humidity values (contour interval is 10 g/kg x 10^{-2}) on peak day for seven cases in the MAM 1988 season. An 'X' indicates the local center of the anomalies. 5° long wind arrows are approximately 15 m/sec.

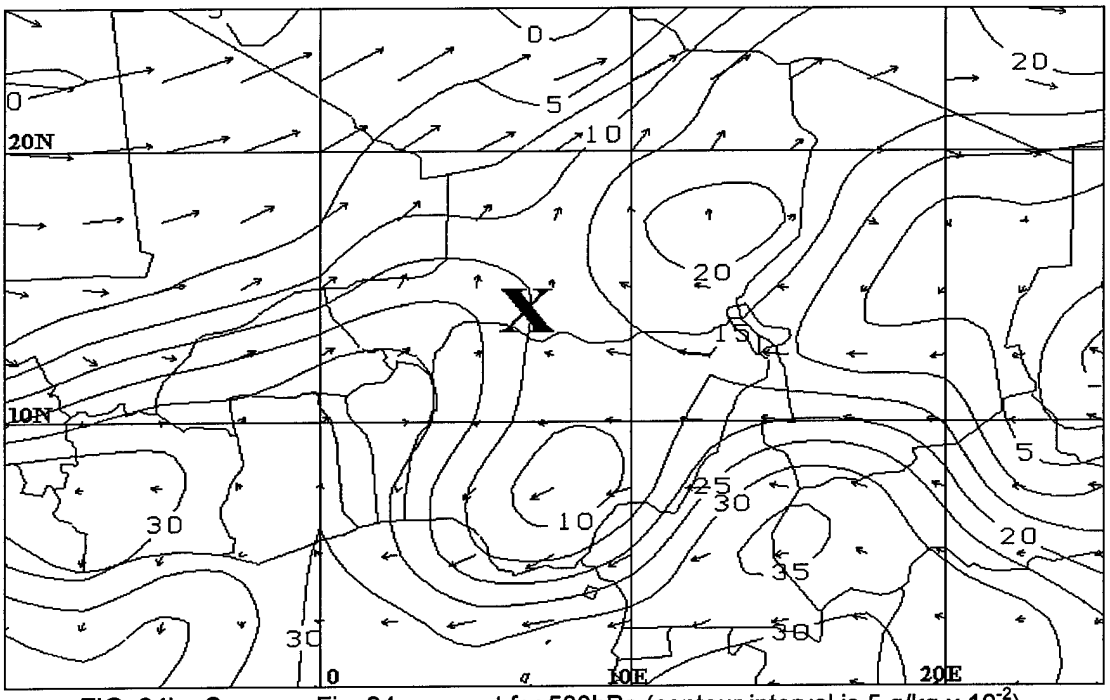

FIG. 24b. Same as Fig. 24a, except for 500hPa (contour interval is 5 g/kg x 10^{-2}).

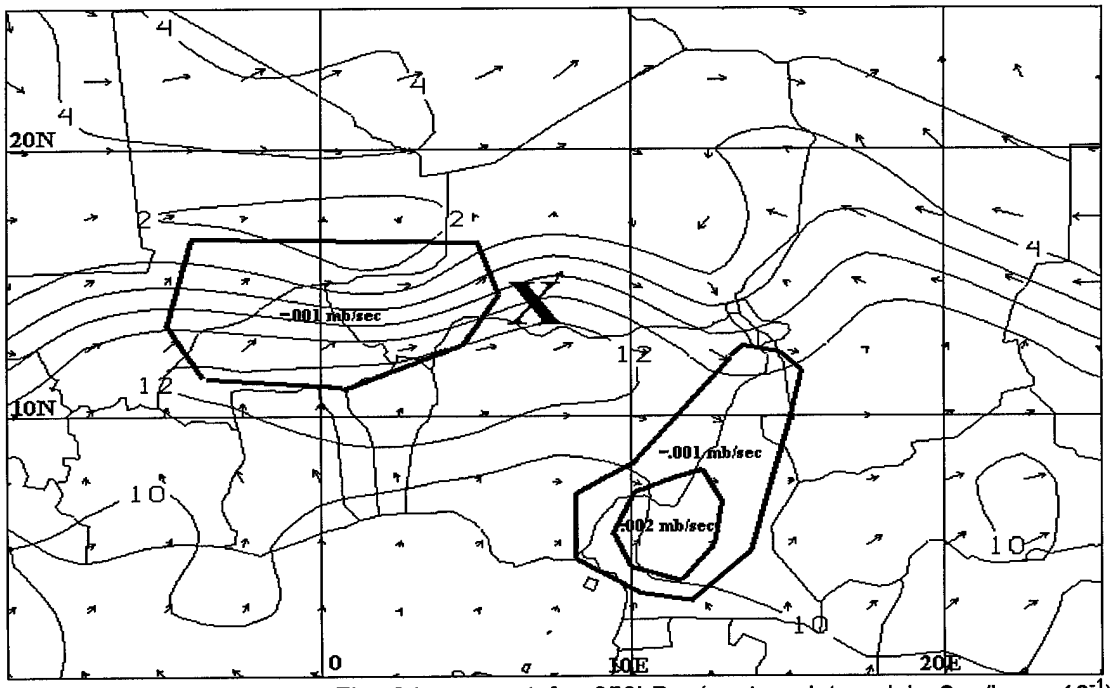

FIG. 24c. Same as Fig. 24a, except for 850hPa (contour interval is 2 g/kg x 10^{-1}). Regions of computed significant 850hPa negative omega (upward vertical motion) for this case are boxed and labeled.

Temperatures yield no real changes in values. A weak (2-3°C) warm temperature anomaly continues to follow within the local area of the PW anomaly at both 250hPa and 500hPa, either as a distinct warm pocket, or a simple warm surge north. These temperature anomalies remained slightly greater than one standard deviation from the mean over the past 72 hours. Figure 25 displays a sample of one case that retains a warm pocket almost centered on the PW signal.

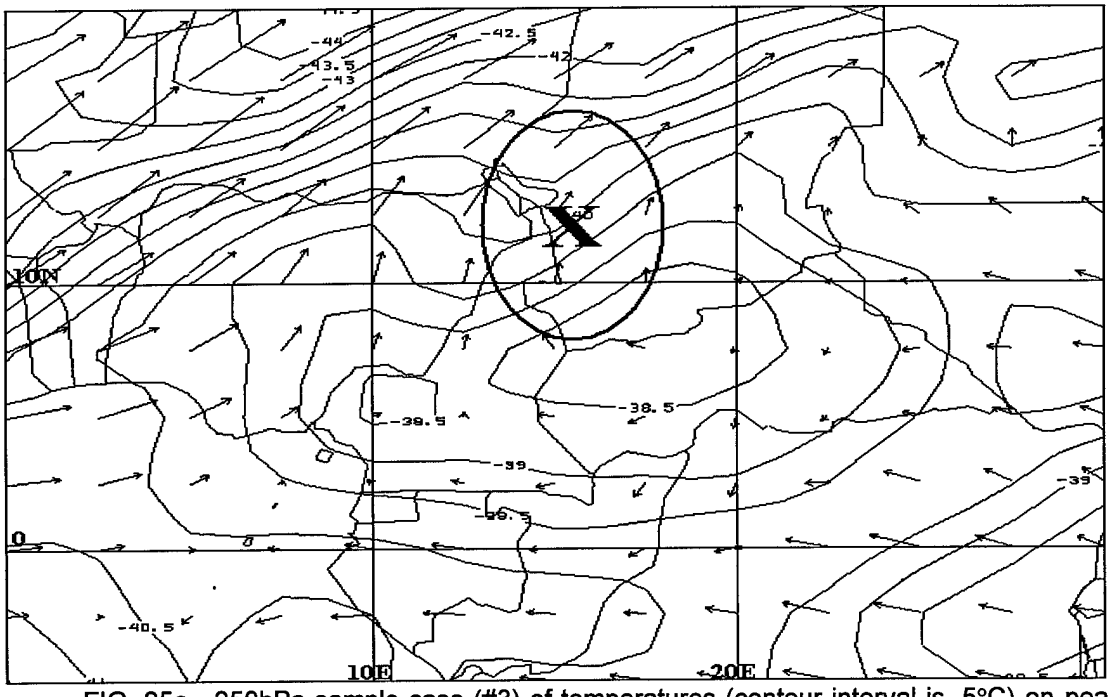

FIG. 25a. 250hPa sample case (#3) of temperatures (contour interval is .5°C) on peak day for seven cases in MAM 1988 season. An 'X' indicates the local center of the anomalies. Oval region indicates core region of the PW signal. 5° long wind arrows are approximately 15 m/sec.

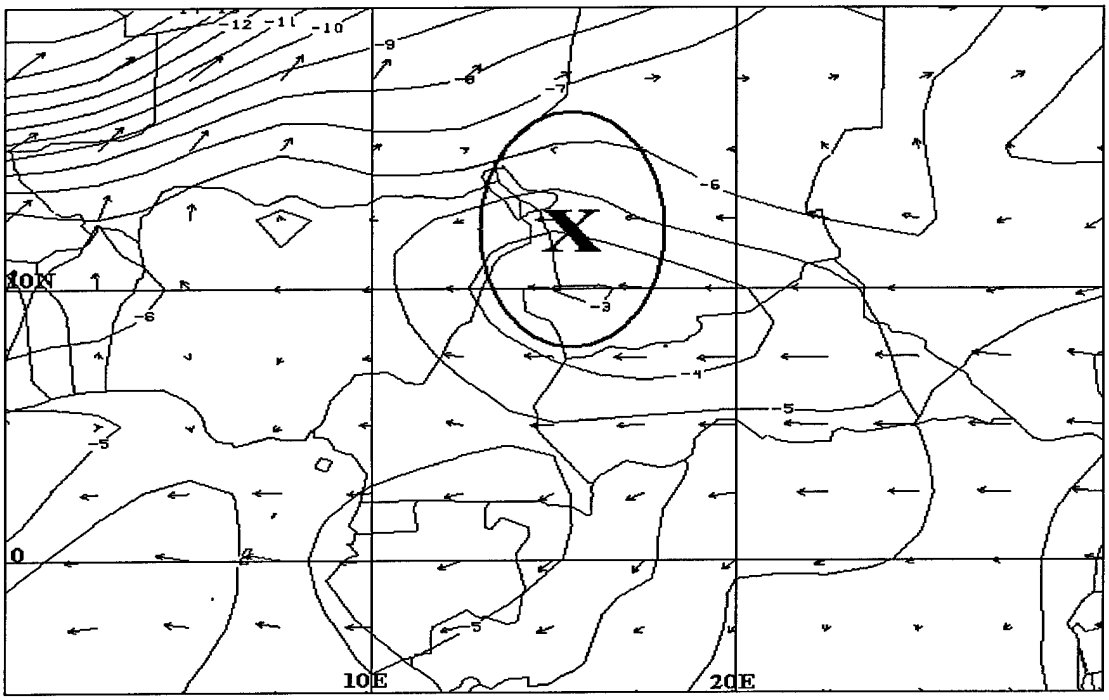

FIG. 25b. Same as Fig. 25a, except for 500hPa (contour interval is 1°C).

The fifth day, or dissipation day, actually marks the point of an anomaly's life cycle in which both the filtered and unfiltered PW signal have begun to noticeably decay or become too difficult to distinguish from higher semi-permanent PW values that frequently exist across east-northeastern Africa. This dissipation occurred within six of the seven anomalies near the same geographic area (see Fig. 3). Only one anomaly's distinguishable center went beyond 20°E.

Omega values at 850hPa continue to become less organized. Analysis becomes difficult when trying to distinguish isolated anomaly-associated upward vertical motion from that of the convergence region (Fig. 26.). Negative values remain to the south along the weakening convergence zone, while weak positive values usually remain to the north.

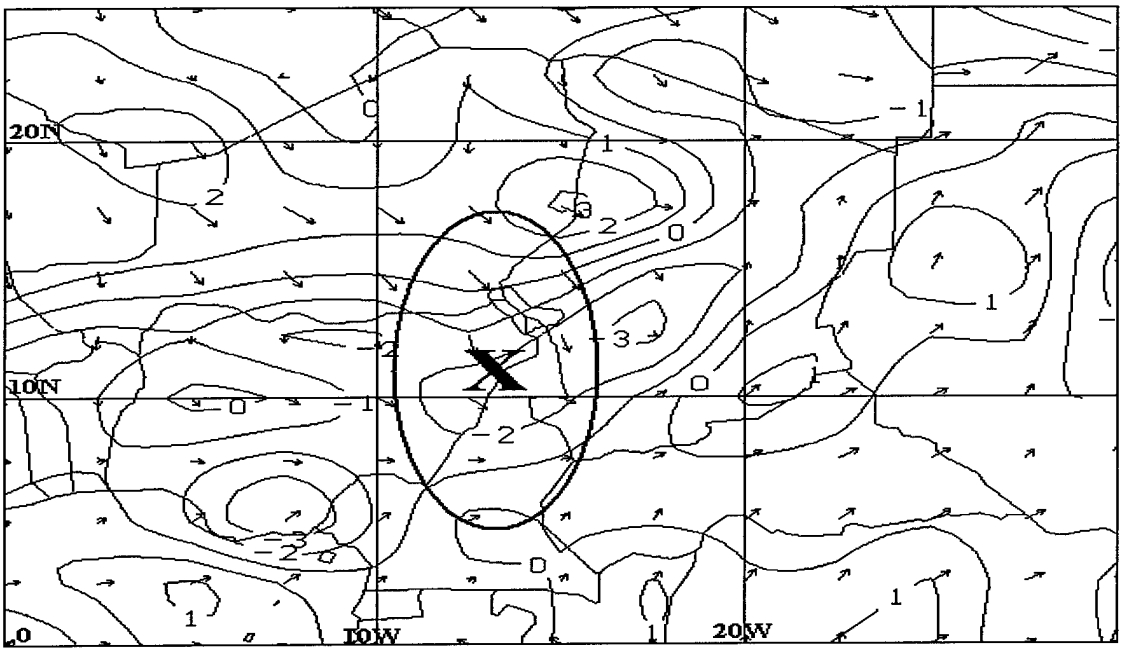

FIG. 26. 850hPa sample case (#1) of computed omega values (contour interval is 1hPa x 10^{-3}/sec) on dissipation day for seven cases in the MAM 1988 season. An 'X' indicates the local center of the anomalies. Oval indicates core region of the PW signal. 5° long wind arrows are approximately 15 m/sec.

Potential vorticity values are very weak around the center of the anomalies by the fifth day. Only two cases had any values greater than +2 near their center. Most of the higher values remained well to the north.

Specific humidity values, though with lessening moisture values, continue to outline the unfiltered PW anomaly structure well across at least one of the two upper levels. The particular case in Fig. 27 developed an isolated "patch" type feature in the unfiltered PW field that is found at both 250hPa and 500hPa in the specific humidity field.

Temperature anomalies also begin to become less apparent. Most of the cases still retain a warm pocket near the anomaly center, though not as pronounced as during the days prior in either size of the warm anomaly or the degree of deviation from the local mean. Due to advection, however, the warm anomalies become displaced slightly northward.

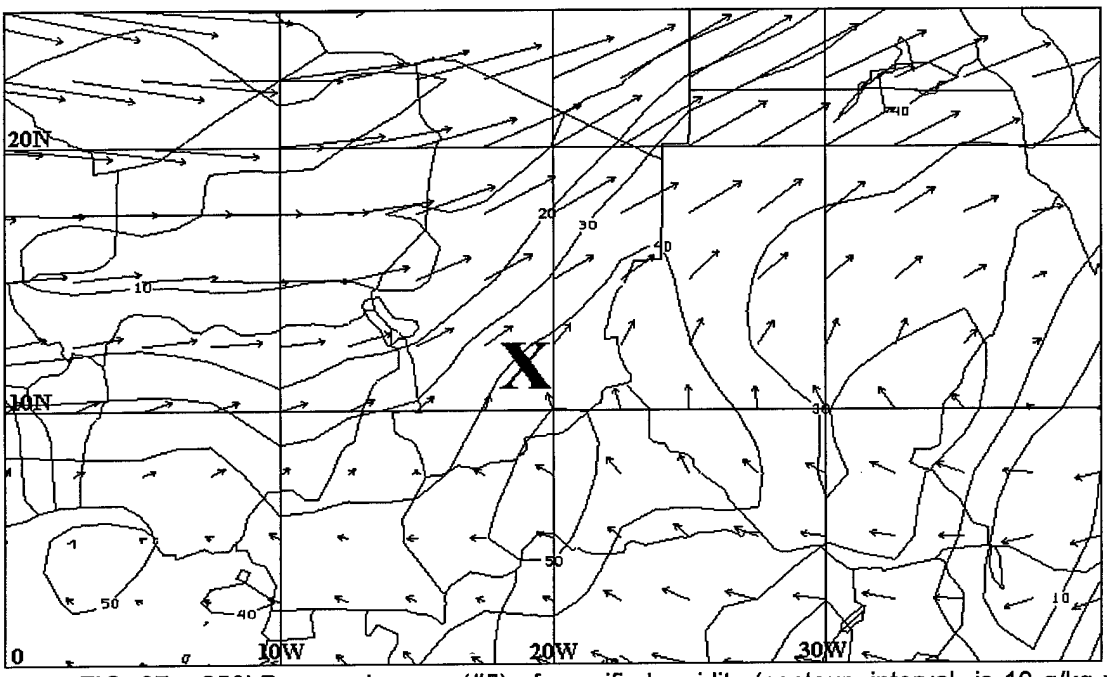

FIG. 27a. 250hPa sample case (#5) of specific humidity (contour interval is 10 g/kg x 10^{-2}) for seven cases on dissipation day for the MAM 1988 season. An 'X' indicates the local center of the anomalies. 5° long wind arrows are approximately 15 m/sec.

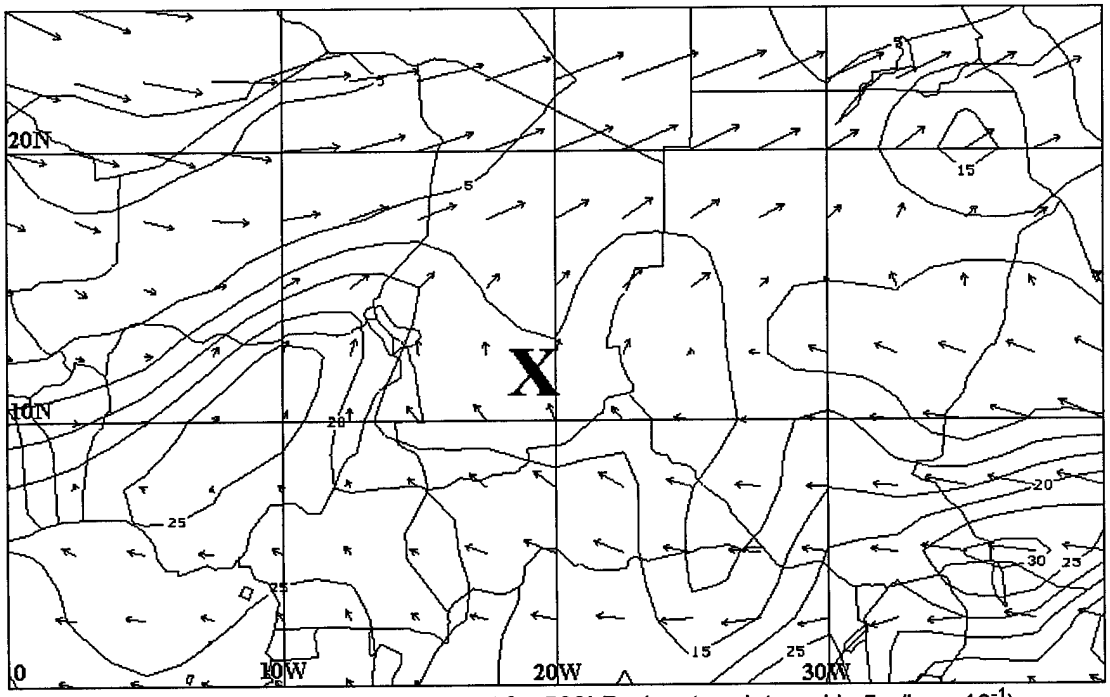

FIG. 27b. Same as Fig. 27a, except for 500hPa (contour interval is 5 g/kg x 10^{-1}).

The northward moistening of the upper levels during the first three days of anomaly development is made even more apparent with composites of the initiation day and peak day, at both 250hPa and 500hPa, for six cases of this case study. One case (#3) is excluded due to its geographic isolation from the others six.

Figures 28 and 29 reveal the apparent moistening found during the first three days of abundant northward advection out of the Gulf of Guinea associated with the passing wave. Notice the northward progression of specific humidity values at both levels across the 10°N latitude band from initiation day to peak day, especially at about 15°E.

Figure 30 displays a six-case composite of the 250hPa standard deviation across the local grid area on initiation and peak day. Comparing these figures to Fig. 18b. in section C of this chapter, typical standard deviations of random days across the local grid would be expected to be have nearly uniform values since the data originates from the same dataset as that from which the seasonal mean is derived. In this figure, however, higher values are found across the PW anomaly propagation region, though not as great as those found across the seasonal mean. This evidence supports the regularity of PW anomalies across this regime.

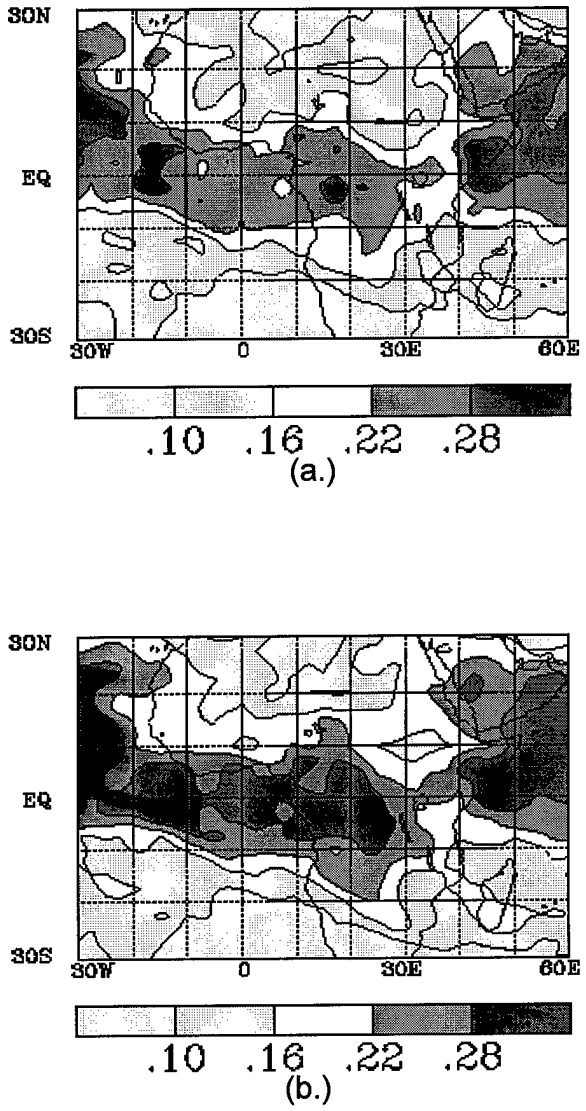

FIG. 28. Six case a.) initiation day and, b.) peak day composite of specific humidity (g/kg) at 250hPa.

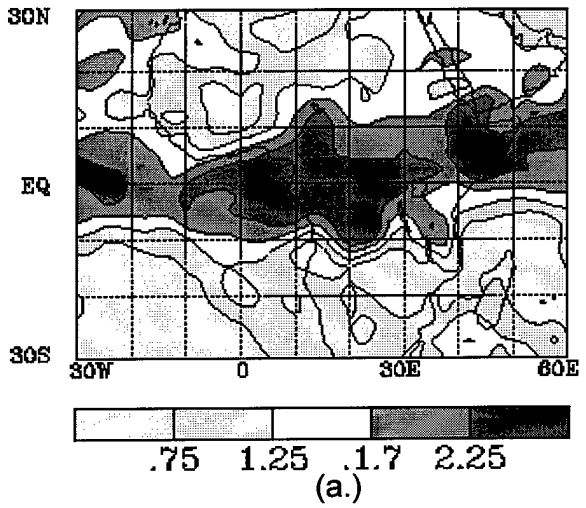

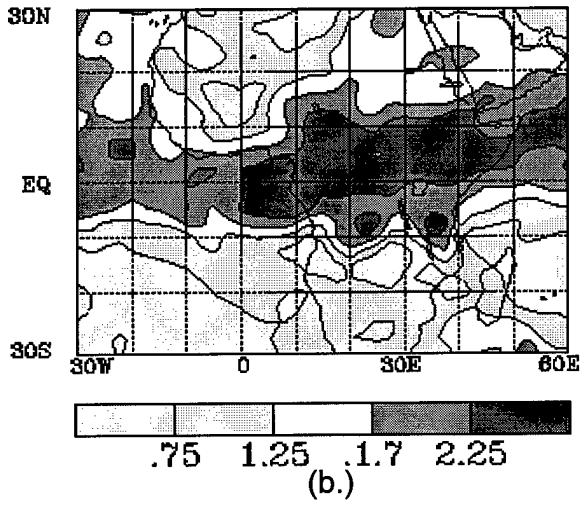

Fig. 29. Same as Fig. 28, except at 500hPa.

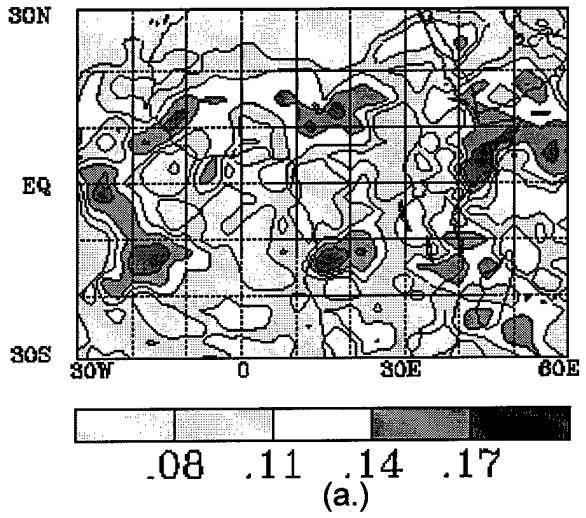

Fig. 30. Six case composite of specific humidity standard deviations at 250hPa on a.) initiation day and, b.) peak day.

The following Chapter provides an empirical model of the development of PW anomalies that initiate northwest of the Gulf of Guinea. The model is developed using the findings of this case study.

CHAPTER V

EMPIRICAL MODEL

An empirical model is, by definition, a verbal or pictorial descriptive model that is based solely on observation and analysis. This study identifies a westward propagating Rossby Wave found within stronger eastward zonal winds which induces a flow that advects anomalous moisture values into an otherwise extremely dry regime across northern Africa.

Each anomaly varies in size and strength of its filtered and unfiltered signal. The signal strength is found primarily to depend on the current local state of atmosphere at the time and location of development. Higher available moisture values to the south, whether due to excess moisture in the atmosphere's mean state, or by way of convective processes, lead to stronger and more coherent filtered and unfiltered signal in the TOVS-generated PW field. Drier conditions to the south result in a weaker and less defined PW signal.

This empirical model identifies four primary stages of the life cycle: 1.) two days prior stage, 2.) initiation stage, 3.) maintenance stage, and 4.) dissipation stage. The cusp-like structure, associated with the Rossby Wave and found during each of the stages, may be located at either 500hPa, 250hPa, or both levels. More intense PW signals contain the structure at both levels

A. STAGE 1 – Two Days Prior

The first stage involves an eastward propagating trough at 250hPa and 500hPa, near 25°N, approaching the west African coastline at approximately 12 m /sec. Removing the mean zonal flow at each 2.5° latitude band reveals a cyclonic (***C***) and anticyclonic (***A***) structure, with an approximate wavelength of 6,100km (wave number 6). The structure is part of an approaching westward propagating Rossby Wave traveling within the greater mean zonal flow. The advective pattern between these two circulations results in a east-northeastwardly tilted cusp-like structure that carries a northeastward advective pattern that moves south into the deep tropics (south of 10°N) .

At upper levels, the region over the east Atlantic contains very low mean specific humidity values (see Figs. 14a.-b.), preventing a high moisture anomaly to develop northward. The feature continues its eastward and slightly southward propagation within the upper level flow. Figure 31 represents stage 1, displaying the cusp-like structure existing in dry upper level conditions and propagating east-southeast into a more moisture rich region as the associated advective pattern sinks closer to the equator. This region also contains warmer temperatures associated with the abundant upper level moisture.

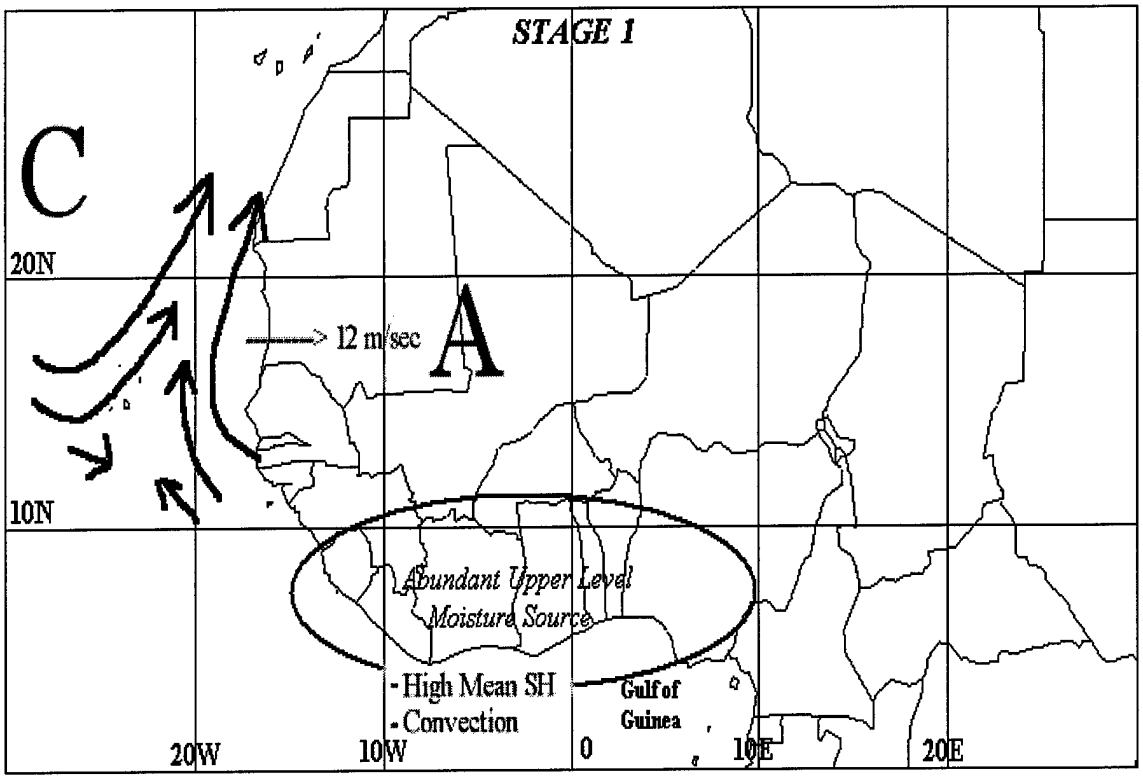

FIG. 31. Represents model stage 1 of PW anomaly life cycle.

B. STAGE 2 – Initiation

Figure 32 represents the second stage. This stage involves the wave propagating east and slightly southward allowing the northeastwardly advective pattern of the cusp-like structure to move close enough to high moisture values near the Gulf of Guinea. This creates a flow that allows for abundant moisture advection northward. Higher moisture values, and associated warm temperature anomalies (+2°C), exceeding two local grid standard deviations above the local mean are advected into the structure, creating a positive PW anomaly. At 250hPa, values well over 0.40 g/kg are advected. At 500 hPa, moisture values greater than 2.5 g/kg are advected, though usually with up to a one day lag behind the 250hPa values due to a weaker flow. Both of these values are well above the local mean state for the season and region. Convective processes may also contribute to the excess moisture found at these upper levels.

The center of the developing PW anomaly, in most cases, may be found within a regional minimum (less than +2 K/kg m^2/sec) of potential vorticity values, with local maximas (exceeding +9 K/kg m^2/sec) to the east and west.

The upper level advective flow also slightly increases 850 hPa upward vertical velocities located near the regional convergence zone. This, too, may carry higher moisture values to the upper levels due to adiabatic cooling with ascent. As the structure moves further inland, it appears to become tilted more northeastward.

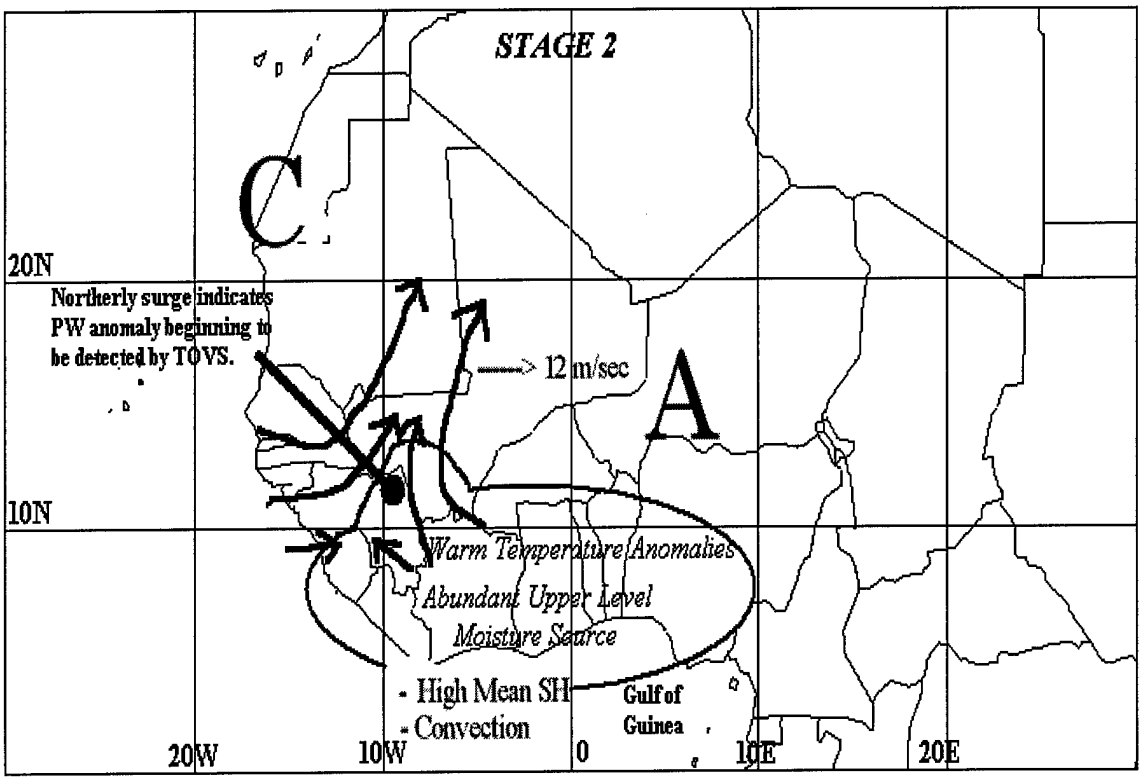

FIG. 32. Represents model stage 2 of PW anomaly life cycle.

C. STAGE 3 - Maintenance

The third stage, usually involving the most pronounced filtered and unfiltered PW signal of the life cycle, entails the beginning of decreasing moisture and associated warm temperature advection from the south due to the PW anomaly's geographic location. The advective pattern of the cusp-like structure begins to move east of its primary moisture source, the Gulf of Guinea. The minimal moisture that does advect into the PW anomaly may rapidly entrain into the local dryer air over the following days as the anomaly moves east, causing the PW signal to become increasingly weaker. Figure 33 displays the structure approaching the center of the continent and beginning to lose its moisture source.

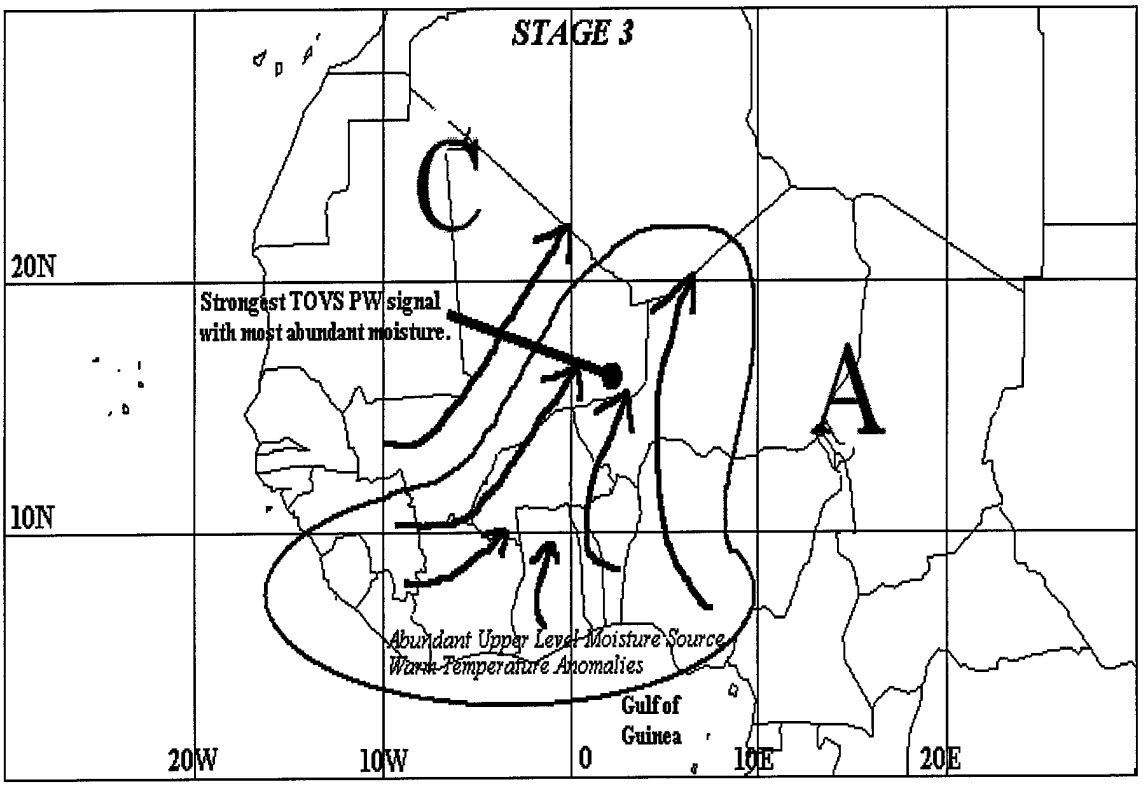

FIG. 33. Represents model stage 3 of PW anomaly life cycle

D. STAGE 4 – Dissipation

The final stage of the anomaly involves the continued weakening of the filtered and unfiltered PW signal, eventually becoming unidentifiable from surrounding data noise. The anomaly rapidly loses its definition due to the decreased moisture available for advection.

Additionally, the propagating wave begins to pull northeastward as it moves off the continent (north of 25°N), even further away from its primary moisture source.

Figure 34 displays the weakening cusp-like structure and the decreasing specific humidity and associated temperature values available for advection into the anomaly.

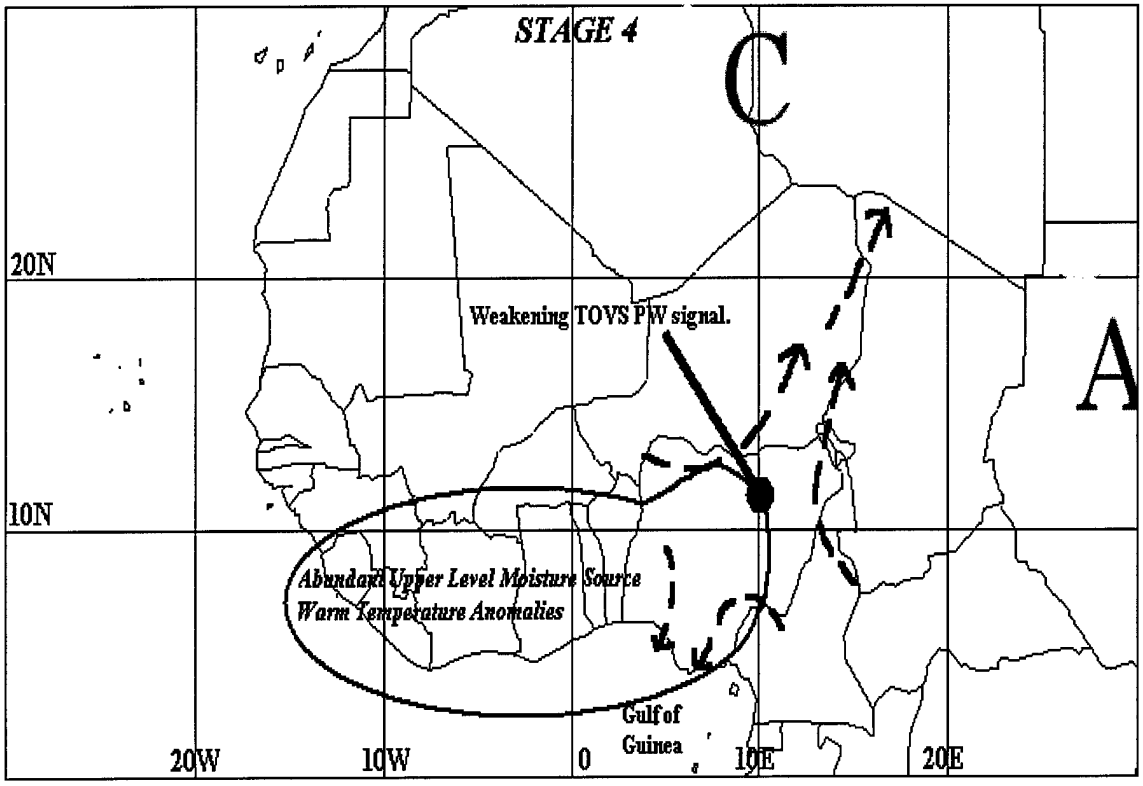

FIG. 34. Represents model stage 4 of PW anomaly life cycle.

CHAPTER VI

SUMMARY AND CONCLUSIONS

The primary objective of this study was to document the evolution and structure of eastward propagating positive PW anomalies that organize near the northwest Gulf of Guinea and maintain their identity into East Africa. The most prominent season, year and location of the TOVS-initiated PW anomalies was previously determined by Mackey (1996) to be across northern Africa during MAM 1988. This source region, one of seven prominent tropical locations, retained the strongest and most coherent signal. Seven cases within the MAM season were chosen to accomplish this goal.

The first step in the research process was to composite the actual wind fields at each level for the seven case (six of which were used in the composites). In addition to the actual wind field, the mean zonal flow was removed to reduce latitudinal shear over the local grid area. This involved subtracting the mean of the latitudinal U component at each 2.5° latitude band and creating a new resultant with the original V component. This process revealed a cyclonic and anticyclonic wave structure that was propagating eastward at approximately 12 m/sec in an eastward mean zonal wind speed (based on 20°N) of approximately 17 m/sec. These findings yielded a Rossby wave of wavenumber 6 propagating to the west at nearly 5 m/sec, and an associated tilted cusp-like structure within its background wind field. The northeastwardly tilted upper level (500hPa and 250hPa) cusp-like structure moved across the region of propagation and advected northeastward abundant

moisture and warm temperatures values from the Gulf of Guinea. Advected moisture values exceed two standard deviations above the local mean, and over one standard deviation above the local mean of temperatures.

The 500hPa and 250hPa flow induced by the wave passage slightly enhanced low level (850hPa) convergence and upward vertical velocities. As the structure moved towards the center of the continent, it begins to lose its moisture source, causing the PW anomaly to weaken and dissipate.

Once the wind field and wave structure was determined, the study utilized NCEP/NCAR numerical model data at 850 hPa, 500 hPa, and 250 hPa of the MAM period to analyze the computed omega, specific humidity, potential vorticity, temperature, and actual wind fields. The resulting dataset was first time averaged, mapped and compared to large-scale structures in the tropical atmosphere. The data revealed regions of known convergence zones, locations of large subtropical highs, and other convectively active regions. These results provided data confidence during analysis.

These values were then used to develop descriptive statistics at two distinct resolutions (2.5° and 10°) of the localized grid that the seven cases propagated through during their seven day life cycle. The 10° spatial resolution further reduced the correlated data by adding temporal filtering to every seventh day of data. Variables found to be statistically significant at both resolutions when correlated with the PW values were then incorporated into a general structure of the PW anomalies as determined by the NCEP/NCAR analysis.

The structure revealed a well-defined specific humidity and temperature field that was directly related to the TOVS-generated positive PW anomalies. The moisture field revealed values as high as 0.5 g/kg at 250 hPa, and 3.0 g/kg at 500 hPa, were advected into the PW anomaly. These values were well

above the maximum mean state values over the Gulf of Guinea, the region in which moisture was being advected out of. The maximum mean moisture values here ranged from 0.28 g/kg at 250 hPa to 2.25 g/kg at 500 hPa.

Lastly, an empirical model was developed to show the four primary stages of PW anomaly formation: two-days prior stage, initiation stage, maintenance stage, and dissipation stage.

In summary, synoptic scale anomalies found in the PW field are found to assist in locating atmospheric waves that cause anomalous flow in the background wind field. The altered wind field then induces intense moisture advection into regions and at levels that are otherwise extremely dry. These anomalous PW signals then aid in determining wave characteristics as they propagate through the upper levels of the atmosphere.

It is unclear whether the PW anomalies discussed in this study interact in any way with westward propagating disturbance, such as easterly waves, moving of the west African coast. During the season in question (MAM), easterly waves and significant westward propagating synoptic disturbances are minimal. Any conclusions that could be drawn regarding interaction between the two events would be difficult, if not impossible, with the dataset used in this study. Future studies of PW anomalies north of equatorial Africa during more convectively active seasons may prove otherwise.

REFERENCES

Burpee, R. W., 1972: The Origin and Structure of Easterly Waves in the Lower Troposphere of North Africa. *J. Atmos. Sci.*, **29**, 77-90.

Carlson, T. N., 1969a: Synoptic Histories of Three African Disturbances That Developed into Atlantic Hurricanes. *Mon. Wea. Rev.*, **97**, 256-276.

-----, 1969b: Some Remarks on African Disturbances and Their Progress Over the Tropical Atlantic. *Mon. Wea. Rev.*, **97**, 716-726.

Chung, H., 1993: Atmospheric Moisture Fields Derived by Satellite Observations over the Tropical Pacific Ocean. PhD. Dissertation, Dept. of Meteorology, Texas A&M University, College Station, TX 77843, 168 pp.

Devlin, K. I., 1995: Application of the 85 GHz Ice Scattering Signature to a Global Study of Mesoscale Convective Systems. M. S. Thesis, Dept. of Meteorology, College Station, TX 77843, 44pp.

Druyan, L. M., P. Lonergan, and J. Cohen, 1997: Case Studies of African Wave Disturbances in Gridded Analyses. *Mon. Wea. Rev.*, **125**, 2520-2530.

Duvel, J., 1988: Analysis of Diurnal, Interdiurnal, and Interannual variations During Northern Hemisphere Summers Using METEOSAT Infrared channels. *J. Climate,* **1**, 471-474.

Frank, N. L., 1969: The "inverted-v" Cloud Pattern—An Easterly Wave?. *Mon. Wea. Rev.*, **97**, 130-140.

-----, 1970: Atlantic Tropical Systems of 1969. *Mon. Wea. Rev.*, **98**, 307 - 314.

Hatfield, E., 1994: Precipitable Water Structure in Tropical Systems as Estimated

from TOVS. M.S. Thesis, Dept. of Meteorology, Texas A&M University, College Station, TX 77843, 127 pp.

Kalnay, E. et al., 1996: The NCEP/NCAR 40 - Year Reanalysis Project. *Bull. Amer. Meteor. Soc.,* **3,** 437-471.

Krishnamurti, T. N., 1979: Tropical Meteorology. *Compendium of Meteorology – Part 4.* **2**, 261-292.

Kuo, H. L., 1949: Dynamic Instability of Two-Dimensional Nondivergent Flow in a Barotropic Atmosphere. *J. Meteor.*, **6**, 105-122.

Landsea, C. W., W. M. Gray, P. W. Mielke, Jr., K. J. Berry, and R. Taft, 1997: June to September Rainfall in North Africa: A Seasonal Forecast for 1997. *<http://tropical.atmos.colostate.edu/forecasts/>*

Lau, K.M., and C. P. Chang, 1987. Planetary Scale Aspects of the Winter Monsoon and Atmospheric Teleconnections. *Monsoon Meteorology*, C. P. Chang and . N. Krishnamurti, Eds., Oxford University Press, 544 pp.

Mackey, M. D., 1996: A Climatology of Tropical Synoptic Scale Behavior from TOVS - Estimated Precipitable Water. M.S. Thesis, Dept. of Meteorology, College Station, TX 77843, 276pp.

Matsuno, T., 1966: Quasi-geostrophic Motions in the Equatorial Area. *J. of the Met. Soc. of Japan*, **44**, 25-43.

McGuirk, J. P., A. H. Thompson, and L. L. Anderson, Jr., 1989: Synoptic Scale Moisture Variations over the Tropical Pacific Ocean. *Mon. Wea. Rev.*, **5,** 1076 - 1091.

Murakami, T., 1980: Temporal Variations of Satellite – Observed Outgoing Longwave Radiation Over the Winter Monsoon Region. Part 1: Long Period (15-30 day) Oscillations. *Mon. Wea. Rev.*, **108**, 408 - 426.

Newell, R. E., J. W. Kidson, D. G. Vincent, and G. J. Boer, 1972: The General Circulation of the Tropical Atmosphere. MIT Press, 258 pp.

Reed, R. J., D. C. Norquist, and E. E. Recker, 1977: The Structure and Properties of African Wave Disturbances as Observed During Phase III of GATE. *Mon. Wea. Rev.*, **105**, 317-333.

Schroeder, S. R., and J. P. McGuirk, 1996: Wavelet Analysis Applied to a Long-Period Data Base of Precipitable Water Derived from TOVS. *Proc. of the 8th Conference on Satellite Meteorology and Oceanography,* Atlanta, GA, 1996, 83-84.

Strager, C.S., 1989: Origins of Convective Activity over Panama. M.S. Thesis, Dept. of Meteorology, Texas A&M University, College Station, TX, 77843, 101 pp.

Takayabu: Y. N., 1994a: Large Scale Cloud Disturbances Associated with Equatorial Waves. Part I: Spectral Features of the Cloud Disturbances. *J. Meteor. Soc. Japan*, **72**, 433-448.

Thompson Jr., R. M., S. W. Payne, E. E. Recker, and R. J. Reed, 1978: Structure And Properties of Synoptic-Scale Wave Disturbances in the Intertropical Convergence Zone of the Eastern Atlantic. *J. of Atmos. Sci.*, **36**, 53-72.

Winton, S. E., 1991: Interactions of Tropical Synoptic-Scale Features as Viewed from a Satellite. M.S. Thesis, Dept. of Meteorology, Texas A&M University, College Station, TX, 77843, 96pp.

Yin, M., 1994: Information Content and Reliability of TOVS Estimates of Precipitable Water. M.S. Thesis, Dept. of Meteorology, Texas A&M University, College Station, TX, 77843, 108 pp.

VITA

Jason Eddy Patla was born on May 10, 1972 in Ft. Eustis, VA to Norbert and Judith Patla. He grew up throughout Virginia, and then onto St. Louis, MO after his eleventh birthday. He attended Marmion Military Academy in Aurora, IL to complete his secondary education, while spending summers in St. Louis. He attended Purdue University in West Lafayette, IN with the Air Force ROTC program and earned his Bachelor of Science degree (May 1994) in Atmospheric Science. Here he became a dedicated Parrot Head (Jimmy Buffett fan).

His first assignment was to the 46th Weather Squadron, Eglin AFB, FL for two years. Afterwards, he attended Texas A&M University, College Station, TX in order to complete his Masters of Science degree in Meteorology, with an emphasis on Tropical Meteorology.

The location of the author may be found via his parents permanent mailing address since he is traveling the world:

Norbert and Judy Patla
144 Oak Hill Rd.
Arab, AL 35016